ETH zürich

Introducing the team, an overview of the project, recent progress

Alexey Kuvshinov

Project Meeting
10 Feb 2021

esa eo

STSE Support To Science Element

SWARM DISC

Introductory remarks

- I am happy that we are back to “old good” times when we had progress meetings during several Science Studies

- Unfortunately meetings are online, D^3 activity is missing

- Hopefully, with “space” vaccine Sputnik-V (and others) we will be able to return to in-person meetings (and D^3 activity) soon

Introducing the team

Dr Alexander Grayver
ETH Zurich
Oberassistant

Dr Mikhail Kruglyakov
University of Otago (NZ)
Research Fellow

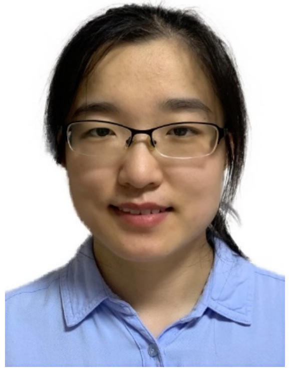

Dr Shan Xu
China University of
Geosciences (Wuhan)
Research Fellow
(Postdoc in ETH is planned)

Chen Chaojian
ETH Zurich
PhD student (third year)

Rafael Rigaud
ETH Zurich
PhD student (first year)

Filippo Cicchetti
ETH Zurich
Master student

Motivation …

Seismology	EM
Velocity	Electrical conductivity
Wave propagation	Diffusion
From surface to core	From surface to mid/lower mantle
Can probe the volume beneath regions without observations	Limited resolution beneath the regions without observations

Examples of global 3D velocity images

From Merignier et al (2020)

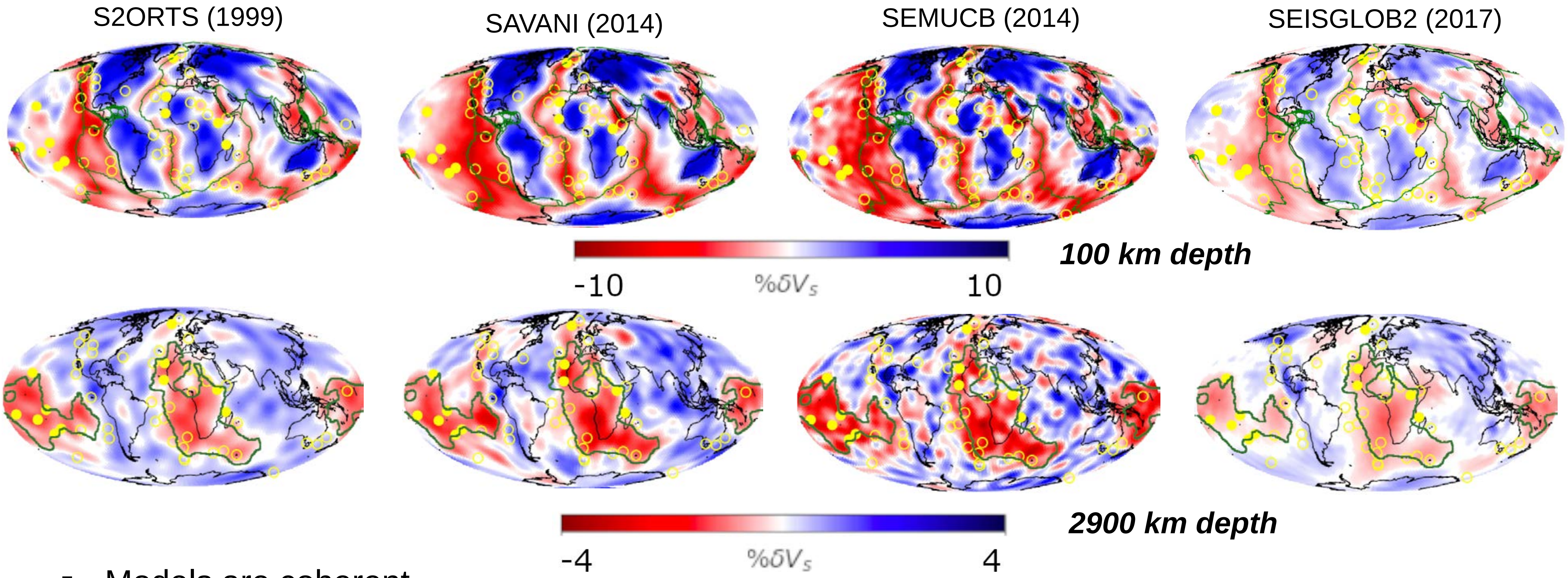

- Models are coherent
- Detailed
- Constrain velocity in the whole mantle

$$3\text{D:}\quad V \equiv V(r,\vartheta,\varphi)$$

From Li et al (2020)

Examples of global 3D conductivity images

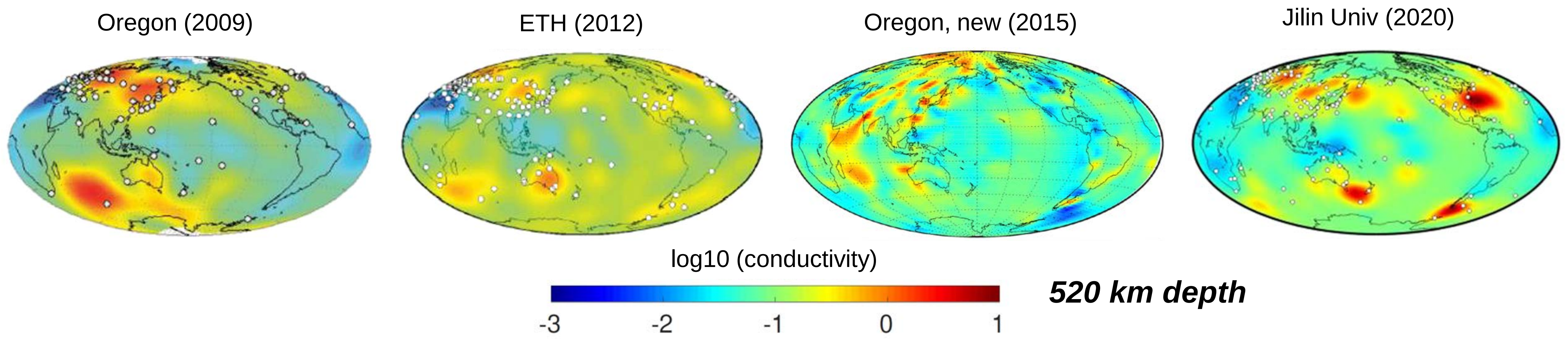

- Models are not coherent (some coherency in NE China)
- A lot of artefacts (in regions with no observations; look, e.g., at “Bermuda” anomaly)
- Unrealistic range of lateral variability (two orders of magnitude)
- Less detailed (compared to seismology)

$$\text{3D:}\quad \sigma \equiv \sigma(r,\vartheta,\varphi)$$

- Constrain(?) conductivity only in depth range ~ 500 – 1500 km (to be discussed later)

Why mantle conductivity at all?

- Proxy for water (hydrogen) and melt content [(1)]; seismology is less sensitive to these parameters

- Geomagnetic modeling of the core, lithosphere, ionosphere, magnetosphere, and ocean signals: requires accurate account for EM effects from conducting Earth [(2)]

- Assessment for Space Weather hazards: modelling geomagnetically induced currents in power lines, etc.; also requires conductivity model of the Earth [(3)]; a lot of activity, e.g., US (2021-2024) program “Living with the Sun”

[(1)] Khan et al 2011; Grayver et al 2017; Munch et al, 2018, 2020,

[(2)] Manoj et al 2006; Sabaka et al 2015, 2016, 2018, 2020; Chulliat et al 2013, 2016; Irrgang et al 2017, 2019; Finlay et al 2020

[(3)] Ivannikova et al 2018; Marshalko et al 2020; 2021

Why the recovery is so poor (and limited to depths of ~ 500 – 1500 km)?

- Are based on observatory data only (coverage is very irregular)
  - No sensible information beneath the regions without observations (e.g. oceans)

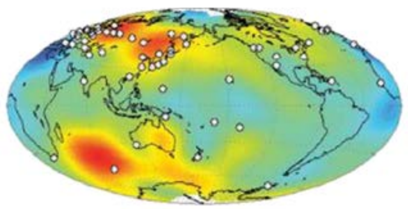

- Variations under consideration are of magnetospheric origin only (ring current source)
  - Periods: days – months (penetration depths ~ 500 – 1500 km)

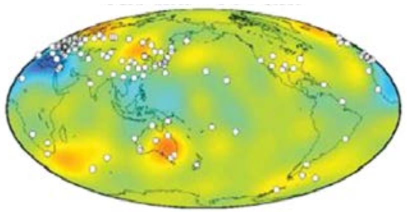

- The source geometry is assumed to be very simple (first zonal harmonic)
  - Allows to implement (standard) C-response concept

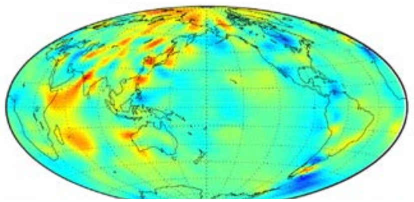

- No information from high latitudes
  - Data there are heavily affected by much more complicated source - auroral electrojet

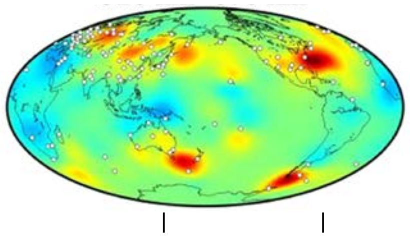

- No information from low latitudes
  - Signal/noise ratio (in radial component) is prohibitively low

Observatory mid-latitude data

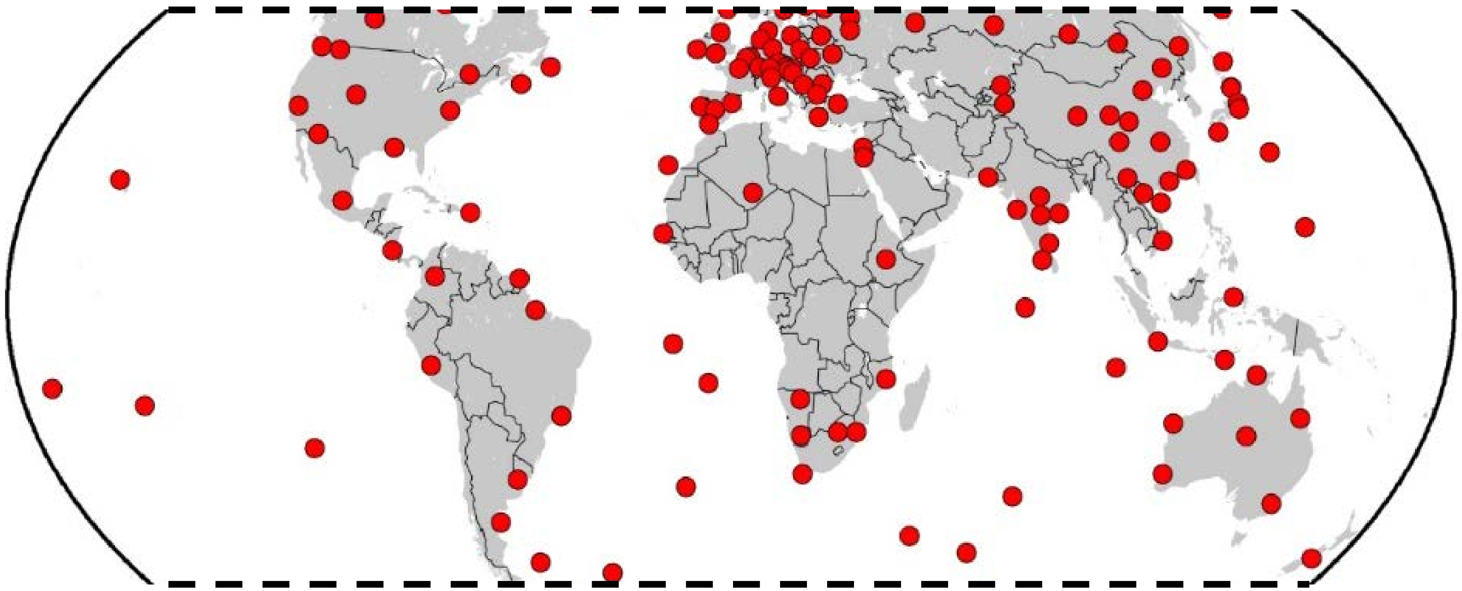

With observatory data only (most probably) it is not to obtain cogent global 3-D conductivity model

Much more ground-based (magnetic field) data exist around the world (at least for inland regions)

(Intermagnet) observatories (< 100)

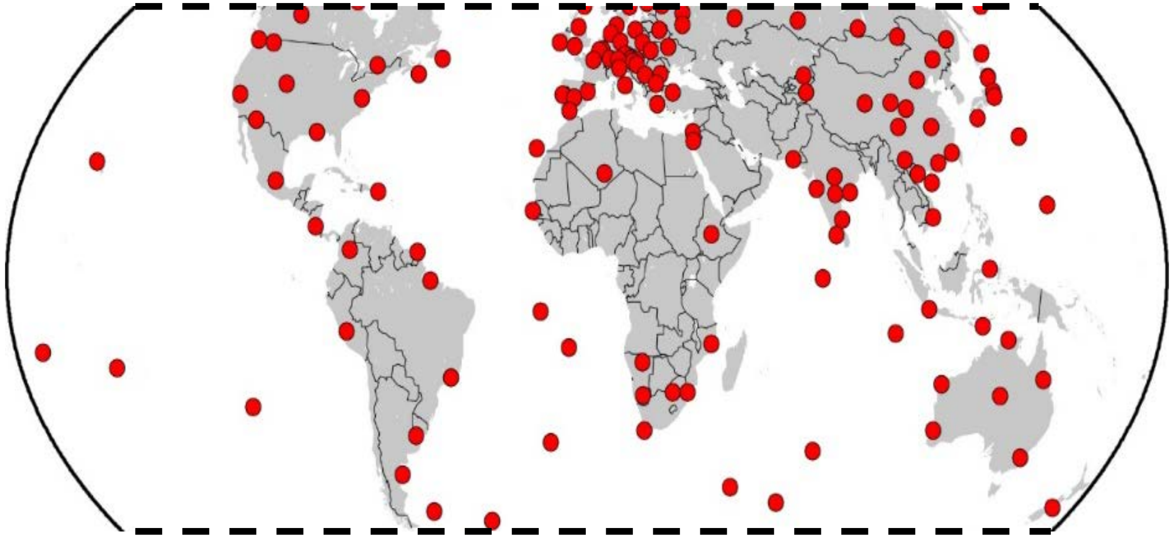

(SuperMag) sites (> 500)

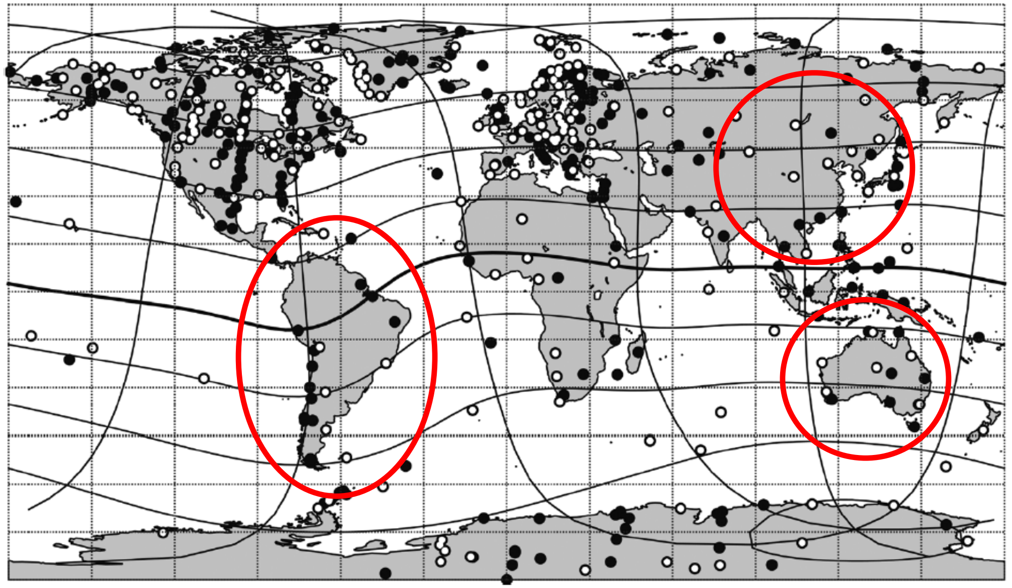

and even more in circled regions…

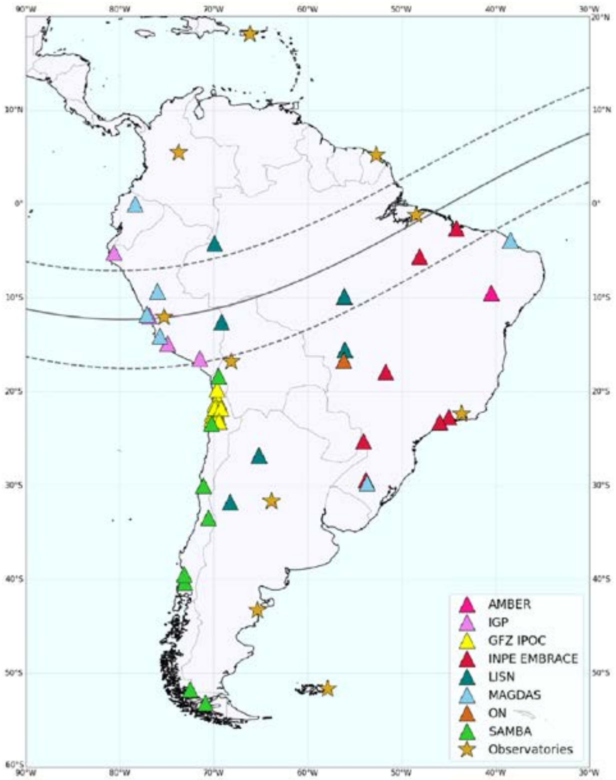
AMBER
IGP
GFZ IPOC
INPE EMBRACE
LISN
MAGDAS
ON
SAMBA
Observatories

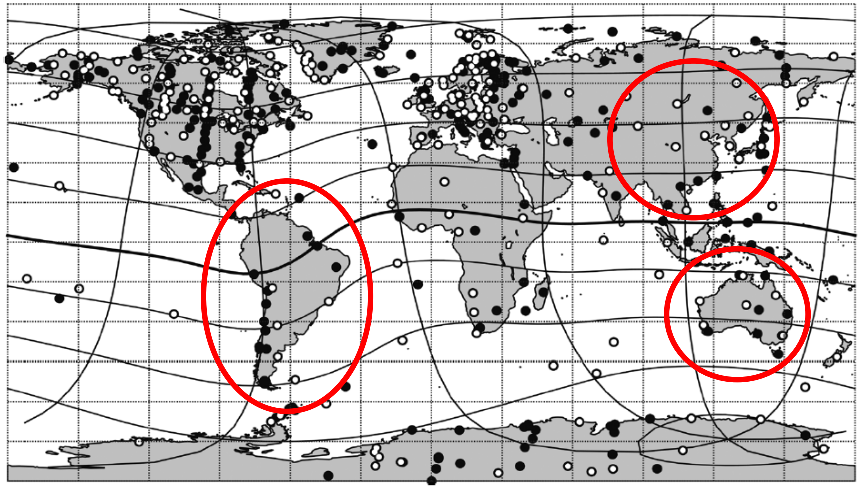

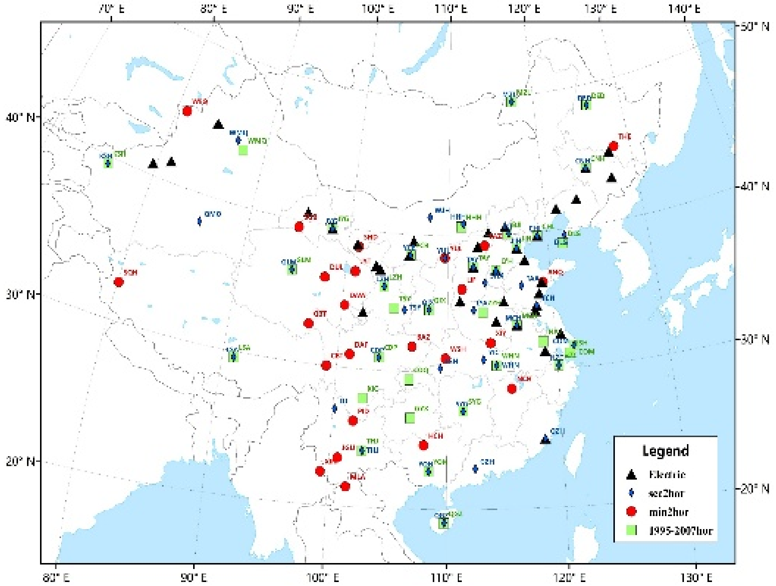
Legend

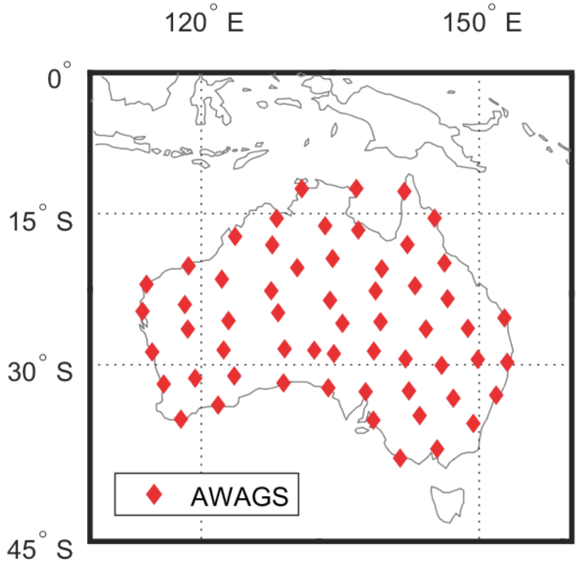
120° E
150° E
0°
15° S
30° S
45° S
AWAGS

Challenges to work with these (additional) data

- Time series are generally shorter than those from the observatories
  - Results at longer periods are expected to be less reliable

- Quality is variable and often poor (gaps, jumps, spikes, no absolute control, etc.)
  - Requires comprehensive preprocessing and calibration (Rafael's talk)

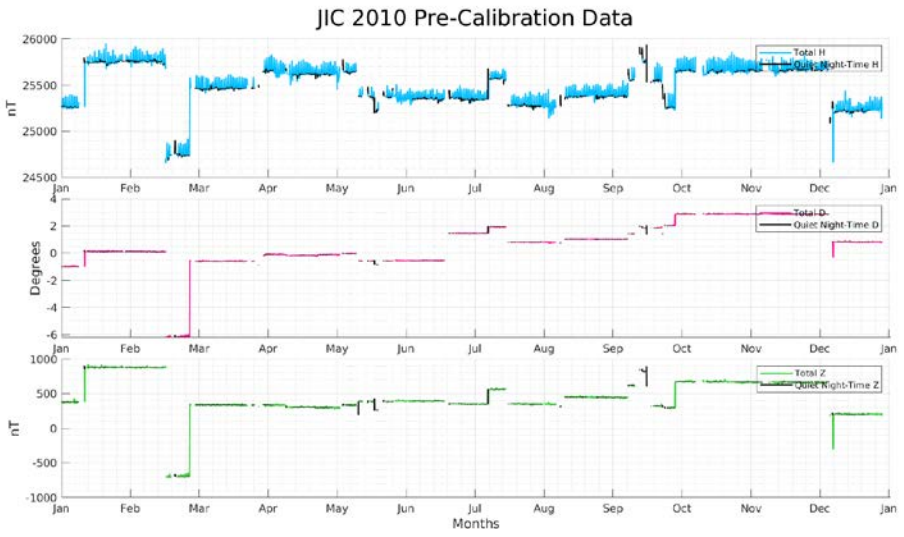

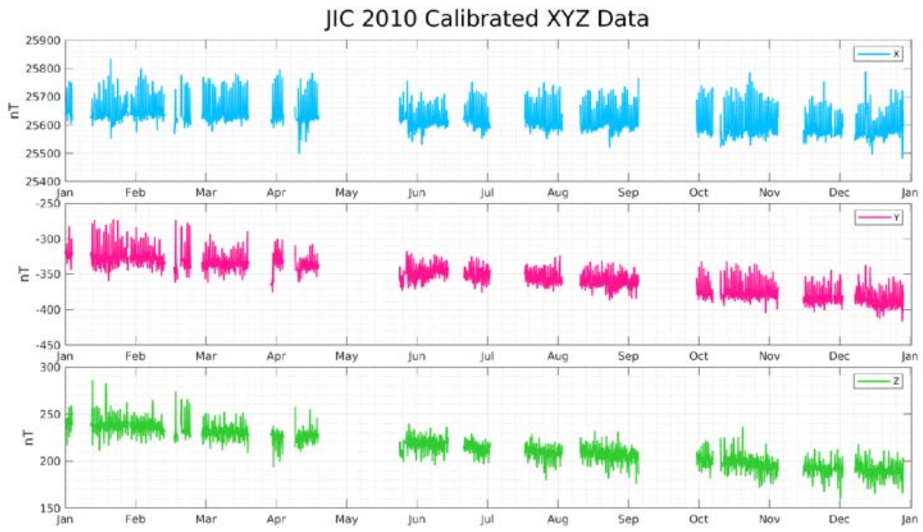

We will have much more (calibrated) inland data regionally, what is next?

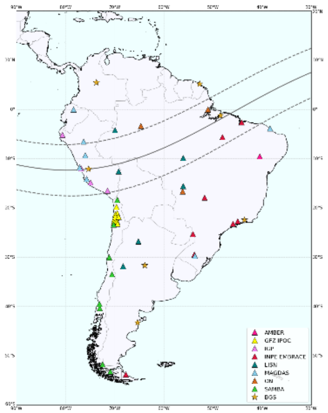

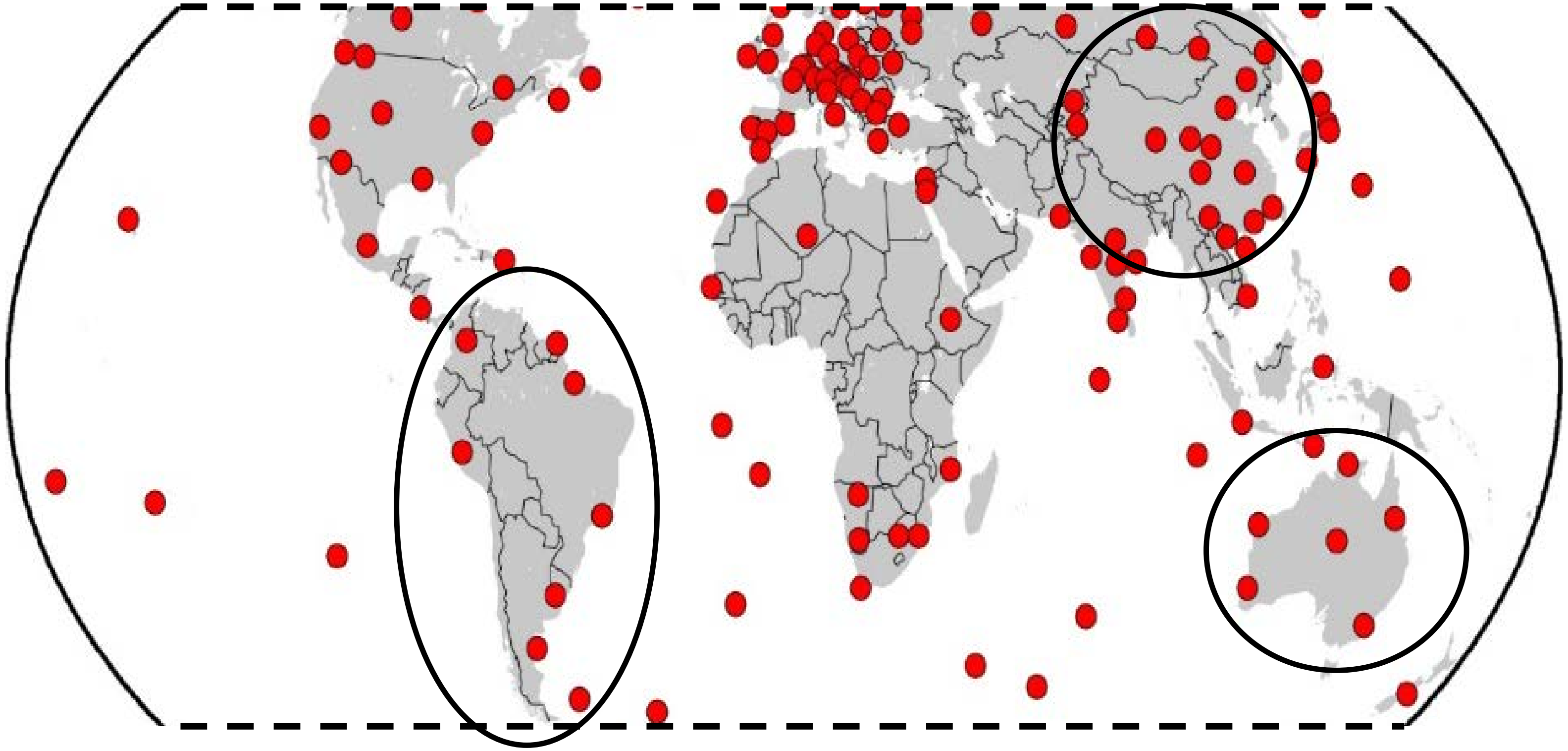

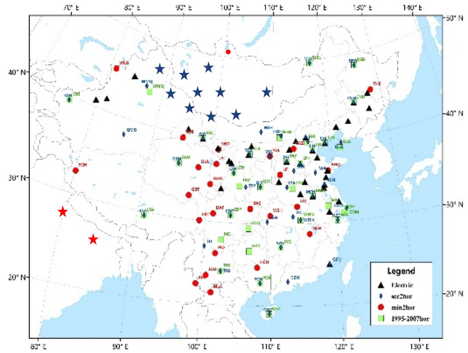

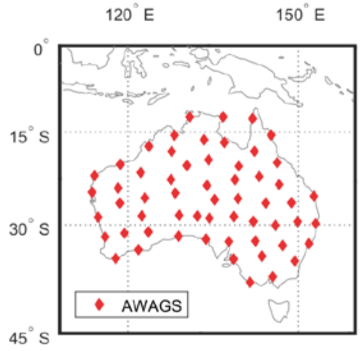

Obtaining regional 3-D conductivity models

What about oceans?

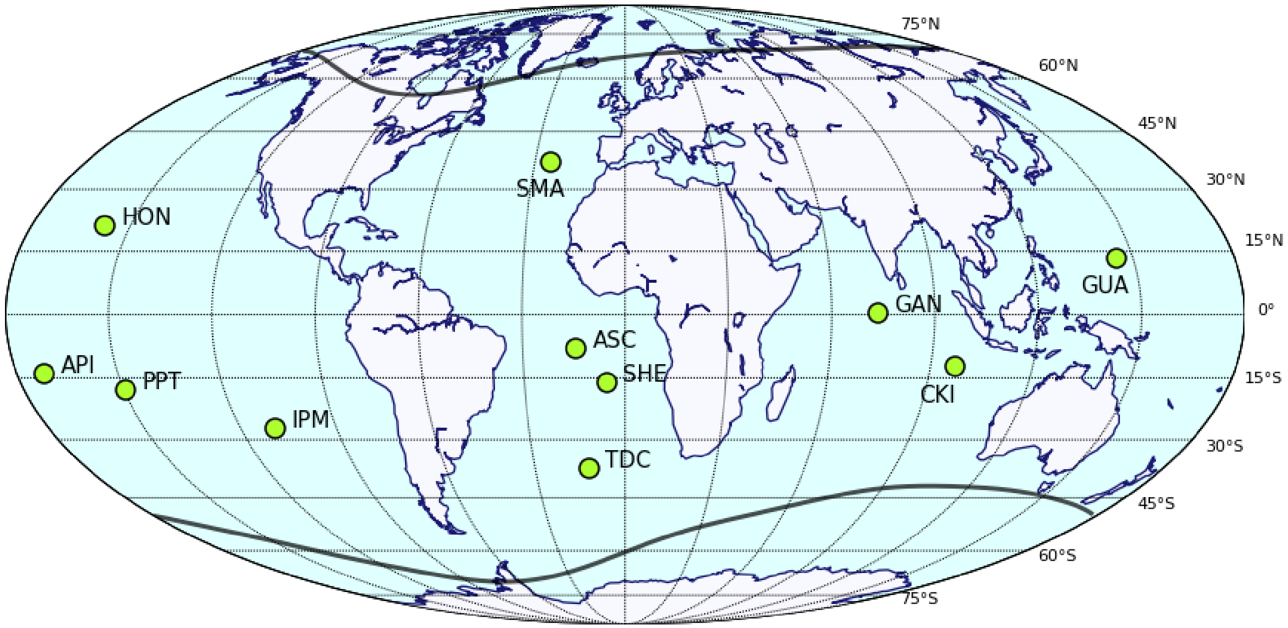

Obtaining local 1D models beneath each island using observatory data

… and satellite data: allow for improving global coverage and even more, e.g., use tidal signals to constrain conductivity below oceans

Observatories

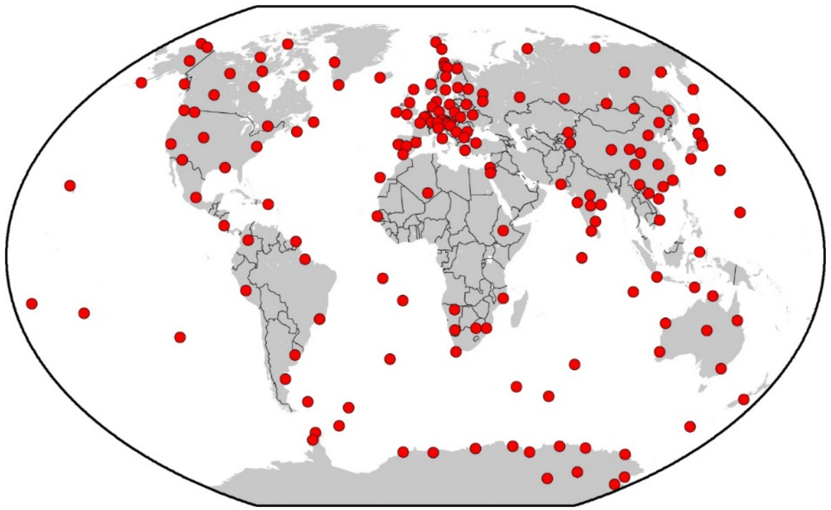

One day of satellite track

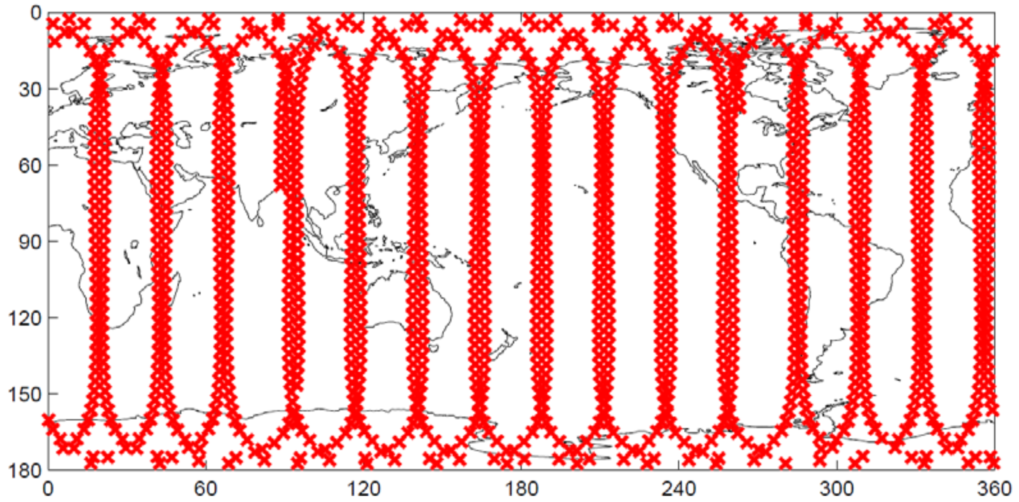

Transfer functions

Global 3D conductivity models were obtained using variations of magnetospheric origin only (ring current (RC) source)

- Periods: days – months (penetration depths ~ 500 – 1500 km)

- The source geometry is assumed to be very simple (first zonal harmonic) allowing ones to use standard local C-response concept*

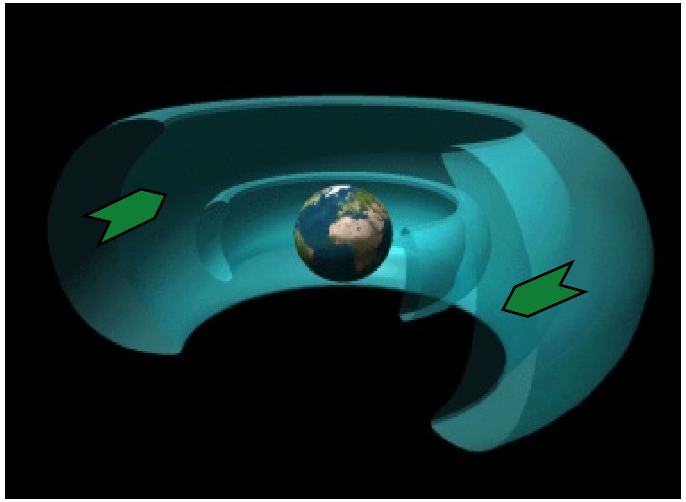

* Banks 1969

Local *C*-response estimation/inversion

Step 1. Take time series of radial and horizontal magnetic field components at a global net of (midlatitude) observatories

$$B_r(\bar{r}_j, t), \quad B_\vartheta(\bar{r}_j, t) \qquad j = 1, 2, \ldots, N$$

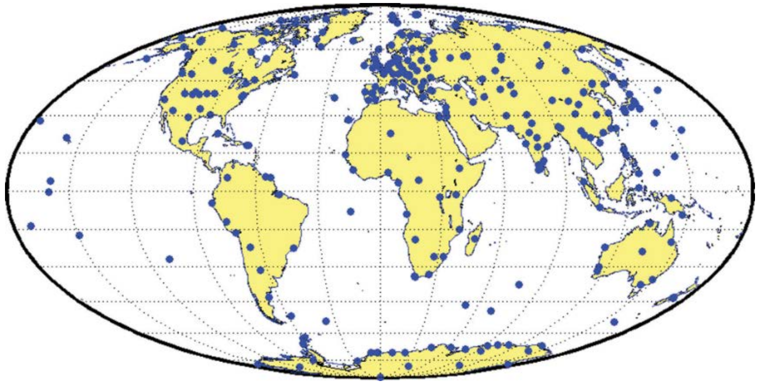

Step 2. Estimate local C-responses

$$C_1(\bar{r}_j, \omega) = -\frac{a}{2} \tan \vartheta_j \frac{B_r(\bar{r}_j, \omega)}{B_\vartheta(\bar{r}_j, \omega)}$$

FUR; Germany

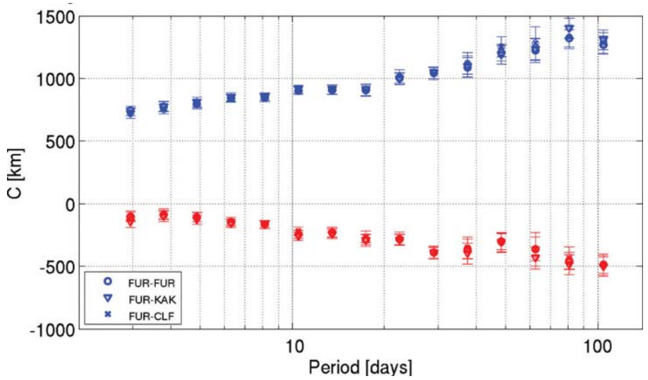

Step 3. Invert them in terms of conductivity

But in reality ring current source is spatially more complex (requiring more SH terms other than S_1^0

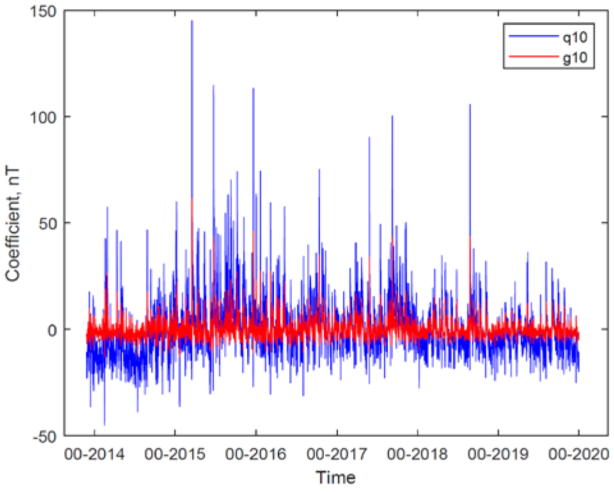

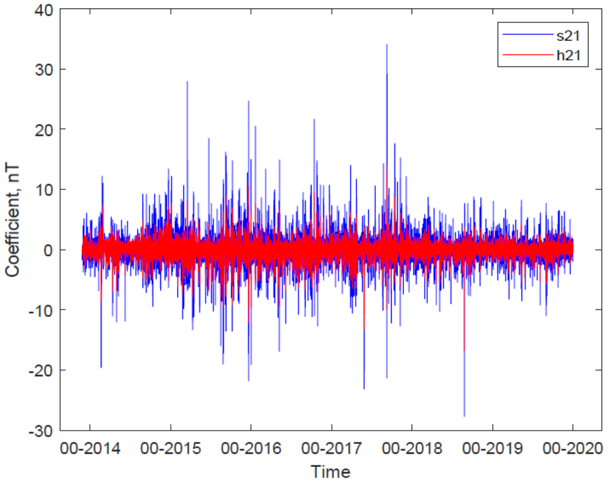

Local C-response concept fails to work

… and how to constrain conductivity at shallower depths (< 500 km)?

One needs considering variations at shorter periods (minutes – days)

Method	Source	Period band	Depth range (km)	Transfer function
Magnetotellurics (MT)	Plane wave (simple)	5 min – 3 hrs	~ 0 – 200	Tippers
Geomagnetic depth sounding (GDS)	Sq (ionospheric) current system (complex)	4 – 24 hrs	~ 100 – 500	?
	Magnetospheric ring current (RC; also complex)	2 – 180 days	~ 500 –1500	?

No attempts so far to jointly invert data from all three methods

- There were no adequate transfer functions to deal with complex (GDS) sources
- There were no adequate tools for a joint inversion (1D or 3D)

Method	Source	Period band	Depth range (km)	Transfer function
Magnetotellurics (MT)	Plane waves (simple)	5 min – 3 hrs	~ 0 – 200	Tippers

$$B_z = W_{zx} B_x + W_{zy} B_y$$

Tippers*

All quantities in this equation depend on location and frequency $(\overline{r}, \omega)$

* Morschhauser et al 2019 (*“quasi” 1D inversion of island tippers*)

ETH zürich

Method	Source	Period band	Depth range (km)	Transfer function
Geomagnetic depth sounding (GDS)	Sq current system (complex)	4 – 24 hrs	~100 – 500	*Sq G2L*
	Magnetospheric ring current (RC; also complex)	2 – 180 days	~ 500 – 1500	*RC G2L*

New global-to-local (G2L) transfer functions*

$$B_r(\overline{r},\omega) = \sum_{n,m} \varepsilon_n^m(\omega) T_n^m(\overline{r},\omega)$$

* Puethe et al 2015 (*concept*); Guzavina et al 2019 (*Sq G2L; 1D*); Munch et al 2020 (*RC G2L + Sq G2L; 1D*)

Method	Source	Period band	Depth range (km)	Transfer function
Magnetotellurics (MT)	Plane wave (simple)	5 min – 3 hrs	~ 0 – 200	Tippers
Geomagnetic depth sounding (GDS)	Sq (ionospheric) current system (complex)	4 – 24 hrs	~ 100 – 500	*Sq G2L*
	Magnetospheric ring current (RC; also complex)	2 – 180 days	~500 – 1500	*RC G2L*

NB: we are discussing (so far) ground-based data

Challenge: satellites move in space

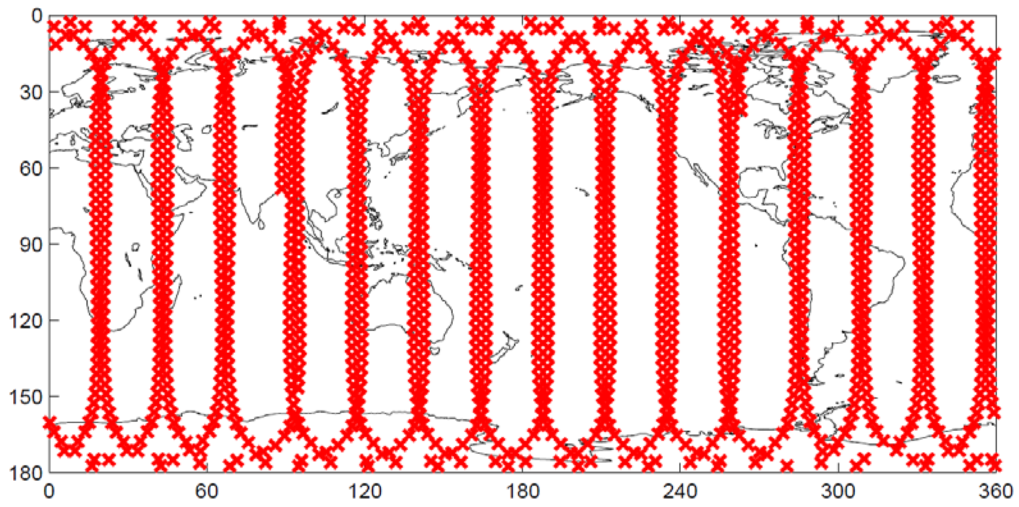

"Ground-based" transfer functions do not work

$$\cancel{B_z(\bar{r},\omega) = W_{zx}(\bar{r},\omega)B_x(\bar{r},\omega) + W_{zy}(\bar{r},\omega)B_y(\bar{r},\omega)}$$

$$\cancel{B_r(\bar{r},\omega) = \sum_{n,m} \varepsilon_n^m(\omega)T_n^m(\bar{r},\omega)}$$

$$\xcancel{B_z(\bar{r},\omega) = W_{zx}(\bar{r},\omega)B_x(\bar{r},\omega) + W_{zy}(\bar{r},\omega)B_y(\bar{r},\omega)}$$

$$\xcancel{B_r(\bar{r},\omega) = \sum_{n,m} \varepsilon_n^m(\omega) T_n^m(\bar{r},\omega)}$$

Alternative transfer functions (suitable for satellite data) are needed: Q-matrices*

$$\iota_k^l(\omega) = \sum_{n,m} Q_{ln}^{km}(\omega)\varepsilon_n^m(\omega)$$

$$V(r,\vartheta,\varphi,\omega) = a\sum_{n,m}\left[\varepsilon_n^m(\omega)\left(\frac{r}{a}\right)^n + \iota_n^m(\omega)\left(\frac{r}{a}\right)^{-(n+1)}\right]S_n^m(\vartheta,\varphi)$$

* Olsen 1999 (*concept*); Puethe and Kuvshinov 1914 (*tools for estimating and 3D inversion of Q-matrices*); Kuvshinov et al 2021 (*3D inversion of Swarm Q-matrices*)

Q-matrices

$$\iota_k^l(\omega) = \sum_{n,m} Q_{ln}^{km}(\omega)\varepsilon_n^m(\omega)$$

- Work with signals of magnetospheric origin only
- Provide global picture (but with *Swarm* data of only very low lateral resolution, continental scale)

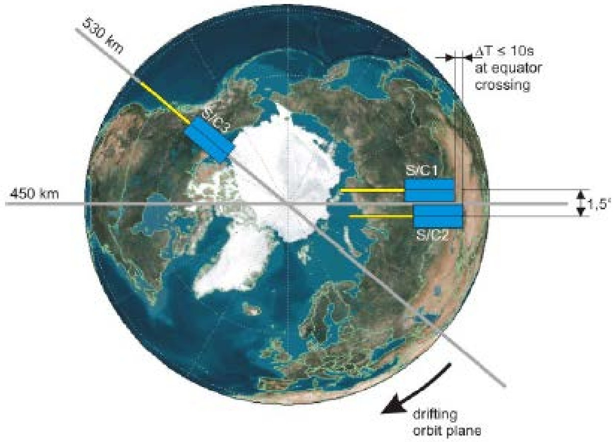

- Global (low resolution) 3D model from satellite data (500 – 1500 km)
- Regional 3D models from ground-based data (0 – 1500 km)
- Local oceanic 1D models from island data (0 – 1500 km)

⇩

Global multi-resolution 3-D model (0 – 1500 km)

Global Multi-Resolution 3-D Mantle Conductivity Model Based on Multi-Source, Multi-Data and Multi-Response Approach

esa eo

STSE Support To Science Element

SWARM DISC

Study logic

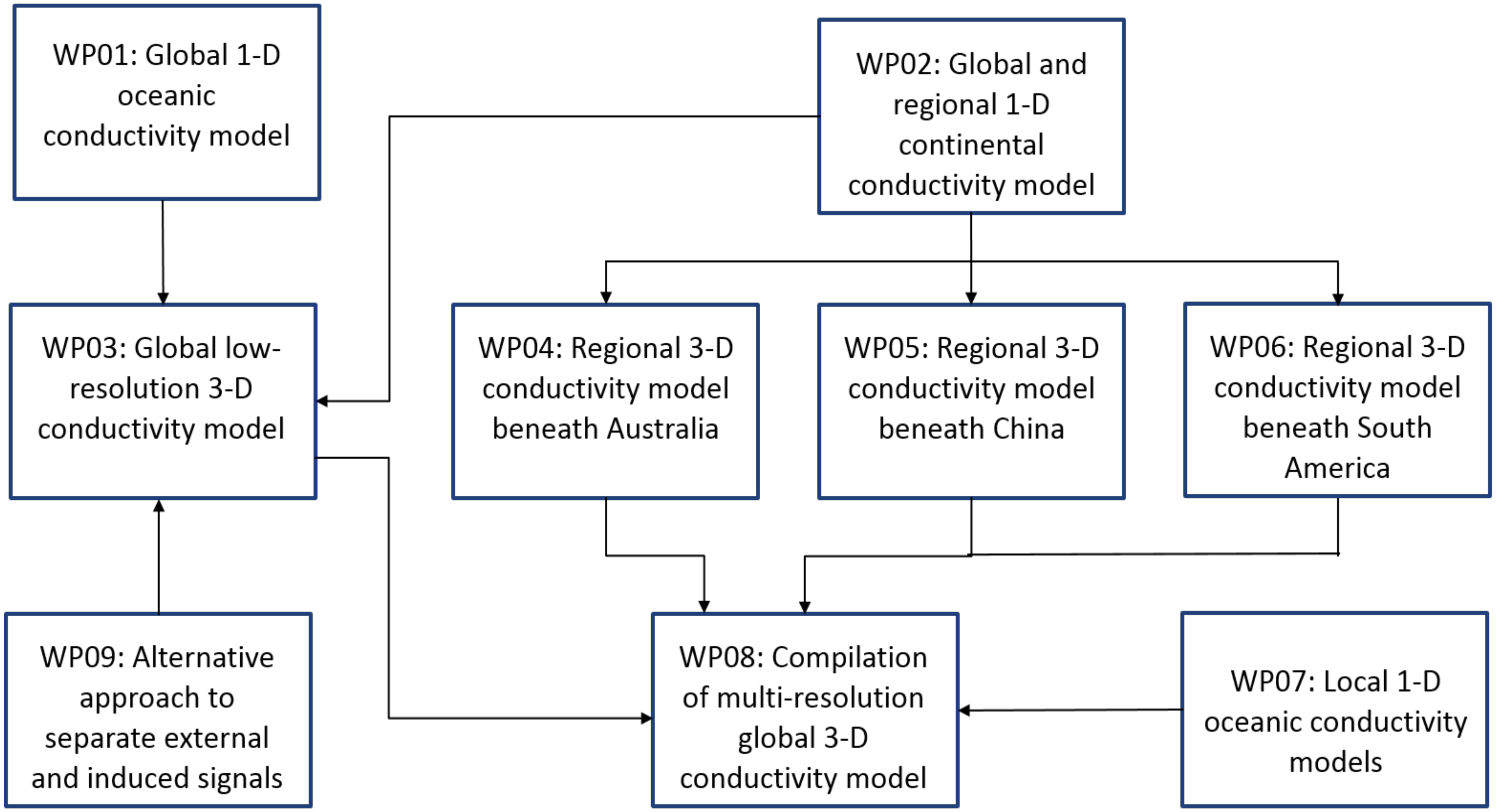
WP01: Global 1-D oceanic conductivity model
WP02: Global and regional 1-D continental conductivity model
WP03: Global low-resolution 3-D conductivity model
WP04: Regional 3-D conductivity model beneath Australia
WP05: Regional 3-D conductivity model beneath China
WP06: Regional 3-D conductivity model beneath South America
WP09: Alternative approach to separate external and induced signals
WP08: Compilation of multi-resolution global 3-D conductivity model
WP07: Local 1-D oceanic conductivity models

Project schedule

Months	07-09	10-12	01-03	04-06	07-09	10-12	01-03	04-06	07-09	10-12	01-03	04-06
Years	2020	2020	2021	2021	2021	2021	2022	2022	2022	2022	2023	2023
WP01				update every year								
WP02				update every year (if the activity will appear to be useful)								
WP03				update every year								
WP04												
WP05												
WP06												
WP07												
WP08												
WP09				update every year (if the activity will appear to be useful)								

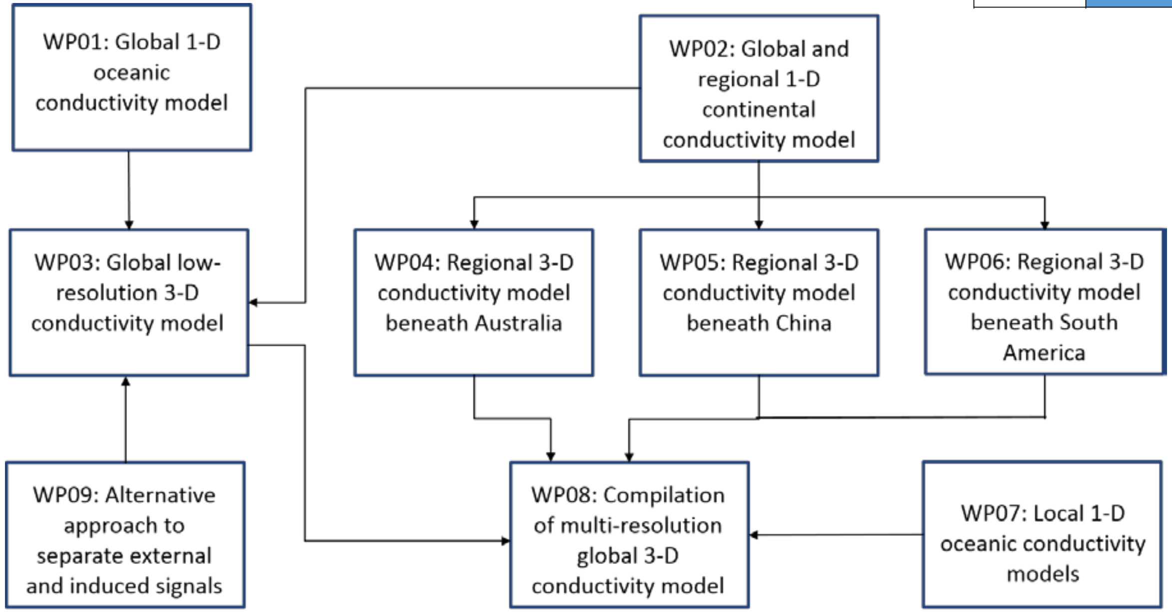

WP01: Global 1-D oceanic conductivity model (A. Grayver)

Months Years	07-09 2020	10-12 2020	01-03 2021	04-06 2021	07-09 2021	10-12 2021	01-03 2022	04-06 2022	07-09 2022	10-12 2022	01-03 2023	04-06 2023
WP01				update every year								
WP02				update every year (if the activity will appear to be useful)								
WP03				update every year								
WP04												
WP05												
WP06												
WP07												
WP08												
WP09				update every year (if the activity will appear to be useful)								

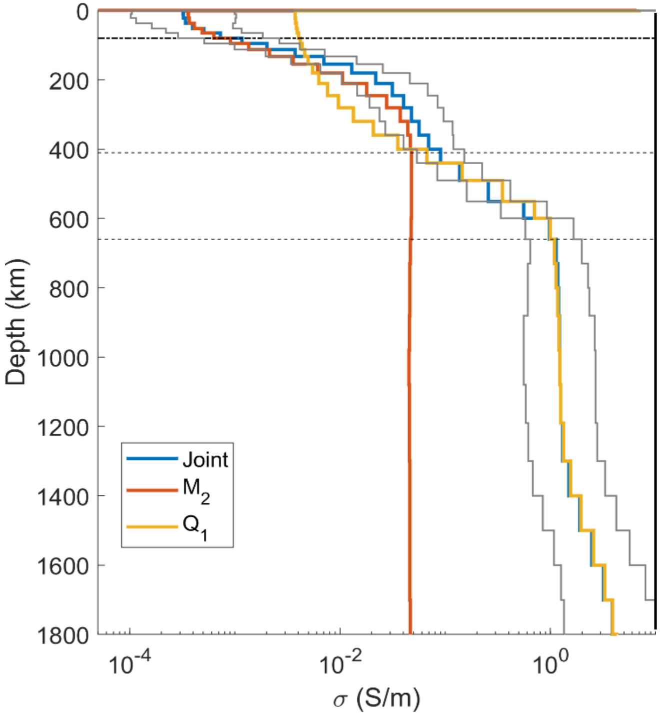

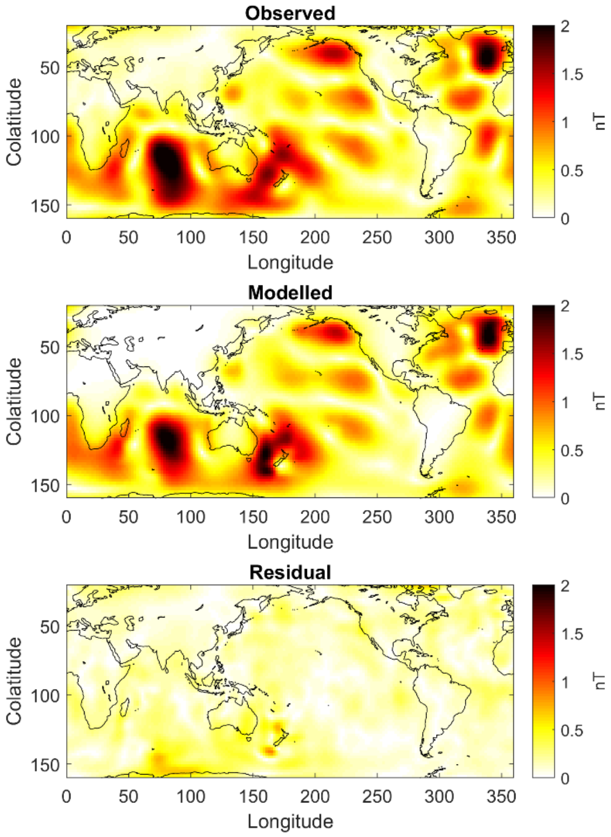

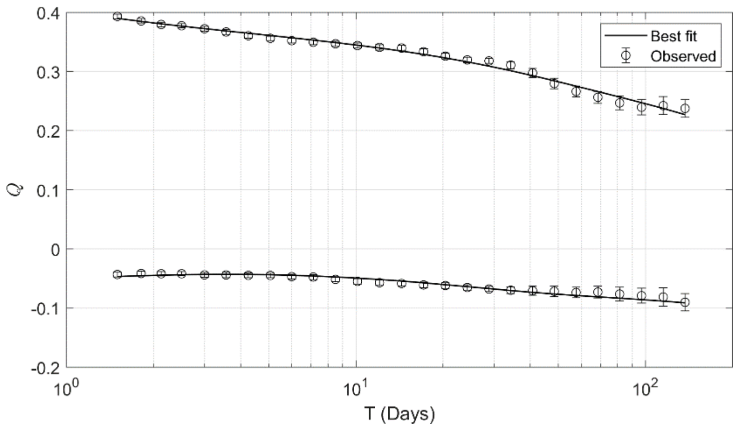

$$\iota_1^0(\omega) = Q_1^0(\omega)\varepsilon_1^0(\omega)$$

Input: satellite tidal signals (M2 Br) + satellite magnetospheric scalar Q-response

Kuvshinov, A., A. Grayver A., L. Toffner-Clausen, N. Olsen, 2021. Probing 3-D electrical conductivity of the mantle using 6 years of Swarm, CryoSat-2 and observatory magnetic data and exploiting matrix Q-responses approach, Earth, Planets Space, accepted.

WP02: Global and regional 1-D conductivity models (A. Grayver, R. Rigaud, A. Kuvshinov)

Months	07-09	10-12	01-03	04-06	07-09	10-12	01-03	04-06	07-09	10-12	01-03	04-06
Years	2020	2020	2021	2021	2021	2021	2022	2022	2022	2022	2023	2023
WP01				update every year								
WP02				update every year (if the activity will appear to be useful)								
WP03				update every year								
WP04												
WP05												
WP06												
WP07												
WP08												
WP09				update every year (if the activity will appear to be useful)								

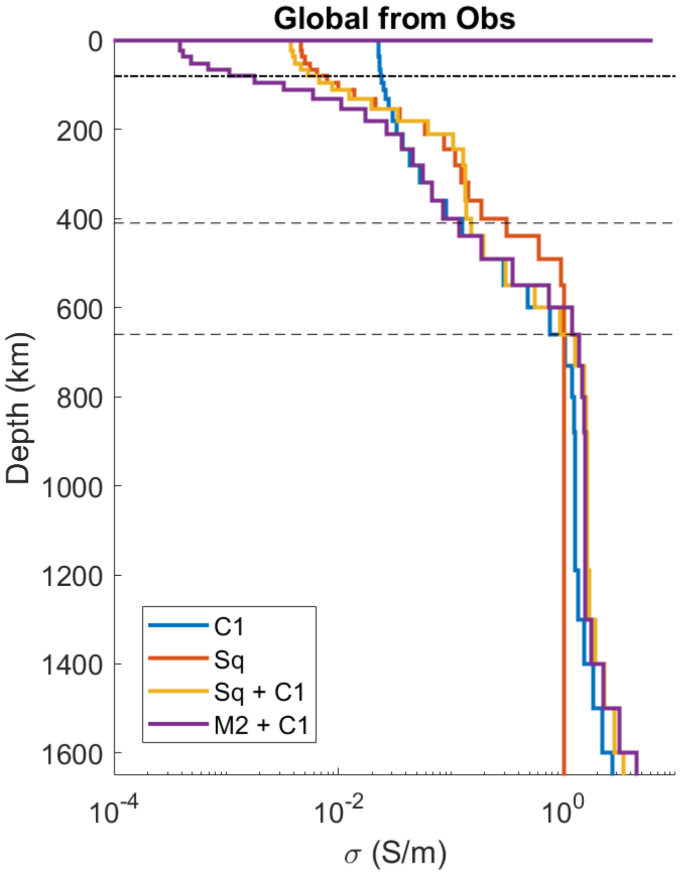

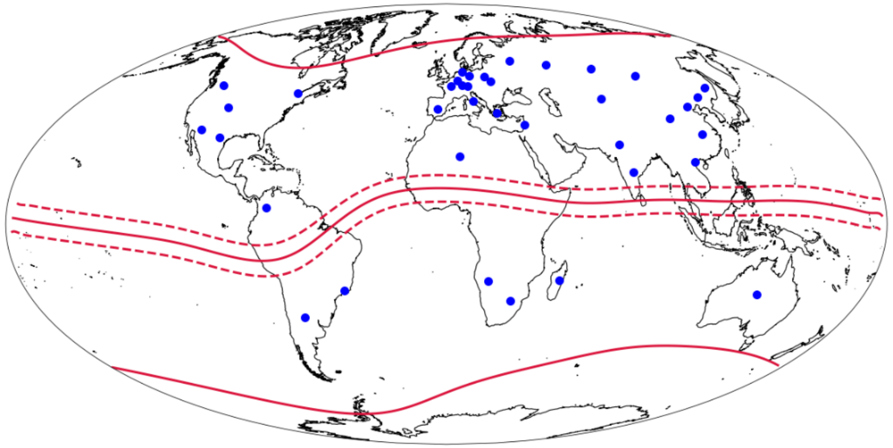

$$B_r(\bar{r},\omega) = \sum_{n,m} \varepsilon_n^m(\omega) T_n^m(\bar{r},\omega)$$

$$\iota_1^0(\omega) = Q_1^0(\omega)\varepsilon_1^0(\omega)$$

Input: inland observatory Sq G2L TFs + satellite magnetospheric scalar Q-response

ETH zürich

WP03: Global low resolution 3-D conductivity model (A. Kuvshinov)

Months	07-09	10-12	01-03	04-06	07-09	10-12	01-03	04-06	07-09	10-12	01-03	04-06
Years	2020	2020	2021	2021	2021	2021	2022	2022	2022	2022	2023	2023
WP01				update every year								
WP02				update every year (if the activity will appear to be useful)								
WP03				update every year								
WP04												
WP05												
WP06												
WP07												
WP08												
WP09				update every year (if the activity will appear to be useful)								

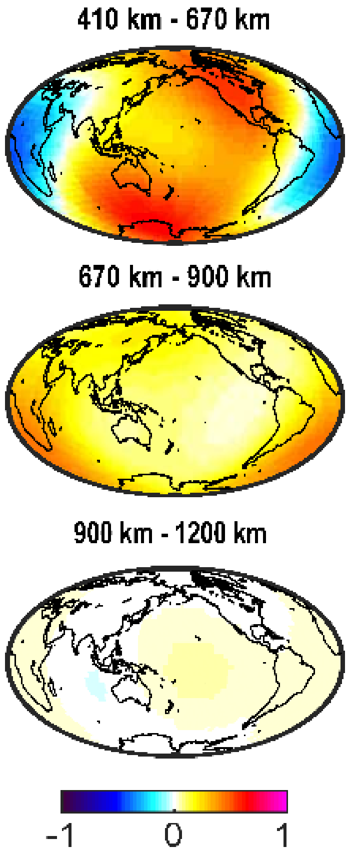

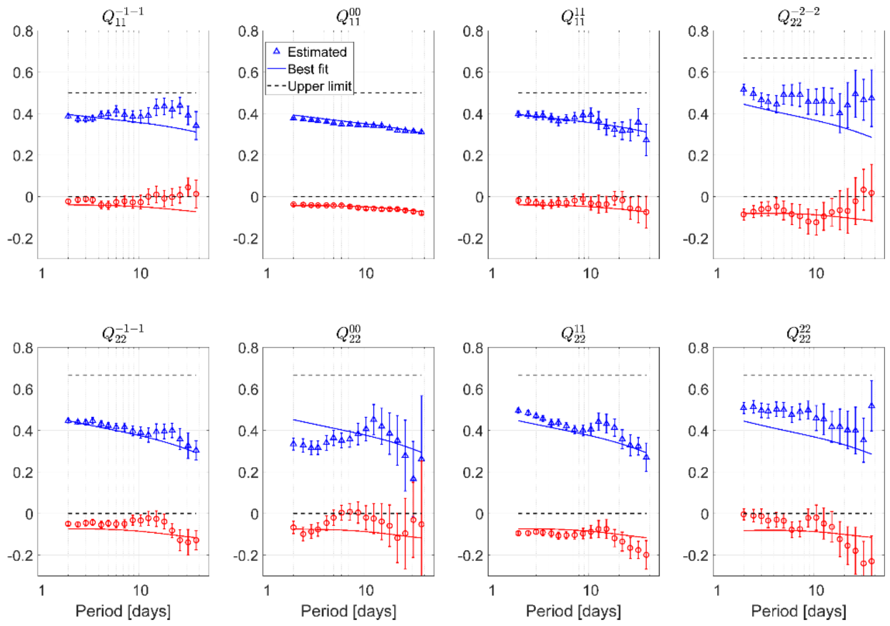

$$\iota_k^l(\omega) = \sum_{n,m} Q_{ln}^{km}(\omega)\varepsilon_n^m(\omega)$$

Input: satellite magnetospheric matrix Q-response

Kuvshinov, A., A. Grayver A., L. Toffner-Clausen, N. Olsen, 2021. Probing 3-D electrical conductivity of the mantle using 6 years of Swarm, CryoSat-2 and observatory magnetic data and exploiting matrix Q-responses approach, Earth, Planets Space, accepted.

WP04: Regional 3-D conductivity model beneath Australia (F. Cicchetti, R. Rigaud, A. Grayver, A. Kuvshinov)

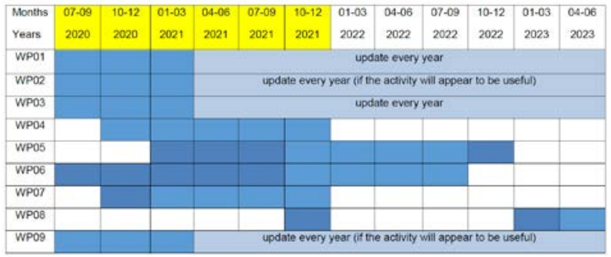

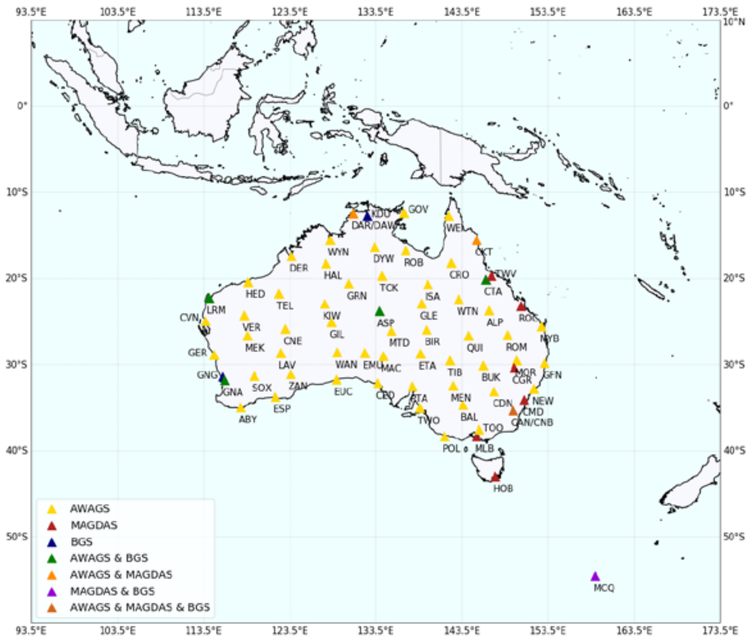

- Data calibrating
- Estimating tippers

$$B_z = W_{zx} B_x + W_{zy} B_y$$

- Developing 3-D tools to jointly invert different responses

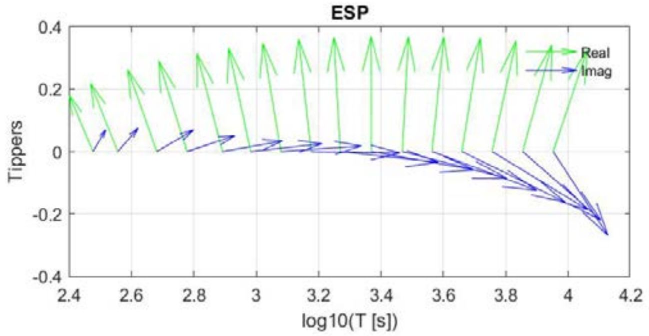

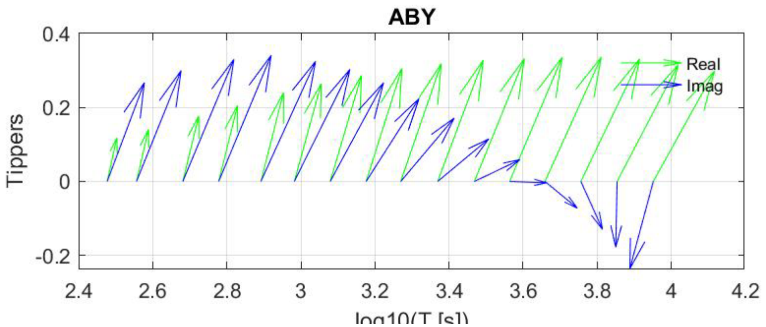

WP05: Regional 3-D conductivity model beneath China (S. Xu, R. Rigaud, A. Kuvshinov)

Months	07-09	10-12	01-03	04-06	07-09	10-12	01-03	04-06	07-09	10-12	01-03	04-06
Years	2020	2020	2021	2021	2021	2021	2022	2022	2022	2022	2023	2023
WP01				update every year								
WP02				update every year (if the activity will appear to be useful)								
WP03				update every year								
WP04												
WP05												
WP06												
WP07												
WP08												
WP09				update every year (if the activity will appear to be useful)								

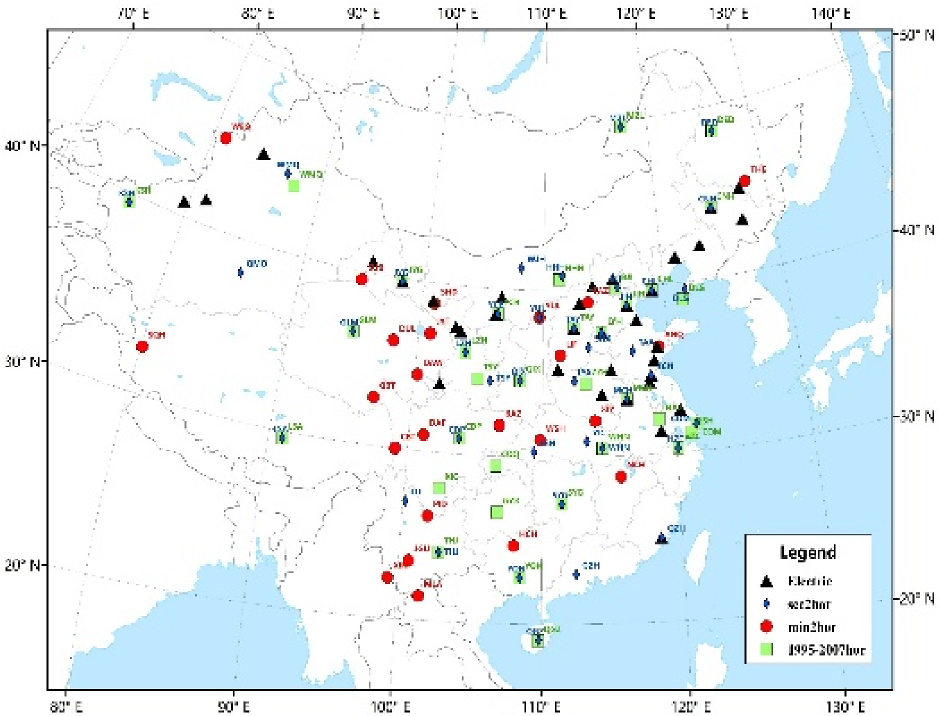

- Data calibrating

WP06: Regional 3-D conductivity model beneath South America (R. Rigaud, A. Grayver, A. Kuvshinov)

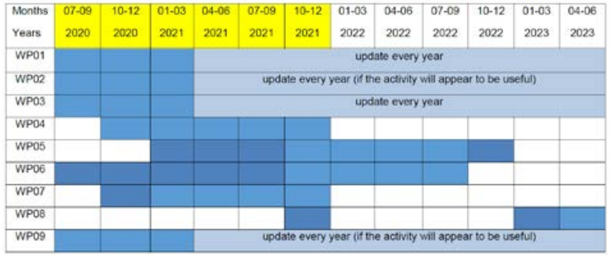

Months	07-09	10-12	01-03	04-06	07-09	10-12	01-03	04-06	07-09	10-12	01-03	04-06
Years	2020	2020	2021	2021	2021	2021	2022	2022	2022	2022	2023	2023
WP01				update every year								
WP02				update every year (if the activity will appear to be useful)								
WP03				update every year								
WP04												
WP05												
WP06												
WP07												
WP08												
WP09				update every year (if the activity will appear to be useful)								

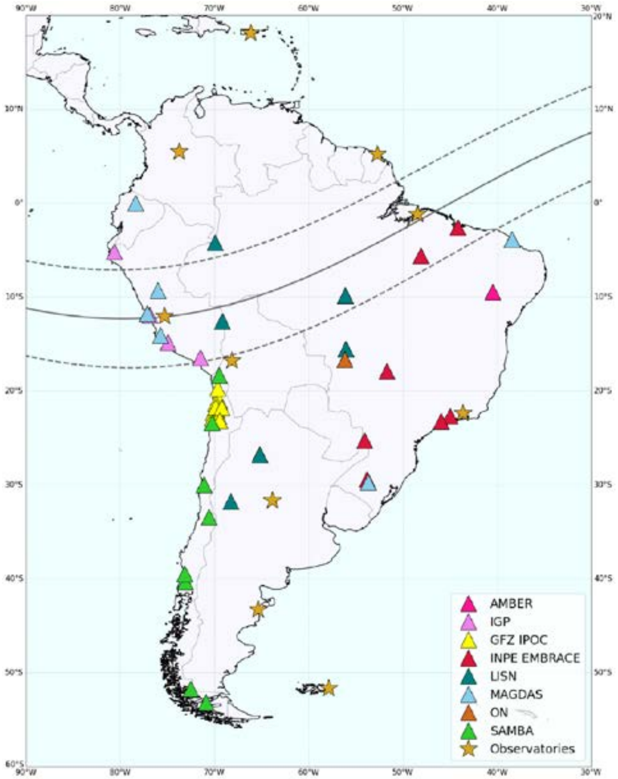

- Data calibrating
- Estimating tippers

Next talk by Rafael Rigaud: “Calibration of ground-based magnetic data for global electromagnetic Induction studies”

WP07: Local 1-D oceanic conductivity models
(C. Chen, R. Rigaud, M. Kruglyakov, A. Kuvshinov)

Months	07-09	10-12	01-03	04-06	07-09	10-12	01-03	04-06	07-09	10-12	01-03	04-06
Years	2020	2020	2021	2021	2021	2021	2022	2022	2022	2022	2023	2023
WP01				update every year								
WP02				update every year (if the activity will appear to be useful)								
WP03				update every year								
WP04												
WP05												
WP06												
WP07												
WP08												
WP09				update every year (if the activity will appear to be useful)								

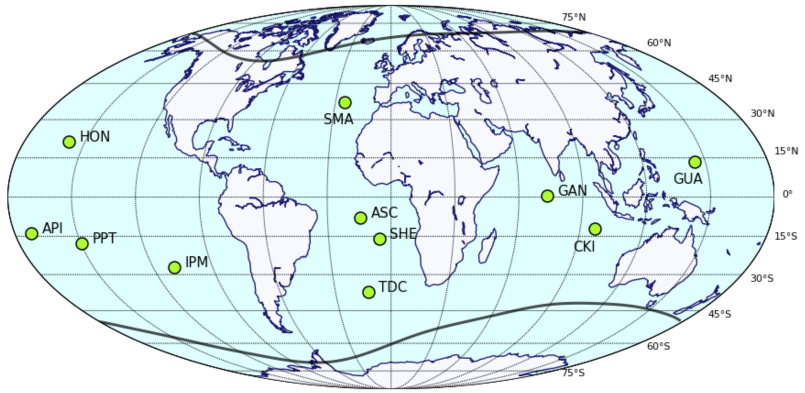

- Estimating tippers
- Estimating Sq and Dst G2L TFs
- Developing quasi 1-D tools to jointly invert different responses

WP08: Compilation of multi-resolution 3-D conductivity model (A. Kuvshinov)

Months	07-09	10-12	01-03	04-06	07-09	10-12	01-03	04-06	07-09	10-12	01-03	04-06
Years	2020	2020	2021	2021	2021	2021	2022	2022	2022	2022	2023	2023
WP01				update every year								
WP02				update every year (if the activity will appear to be useful)								
WP03				update every year								
WP04												
WP05												
WP06												
WP07												
WP08												
WP09				update every year (if the activity will appear to be useful)								

- Not started yet

WP09: Alternative approach to separate inducing and induced signals (A. Grayver, A. Kuvshinov)

Months	07-09	10-12	01-03	04-06	07-09	10-12	01-03	04-06	07-09	10-12	01-03	04-06
Years	2020	2020	2021	2021	2021	2021	2022	2022	2022	2022	2023	2023
WP01				update every year								
WP02				update every year (if the activity will appear to be useful)								
WP03				update every year								
WP04												
WP05												
WP06												
WP07												
WP08												
WP09				update every year (if the activity will appear to be useful)								

Third talk by Alexander Grayver: “One equation, two unknowns: towards reconstruction of source current and subsurface conductivity structures”

New papers

- Kuvshinov, A., A. Grayver A., L. Toffner-Clausen, N. Olsen, 2021. Probing 3-D electrical conductivity of the mantle using 6 years of Swarm, CryoSat-2 and observatory magnetic data and exploiting matrix Q-responses approach, Earth, Planets Space, accepted.

- Grayver A., A. Kuvshinov, D. Werthmuller, 2021. Time-domain modeling of three-dimensional Earth's and planetary electromagnetic induction effect in ground and satellite observations, J. Geophys. Res, accepted.

- Chen, C., M. Kruglyakov, A. Kuvshinov, 2021, Advanced three-dimensional electromagnetic modeling using a nested integral equation approach, Geophys. J. Int, accepted.

- Marshalko E., M. Kruglyakov, A. Kuvshinov, L. Juusola, N. Kwagala, E. Sokolova, V. Pilipenko, 2021. Comparing three approaches to the inducing source setting for the ground electromagnetic field modeling due to space weather events, Space Weather, accepted.

with the aknowledgement:

“ Author(s) (study) has been supported in the framework of Swarm DISC activities, funded by ESA contract no. 4000109587, with the support from EO Science for Society”

ETH zürich

Calibration of Ground-Based Magnetic Data For Global Electromagnetic Induction Studies

Rafael Rigaud

Project Meeting
10 Feb 2021

Constraining Electrical Conductivity From Ground-Based Transfer Functions - Methodology

- Compilation of all available data
  - Geomagnetic Observatories
  - Magnetometer Arrays (e.g. Space weather studies)

- Development of data calibration tool

- Estimation of experimental tippers, Sq and RC G2L TFs

- Forward and inverse 3-D modelling

Constraining Electrical Conductivity From Ground-Based Transfer Functions - Methodology

- **Compilation of all available data**
  - **Geomagnetic Observatories**
  - **Magnetometer Arrays (e.g. Space weather studies)**

- **Development of data calibration tool**

- Estimation of experimental tippers, Sq and RC G2L TFs

- Forward and inverse 3-D modelling

Compilation of South American Magnetometer Data

- African Meridian B-Field Education and Research (AMBER) and South American Meridional B-Field Array (SAMBA) - NSF / NASA / Boston College / UCLA

Code	Name	lat^{GG}	lon^{GG}	lat^{GM}	lon^{GM}	Measured Components	Units	Sampling Rate
PETR	Petrolina	−9.50	−40.50	−6.95	30.2	X, Y, Z	nT, Degree	Minute

Code	Name	lat^{GG}	lon^{GG}	lat^{GM}	lon^{GM}	Measured Components	Units	Sampling Rate
ANT	Antofagasta	−23.39	−70.24	−10.31	0.72	X, Y, Z	nT, Degree	Minute
CERR	Los Cerrillos	−33.45	−70.60	−19.80	0.75	X, Y, Z	nT, Degree	Minute
OSNO	Osorno	−40.34	−73.09	−26.39	359.73	X, Y, Z	nT, Degree	Minute
PAC	Puerto Arenas	−53.20	−70.90	−38.27	2.87	X, Y, Z	nT, Degree	Minute
PNT	Puerto Natales	−51.73	−72.51	−37.16	1.55	X, Y, Z	nT, Degree	Minute
PUT	Putre	−18.33	−69.50	−5.50	−1.44	X, Y, Z	nT, Degree	Minute
SER	La Serena	−30.00	−71.13	−16.55	0.17	X, Y, Z	nT, Degree	Minute
VLD	Valdivia	−39.48	−73.14	−25.58	−0.4	X, Y, Z	nT, Degree	Minute

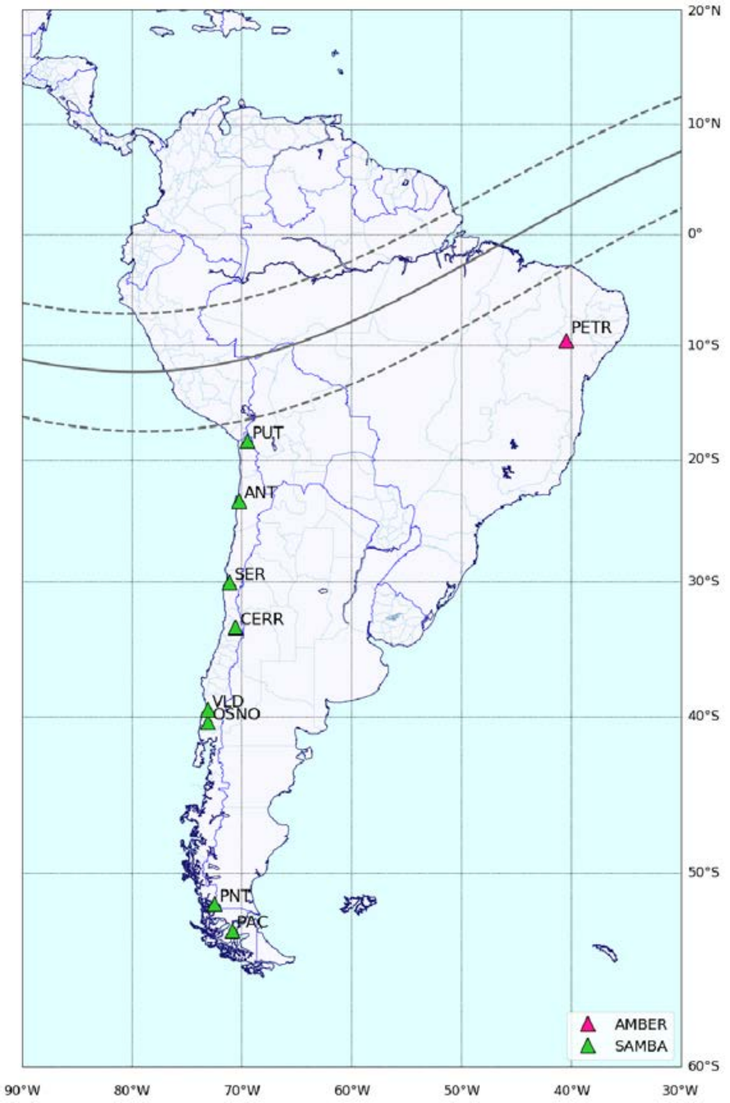

Compilation of South American Magnetometer Data

- Integrated Plate Boundary Observatory Chile (IPOC) Array - GFZ

Station	Latitude	Longitude	Elevation	Starting Date	E_x Length (m)	E_y Length (m)	Dipole Configuration
PB01	−21.04323	−69.48740	900	02.05.2007	80.3	81.4	L
PB02	−21.31973	−69.89603	1015	03.05.2007	80.9	84.8	T
PB03	−22.04847	−69.75310	1460	07.03.2007	80.4	71.5	L
PB04	−22.33369	−70.14918	1530	10.03.2007	100	101.3	L
PB05	−22.85283	−70.20235	1150	09.03.2007	80	81.3	T
PB06	−22.70580	−69.57188	1440	08.03.2007	79.3	80.8	L
PB07	−21.72667	−69.88618	1560	06.03.2007	81.3	80.5	L
PB09	−21.79638	−69.24192	1530	22.04.2010	80.8	80	L
PB11	−19.76096	−69.65582	1410	08.10.2014	99.3	99.7	L
PB15	−23.20833	−69.47092	1830	04.08.2011	80.8	80.7	cross
A01	−20, 7636	−69, 8887	980	06.10.2014	100.3	99.8	L

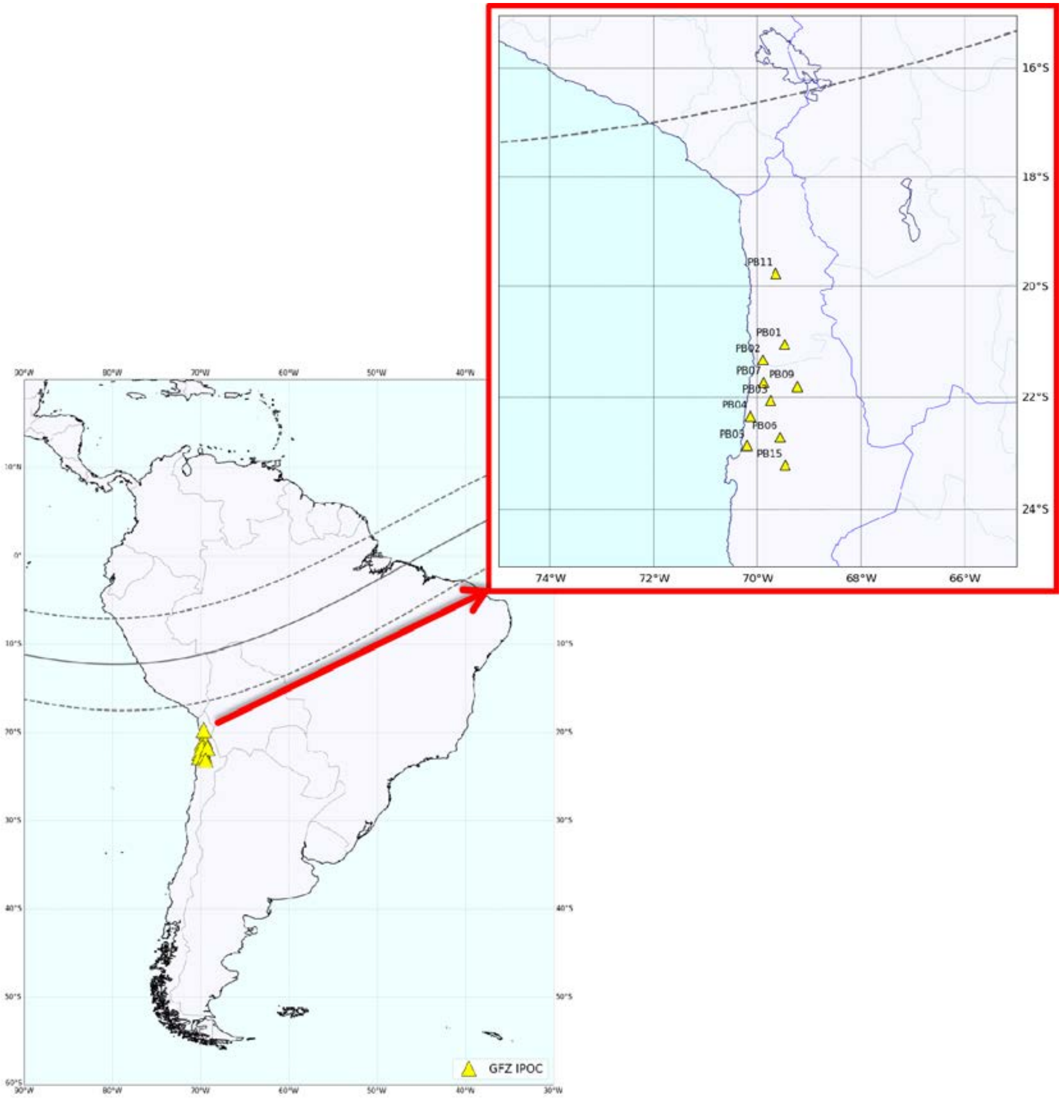

Compilation of South American Magnetometer Data

- Low-Latitude Ionospheric Sensor (LISN) - NSF / NASA / Instituto Geofisico del Perú (IGP)

Code	Name	lat^{GG}	lon^{GG}	lat^{GM}	lon^{GM}	Measured Components	Units	Sampling Rate
ALF	Alta Floresta	−9.87	−56.10	−0.78	16.33	H, D, Z	nT, Degrees	Minute
CBA	Cuiaba	−15.56	−56.07	−6.43	16.10	H, D, Z	nT, Degrees	Minute
LEO	El Leoncito	−31.80	−69.29	−22.23	3.12	H, D, Z	nT, Degrees	Minute
LET	Leticia	−4.19	−69.94	5.24	2.74	H, D, Z	nT, Degrees	Minute
PMO	Puerto Maldonato	−12.59	−69.19	−3.12	3.41	H, D, Z	nT, Degrees	Minute
TUC	Tucumán	−26.81	−65.18	−17.32	7.02	H, D, Z	nT, Degrees	Minute

Code	Name	lat^{GG}	lon^{GG}	lat^{GM}	lon^{GM}	Measured Components	Units	Sampling Rate
ANC	Ancon	−11.78	−77.15	−2.11	−4.43	H, D, Z	nT, Degrees	Minute
ARE	Arequipa	−16.47	−71.49	−6.96	1.15	H, D, Z	nT, Degrees	Minute
DJP	Delta-Jicamarca Piura	−11.95	−76.88	−2.49	−4.11	H, D, Z	nT, Degrees	Minute
JIC	Jicamarca	−11.95	−76.88	−2.49	−4.11	H, D, Z	nT, Degrees	Minute
NAZ	Nazca	−14.83	−74.92	−5.33	−2.18	H, D, Z	nT, Degrees	Minute
PIU	Piura	−5.17	−80.64	4.18	7.95	H, D, Z	nT, Degrees	Minute

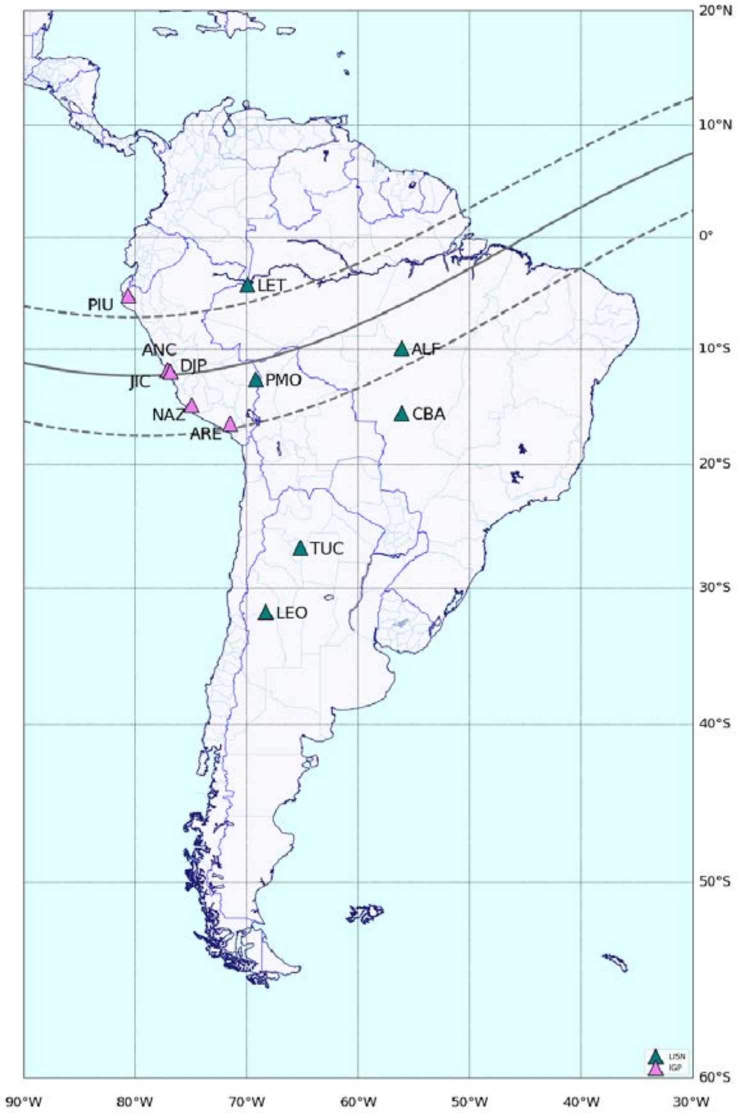

Compilation of South American Magnetometer Data

- Estudo e Monitoramento BRAsileiro de Clima Espacial (EMBRACE) Magnetic Network (Embrace MagNet) - INPE

Code	Name	lat^{GG}	lon^{GG}	lat^{GM}	lon^{GM}	Measured Components	Units	Sampling Rate
ALF	Alta Floresta	−9.87	−56.10	−0.78	16.33	H, D, Z	nT, Degrees	Minute
ARA	Araguatins	−5.60	−48.10	3.00	24.49	H, D, Z	nT, Degrees	Minute
CBA	Cuiaba	−15.56	−56.07	−6.43	16.10	H, D, Z	nT, Degrees	Minute
CXP	Cachoeira Paulista	−22.70	−45.00	−14.17	26.26	H, D, Z	nT, Degrees	Minute
EUS	Eusebio	−3.88	−38.43	4.14	34.21	H, D, Z	nT, Degrees	Minute
JAT	Jatai	−17.92	−51.71	−9.00	20.18	H, D, Z	nT, Degrees	Minute
MED	Medianeira	−25.29	−54.09	−16.19	17.49	H, D, Z	nT, Degrees	Minute
RGA	Rio Grande	−53.79	−67.75	−44.23	4.08	H, D, Z	nT, Degrees	Minute
SJC	São José dos Campos	−23.21	−45.95	−14.61	25.32	H, D, Z	nT, Degrees	Minute
SLZ	São Luis	−2.59	−44.20	5.70	28.60	H, D, Z	nT, Degrees	Minute
SMS	São Martinho da Serra	−29.44	−53.82	20.33	17.50	H, D, Z	nT, Degrees	Minute
TUC	Tucumán	−26.81	−65.18	−17.32	7.02	H, D, Z	nT, Degrees	Minute

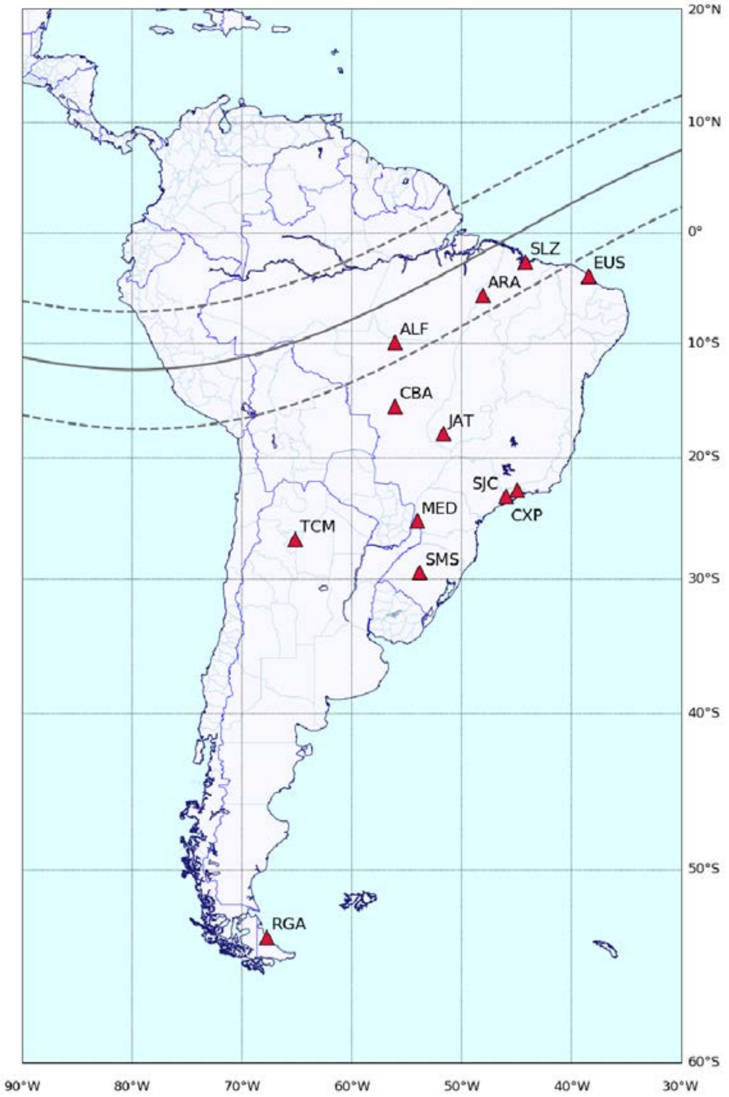

Compilation of South American Magnetometer Data

- Temporary magnetic stations maintained by Observatório Nacional (ON)

Code	Name	lat^{GG}	lon^{GG}	lat^{GM}	lon^{GM}	Measured Components	Units	Sampling Rate
MAA	Macapá	0.01	−51.05	9.07	21.85	H, D, Z, F	nT, Degree	Minute
PNL	Pantanal	−16.68	−56.18	−7.54	15.94	X, Y, Z, F	nT, Degree	Minute
TEF	Tefé	−3.33	−64.70	6.33	7.95	–	–	–

Compilation of South American Magnetometer Data

- Magnetic Data Acquisition System (MAGDAS) - Kyushu University

Code	Name	lat^{GG}	lon^{GG}	lat^{GM}	lon^{GM}	Measured Components	Units	Sampling Rate
ANC	Ancon	−11.78	−77.15	−2.11	−4.43	HN, HE, Z	nT	Second
EUS	Eusebio	−3.88	−38.43	4.14	34.21	HN, HE, Z	nT	Second
ICA	Ica	−14.09	−75.74	−4.42	−3.03	HN, HE, Z	nT	Second
JRS	Jerusalem	0.00	−78.36	9.82	−5.77	HN, HE, Z	nT	Second
SMA	Santa Maria	−29.72	−53.72	−19.30	13.24	HN, HE, Z	nT	Second
TMA	Tingo Maria	−9.31	−76.00	0.36	−3.33	HN, HE, Z	nT	Second
TPT	Tarapoto	−6.50	−76.36	3.17	−3.72	HN, HE, Z	nT	Second

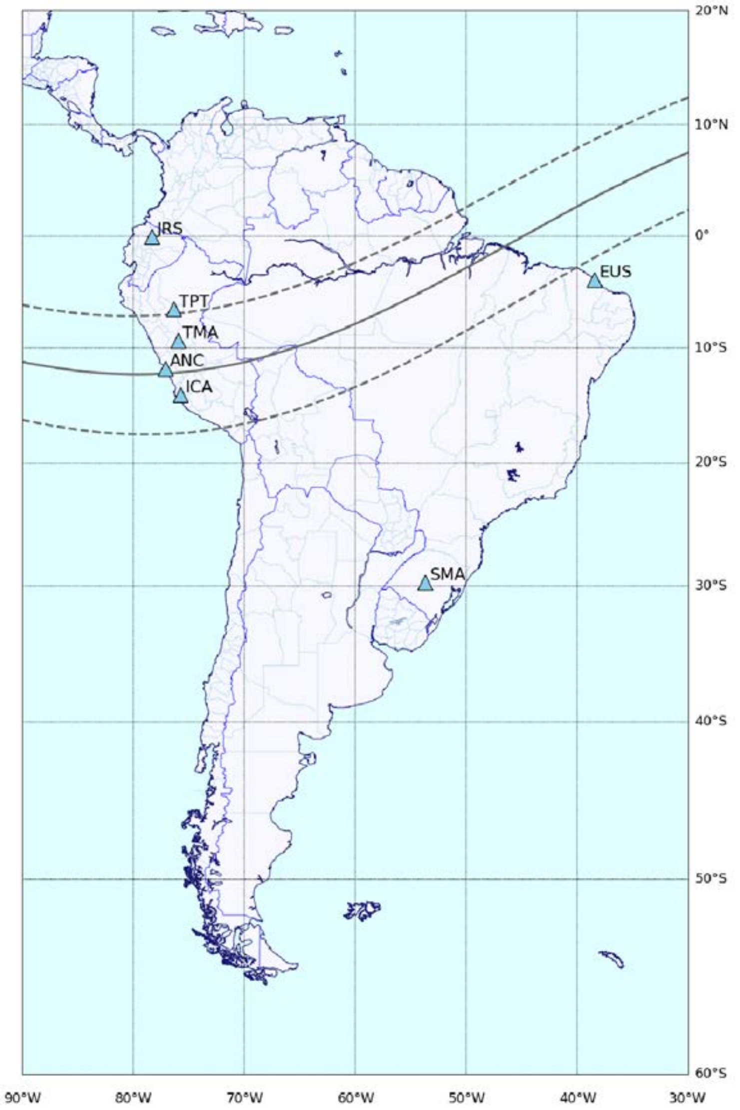

Compilation of South American Magnetometer Data

- Magnetic Observatories (BGS Swarm Database* / INTERMAGNET)

Code	Name	lat^{GG}	lon^{GG}	lat^{GM}	lon^{GM}	Measured Components	Units	Sampling Rate
FUQ	Fuquene	5.43	286.27	15.06	358.86	X, Y, Z, F	nT, Degree	Hour (Definite)
HUA	Huancayo	−12.05	−75.33	−2.57	−2.60	X, Y, Z, F	nT, Degree	Minute (Definite)
KOU	Kourou	5.21	−52.73	14.22	20.48	X, Y, Z, F	nT, Degree	Minute (Definite)
PIL	Pilar	−31.67	−63.88	21.97	8.04	X, Y, Z, F	nT, Degree	Minute (Definite)
PST	Port Stanley	-51.51	302.10	-42.15	12.32	X, Y, Z, F	nT, Degree	Minute (Definite)
SJG	San Juan	18.00	293.85	27.57	6.95	X, Y, Z, F	nT, Degree	Minute (Definite)
TRW	Trelew	−43.27	−65.38	−33.51	6.35	X, Y, Z, F	nT, Degree	Minute (Definite)
TTB	Tatuoca	1.20	−48.51	9.77	24.54	X, Y, Z, F	nT, Degree	Minute (Definite)
VRE	Vila Remedios	-16.77	291.83	-7.03	4.35	X, Y, Z, F	nT, Degree	Hour (Definite)
VSS	Vassouras	−22.40	−43.65	−13.78	27.49	X, Y, Z, F	nT, Degree	Minute (Definite)

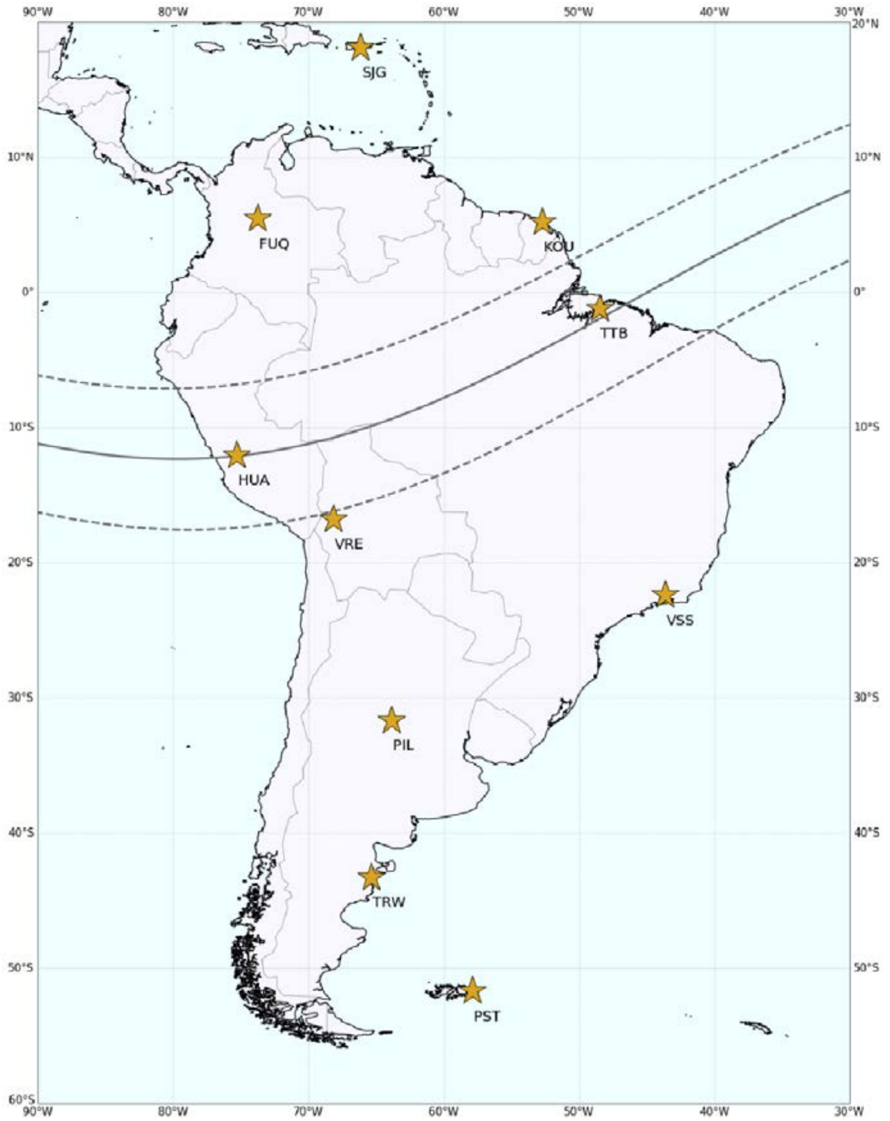

* MacMillan and Olsen (2013)

Constraining Electrical Conductivity Beneath South America

- The use of magnetometer arrays data presents significant challenges in comparison with standard magnetic observatory data

- This prompted the development of a data calibration tool to prepare this data for estimation of EM transfer functions (in collaboration with Dr. Jürgen Matzka, GFZ-Potsdam)

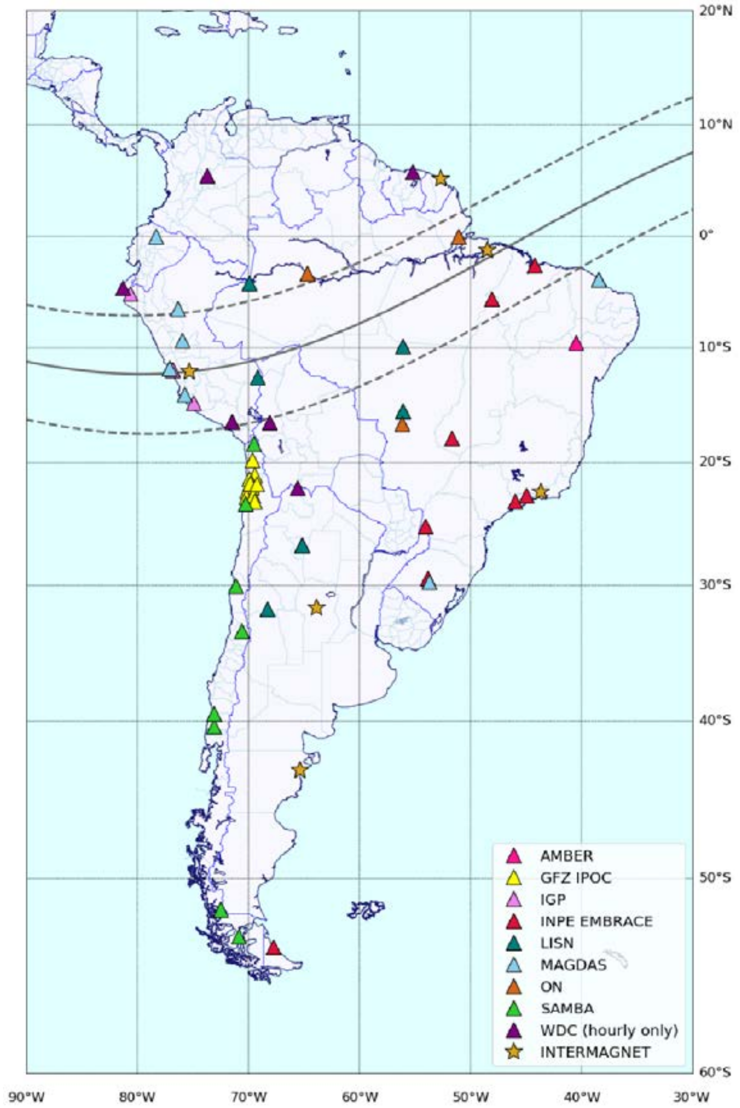

Measuring the Geomagnetic Field: Fundamentals

- Variometer and absolute instruments are used in geomagnetic observatories

- Variometer measurements: Measure the field variations along a sensor-oriented axis

- Most used variometer: FGE Fluxgate Magnetometer (DTU - Denmark)

Measuring the Geomagnetic Field: Fundamentals

- Absolute instruments measure the field strength (F) (with scalar magnetometers) and the direction of the field (with fluxgate teodolites)

- Absolute measurements are used to determine baselines and to calibrate variometer data

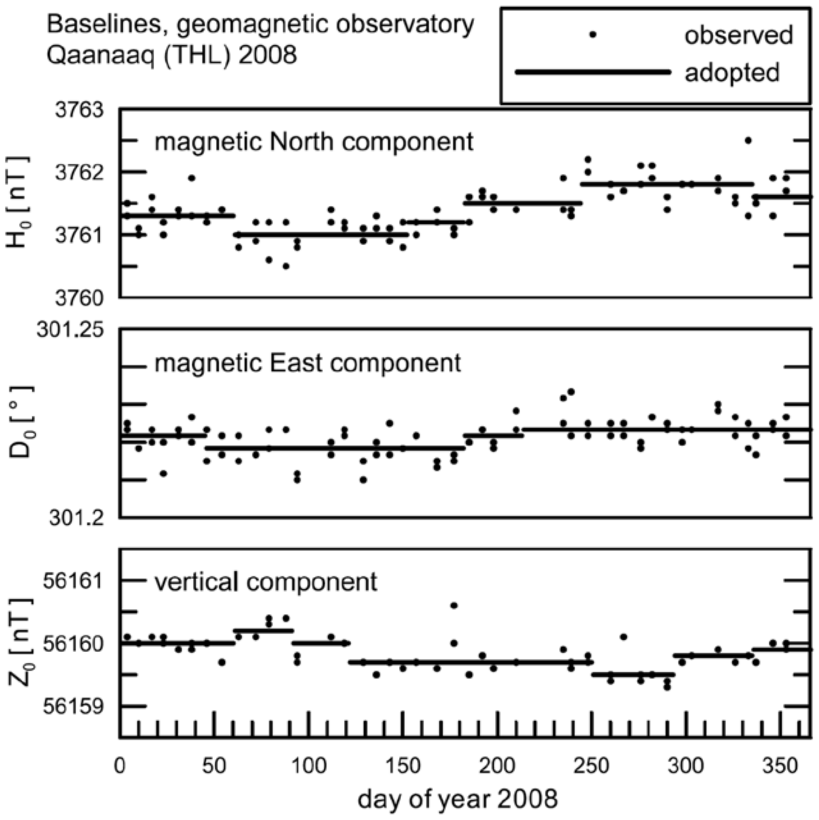

Matzka et al (2010)

FGE Fluxgate Magnetometer

- The fluxgate magnetometer has two horizontal sensors and one vertical sensor. The horizontal sensors can be rotated around the vertical axis and the field is measured along each sensor direction. Most used orientations:
  - H-D-Z: Horizontal sensors oriented towards magnetic north and east;
  - X-Y-Z: Horizontal sensors oriented towards geographic north and east

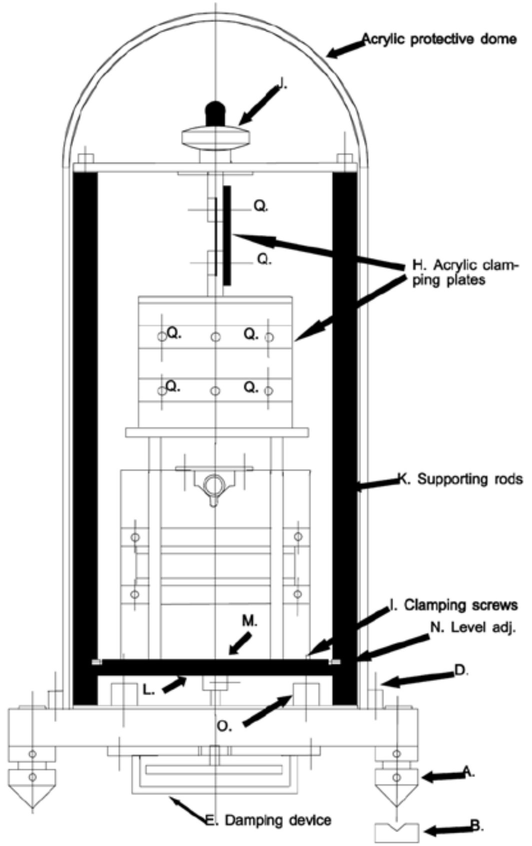

FGE Fluxgate Magnetometer

- The fluxgate magnetometer has two horizontal sensors and one vertical sensor. The horizontal sensors can be rotated around the vertical axis and the field is measured along each sensor direction. Most used orientations:
  - **H-D-Z: Horizontal sensors oriented towards magnetic north and east;**
  - X-Y-Z: Horizontal sensors oriented towards geographic north and east

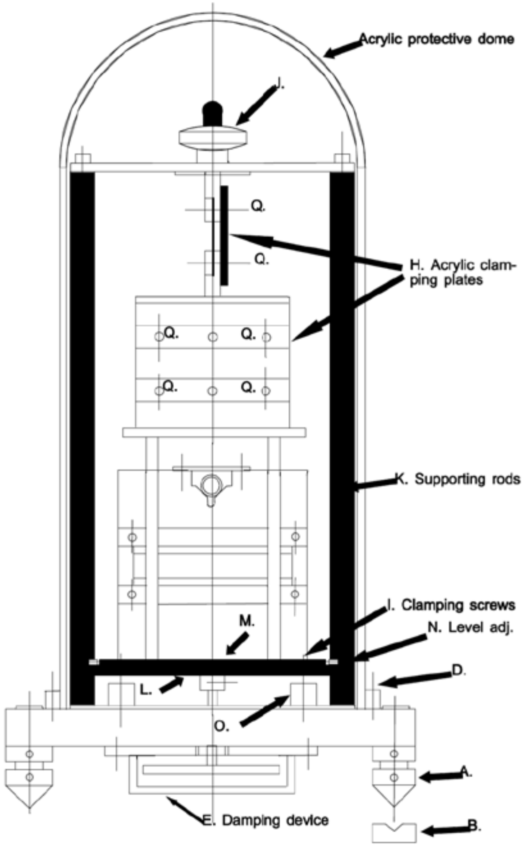

Why Calibrate?

- Magnetometer arrays tipically use variometer instruments only
- If data is provided with baselines, most often there is no information available on how they were determined and how data was calibrated
- Data is generally of poorer quality in comparison with observatory data

Station: JIC (Jicamarca), Year: 2010, lat = -11.95o, lon = -76.88o

Why Calibrate?

- Magnetometer data are often provided as uncalibrated data in a local magnetic coordinates reference frame even though they are reported as geomagnetic field components

ICA (Ica) Station, year: 2014, lat = -14.09º, lon = -75.74º

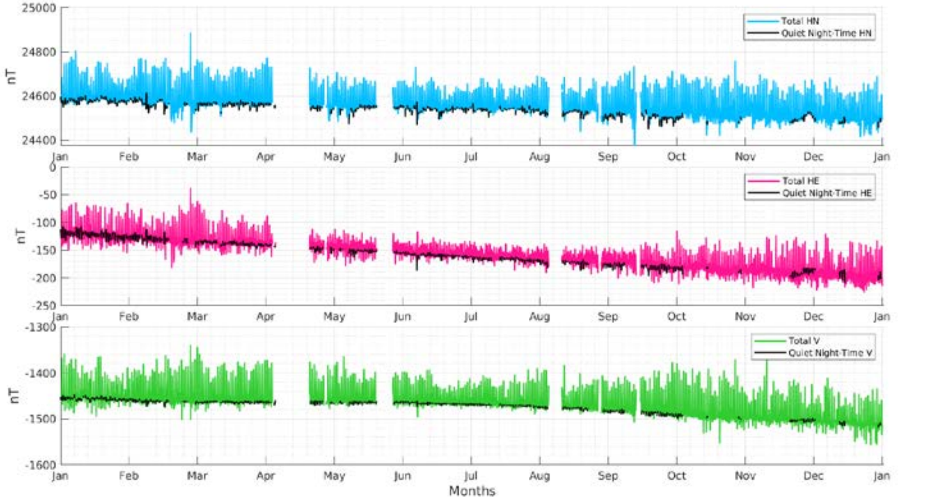

Huancayo (HUA) Magnetic Observatory, year: 2014, lat = -12.05º, lon = -75.33º

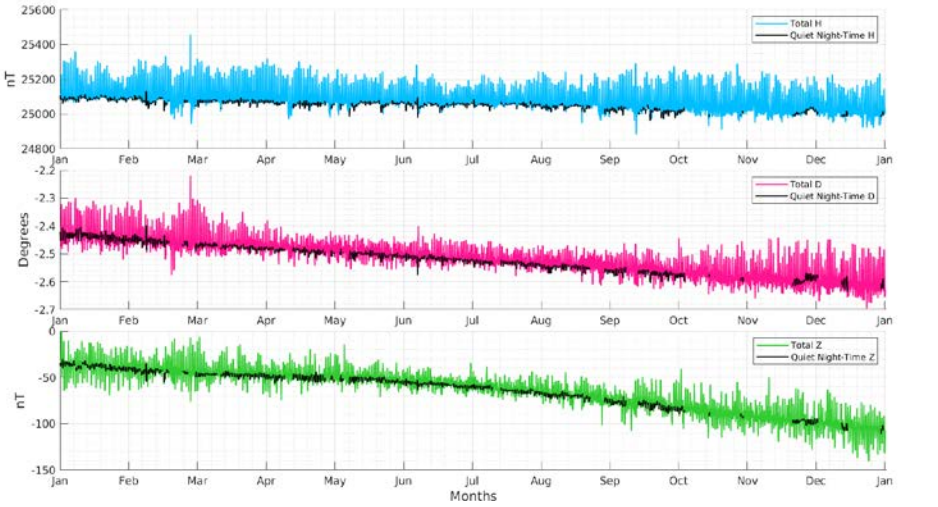

Why Calibrate?

- Magnetometer data are often provided as uncalibrated data in a local magnetic coordinates reference frame even though they are reported as geomagnetic field components

ICA (Ica) Station data file for 01.02.2014

```
 Format                   IAGA-2002
 Source of Data           Kyushu University (KU)
 Station Name             Ica
 IAGA CODE                ICA (KU code)
 Geodetic Latitude        -14.090
 Geodetic Longitude       284.260
 Elevation                8888.88
 Reported                  HDZ
 Sensor Orientation       HDZF
 Digital Sampling         1 second
 Data Interval Type       1-second
 Data Type                Provisional
DATE TIME DOY ICAH ICAD ICAZ ICAF
2014-02-01 00:00:00.000 032  24590.91   -126.63  -1455.88   99999.99
2014-02-01 00:00:01.000 032  24590.92   -126.59  -1455.88   99999.99
2014-02-01 00:00:02.000 032  24590.92   -126.58  -1455.89   99999.99
2014-02-01 00:00:03.000 032  24590.90   -126.56  -1455.88   99999.99
2014-02-01 00:00:04.000 032  24590.85   -126.60  -1455.88   99999.99
2014-02-01 00:00:05.000 032  24590.79   -126.67  -1455.88   99999.99
2014-02-01 00:00:06.000 032  24590.77   -126.74  -1455.88   99999.99
2014-02-01 00:00:07.000 032  24590.77   -126.81  -1455.88   99999.99
2014-02-01 00:00:08.000 032  24590.79   -126.83  -1455.89   99999.99
2014-02-01 00:00:09.000 032  24590.82   -126.82  -1455.89   99999.99
```

ICA (Ica) Station, year: 2014, lat = -14.09º, lon = -75.74º

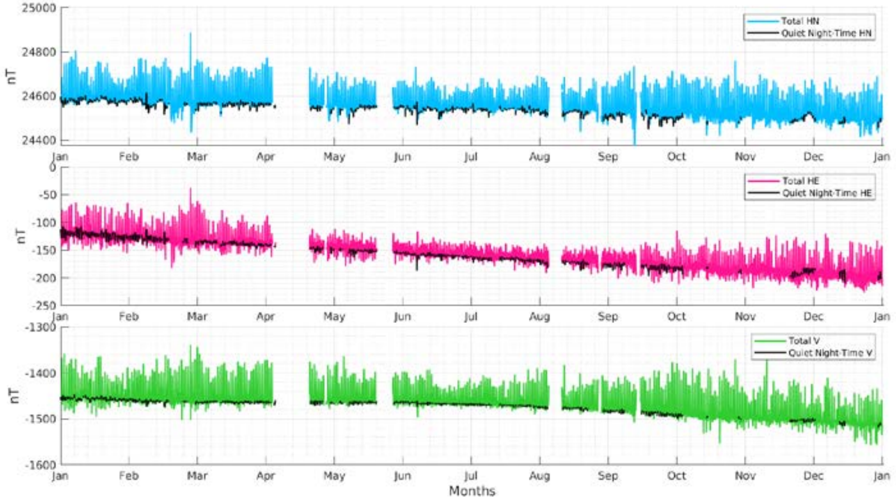

Huancayo (HUA) Magnetic Observatory, year: 2014, lat = -12.05º, lon = -75.33º

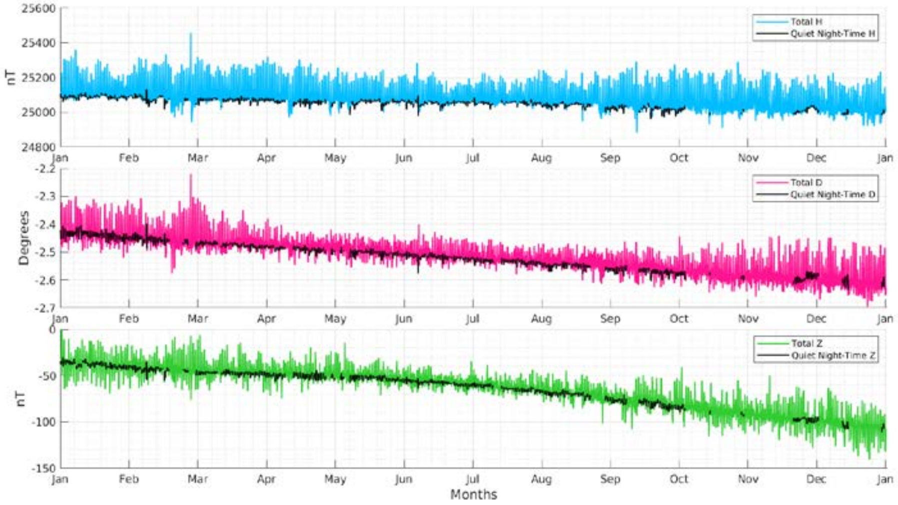

Geomagnetic Data Calibration – Non-Linear Formulas

- We introduce a local magnetic coordinate frame* as
    - B = *(N, E, V)*
- where *N, E,* and *V* are axis approximately aligned towards the Geomagnetic North, East and vertically down and aligned with the corresponding sensors axis

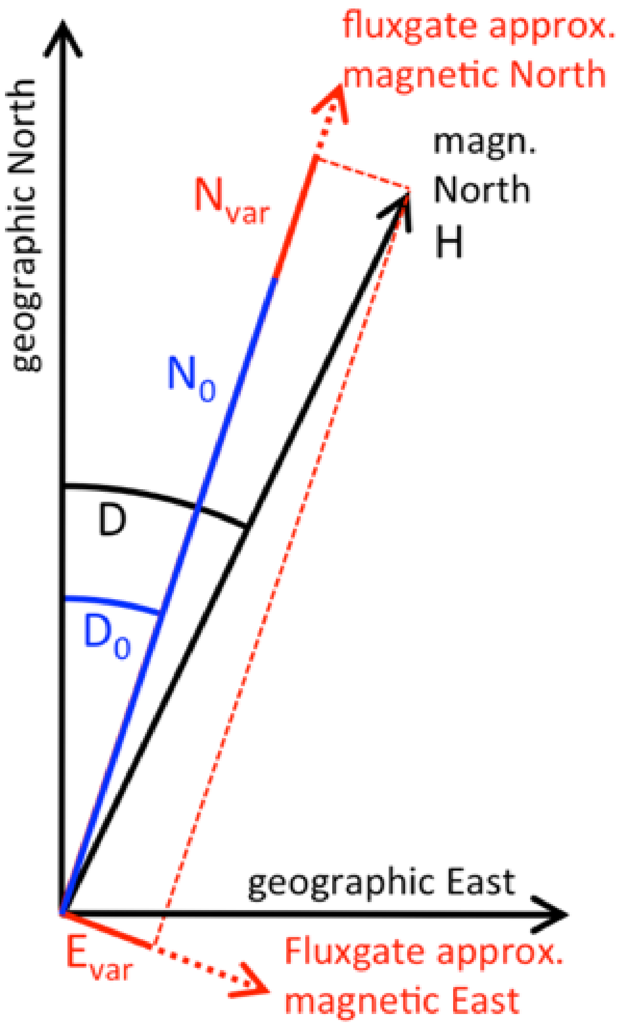

* Gjoerlev(2012)

Geomagnetic Data Calibration Formulas

- The sensor aligned components are defined as

$$
\begin{aligned}
N(t) &= N_0 + N_{var}(t) \\
E(t) &= E_0 + E_{var}(t) \\
V(t) &= V_0 + V_{var}(t)
\end{aligned}
$$

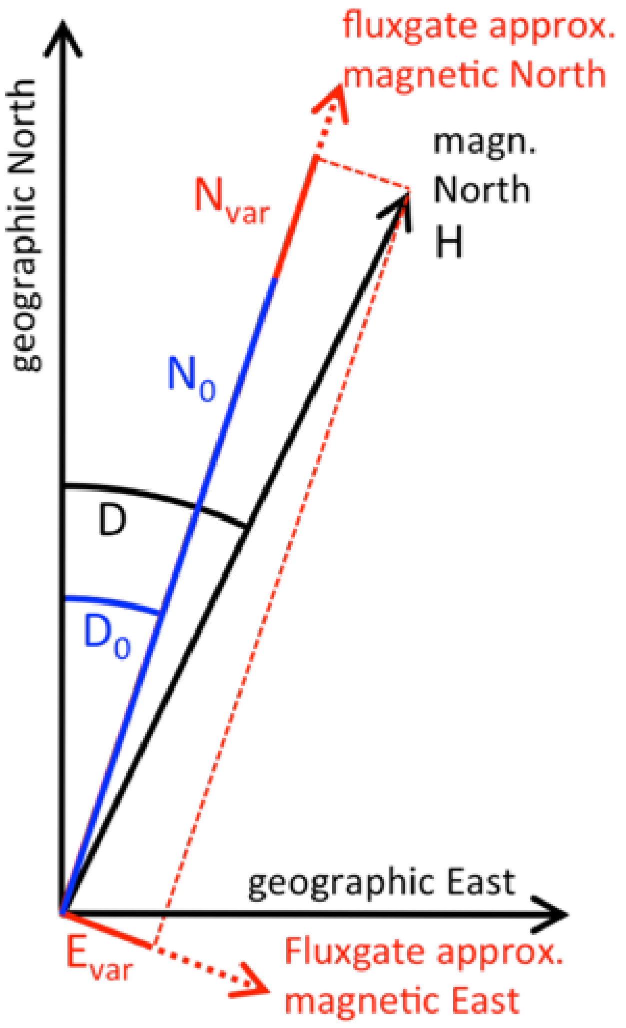

* Gjoerlev(2012)

Geomagnetic Data Calibration Formulas

- The sensor aligned components are defined as

$$
\begin{aligned}
\mathbf{N}(\mathbf{t}) &= \mathrm{N}_0 + \mathrm{N}_{\mathrm{var}}(\mathrm{t}) \\
\mathbf{E}(\mathbf{t}) &= \mathrm{E}_0 + \mathrm{E}_{\mathrm{var}}(\mathrm{t}) \\
\mathbf{V}(\mathbf{t}) &= \mathrm{V}_0 + \mathrm{V}_{\mathrm{var}}(\mathrm{t})
\end{aligned}
$$

- where **N**, **E**, **V** are the geomagnetic field components oriented approximately towards the magnetic North, East and vertically downwards and aligned with the corresponding variometer sensor axis

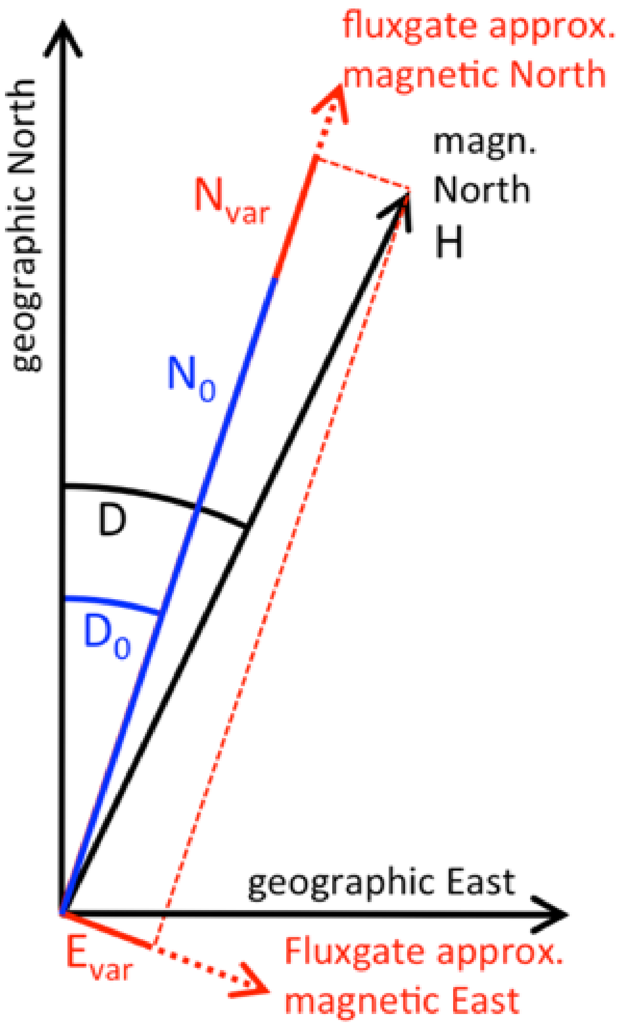

* Gjoerlev(2012)

Geomagnetic Data Calibration Formulas

- The sensor aligned components are defined as

$$
\begin{aligned}
N(t) &= \mathbf{N_0} + N_{var}(t)\\
E(t) &= \mathbf{E_0} + E_{var}(t)\\
V(t) &= \mathbf{V_0} + V_{var}(t)
\end{aligned}
$$

- $\mathbf{N_0}$, $\mathbf{E_0}$, $\mathbf{V_0}$ are the baselines of the components N, E, V

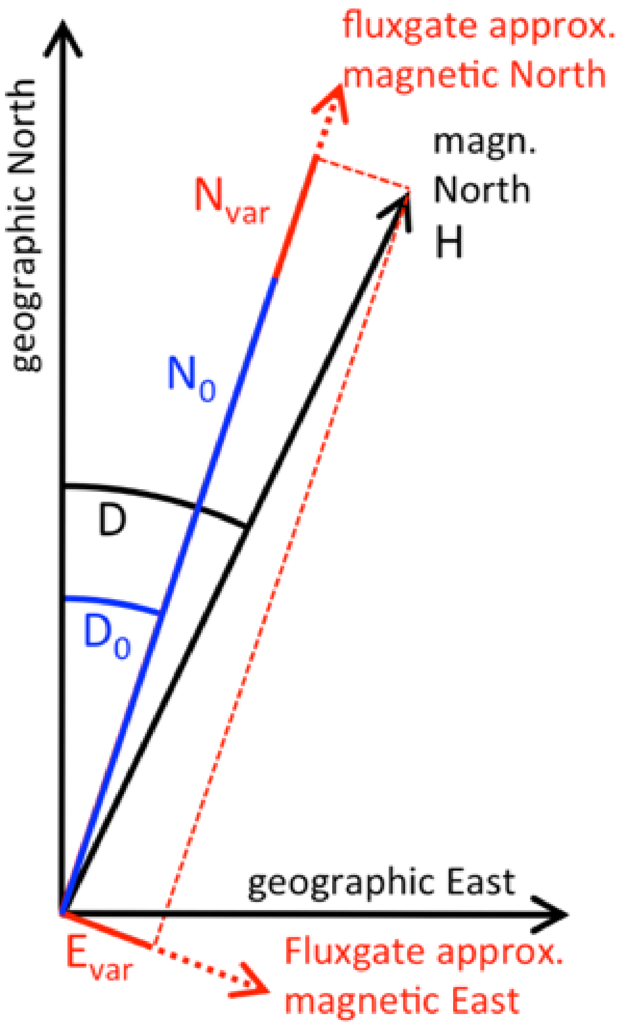

* Gjoerlev(2012)

Geomagnetic Data Calibration Formulas

- The sensor aligned components are defined as

$$
\begin{aligned}
\mathrm{N(t)} &= \mathrm{N_0} + \mathbf{N_{var}(t)} \\
\mathrm{E(t)} &= \mathrm{E_0} + \mathbf{E_{var}(t)} \\
\mathrm{V(t)} &= \mathrm{V_0} + \mathbf{V_{var}(t)}
\end{aligned}
$$

- $\mathbf{N_{var}}$, $\mathbf{E_{var}}$, $\mathbf{V_{var}}$ are the variometer sensor readings approximatly oriented towards magnetic North, East and vertically downwards

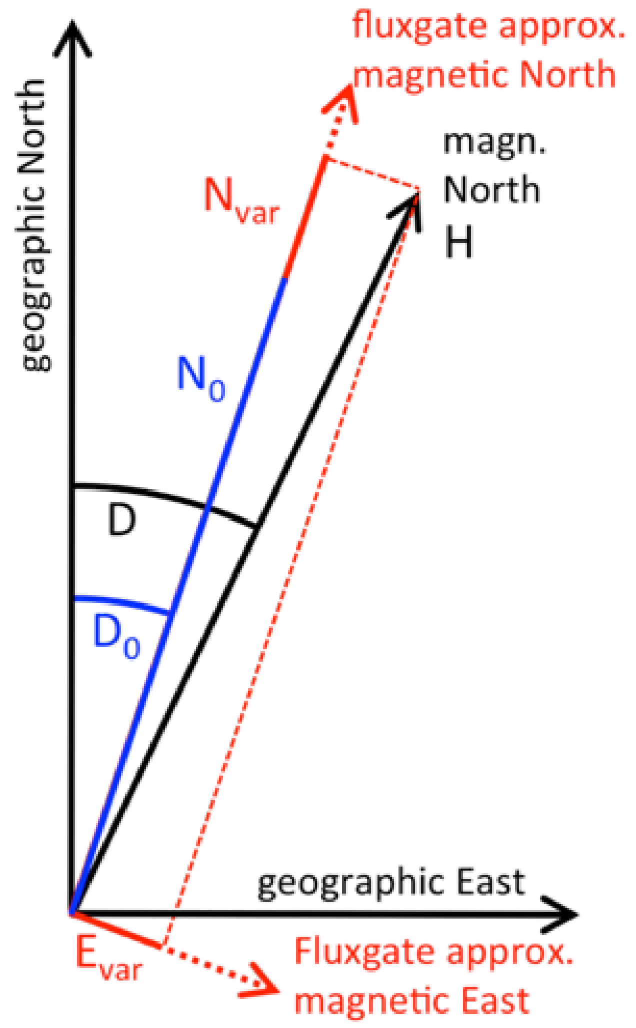

* Gjoerlev(2012)

Geomagnetic Data Calibration Formulas

- Assuming the variometer sensors are aligned to the geomagnetic coordinates in a way that N is maximum and E is approximately zero, the geomagnetic field components can be calculated at each time t using:

$$H(t) = \sqrt{(N_0(t) + N_{var}(t))^2 + E_{var}^2(t)}$$

$$D(t) = D_0(t) + \tan^{-1}\left(\frac{E_{var}(t)}{N_0(t) + N_{var}(t)}\right)$$

$$Z(t) = V_0(t) + V_{var}(t)$$

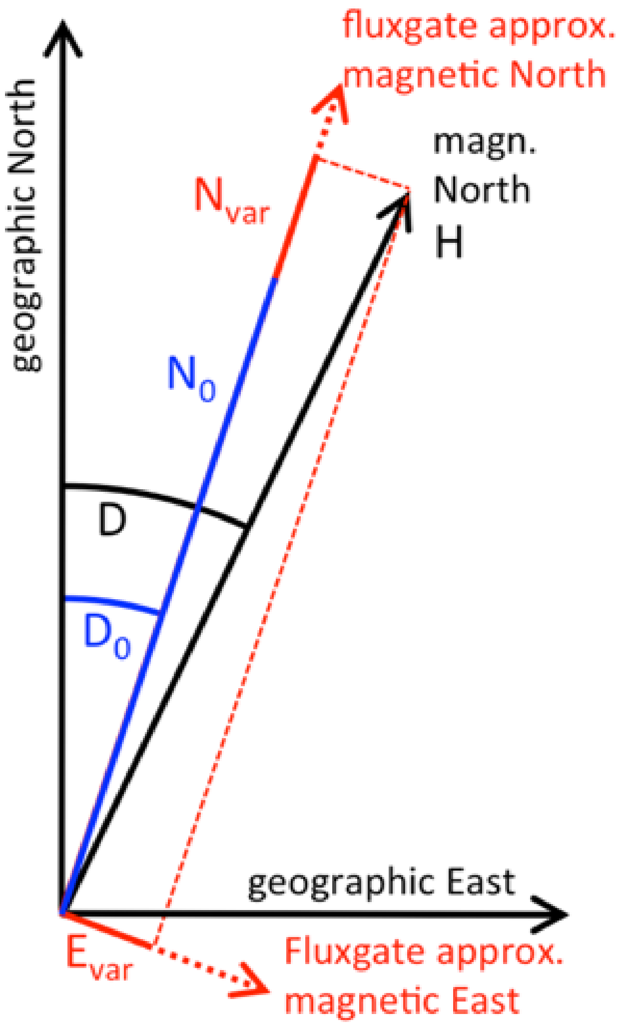

Geomagnetic Data Calibration Formulas

- Assuming the variometer sensors are aligned to the geomagnetic coordinates in a way that N is maximum and E is approximately zero, the geomagnetic field components can be calculated at each time t using:

$$H(t) = \sqrt{(N_0(t) + N_{var}(t))^2 + E_{var}^2(t)}$$

$$D(t) = D_0(t) + \tan^{-1}\left(\frac{E_{var}(t)}{N_0(t) + N_{var}(t)}\right)$$

$$Z(t) = V_0(t) + V_{var}(t)$$

- The complete calibration scheme will be the subject of a future publication

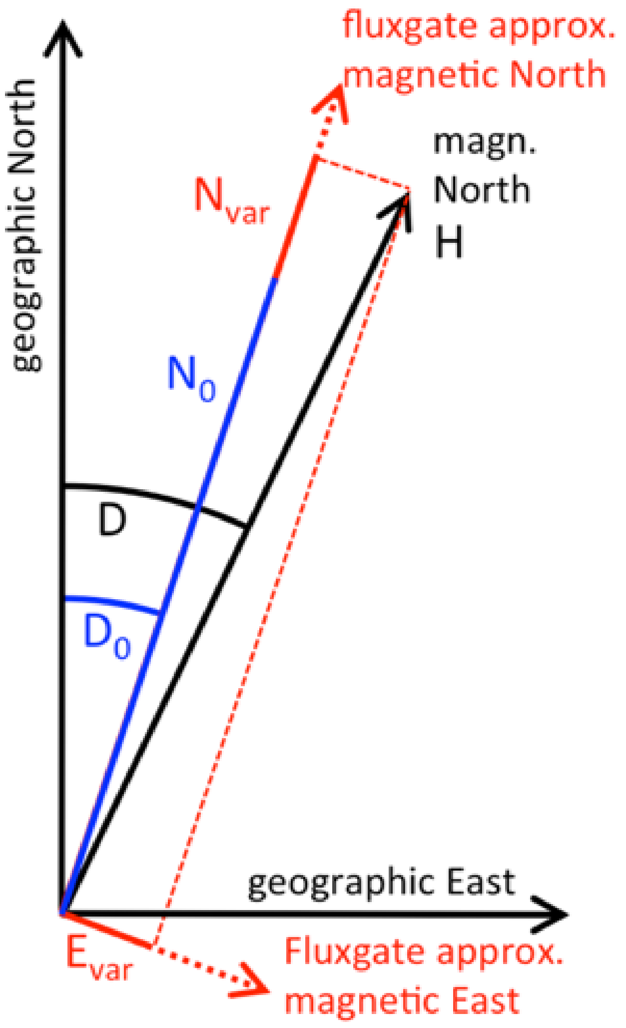

Geomagnetic Data Calibration Example – Step 1

- From the raw times series of N, E and V components measured at Ancon magnetic station (ANC; lat = -11.78º, lon = -77.15º) at May 2011, from MAGDAS database:

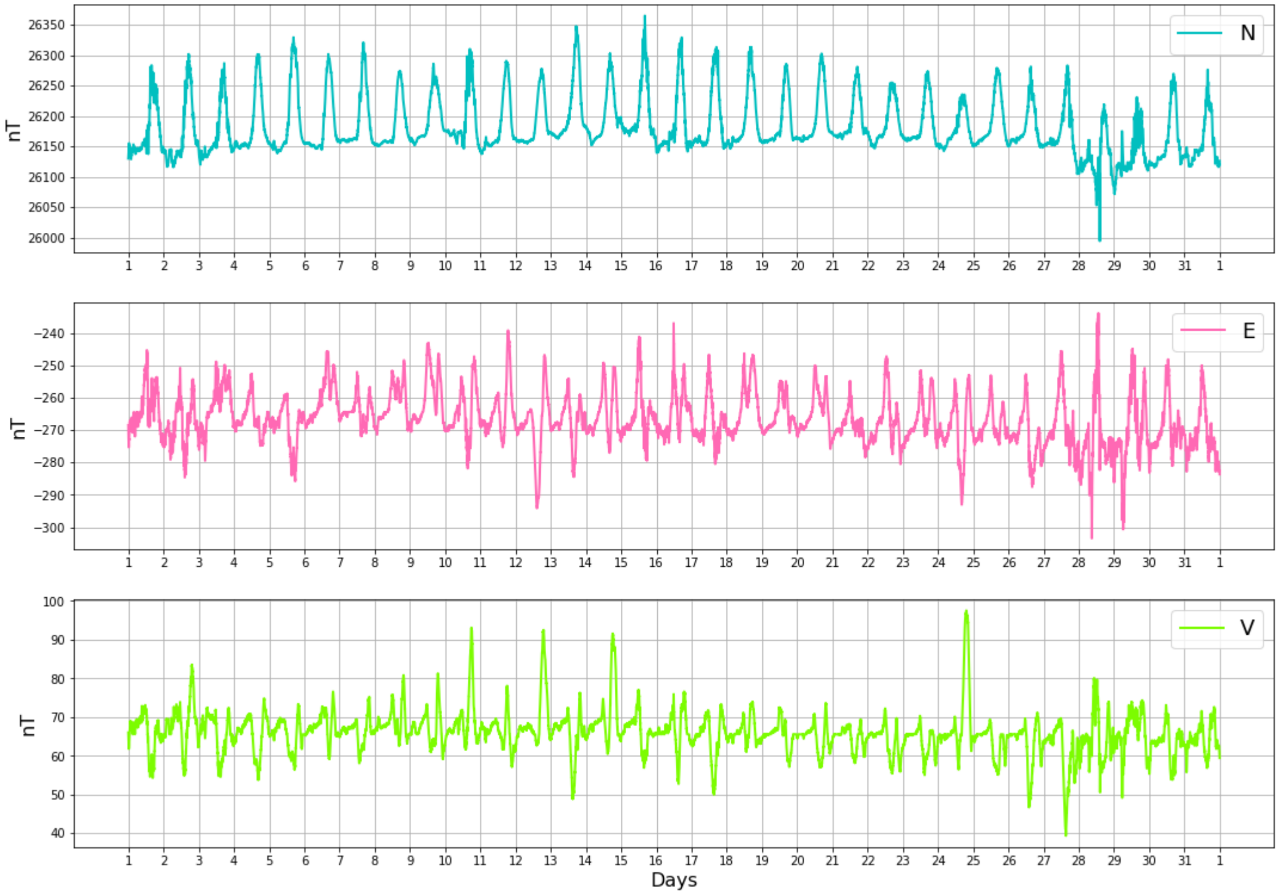

Geomagnetic Data Calibration Example – Step 2

- Determine the baselines N_0, E_0 and V_0 from the mean of the quiet night time N, E and V data

- We adopt 22 – 4 LT and $|Dst*\cos(\theta_{gm})| < 40$ nT as the night time and geomagnetic activity criterias, respectively

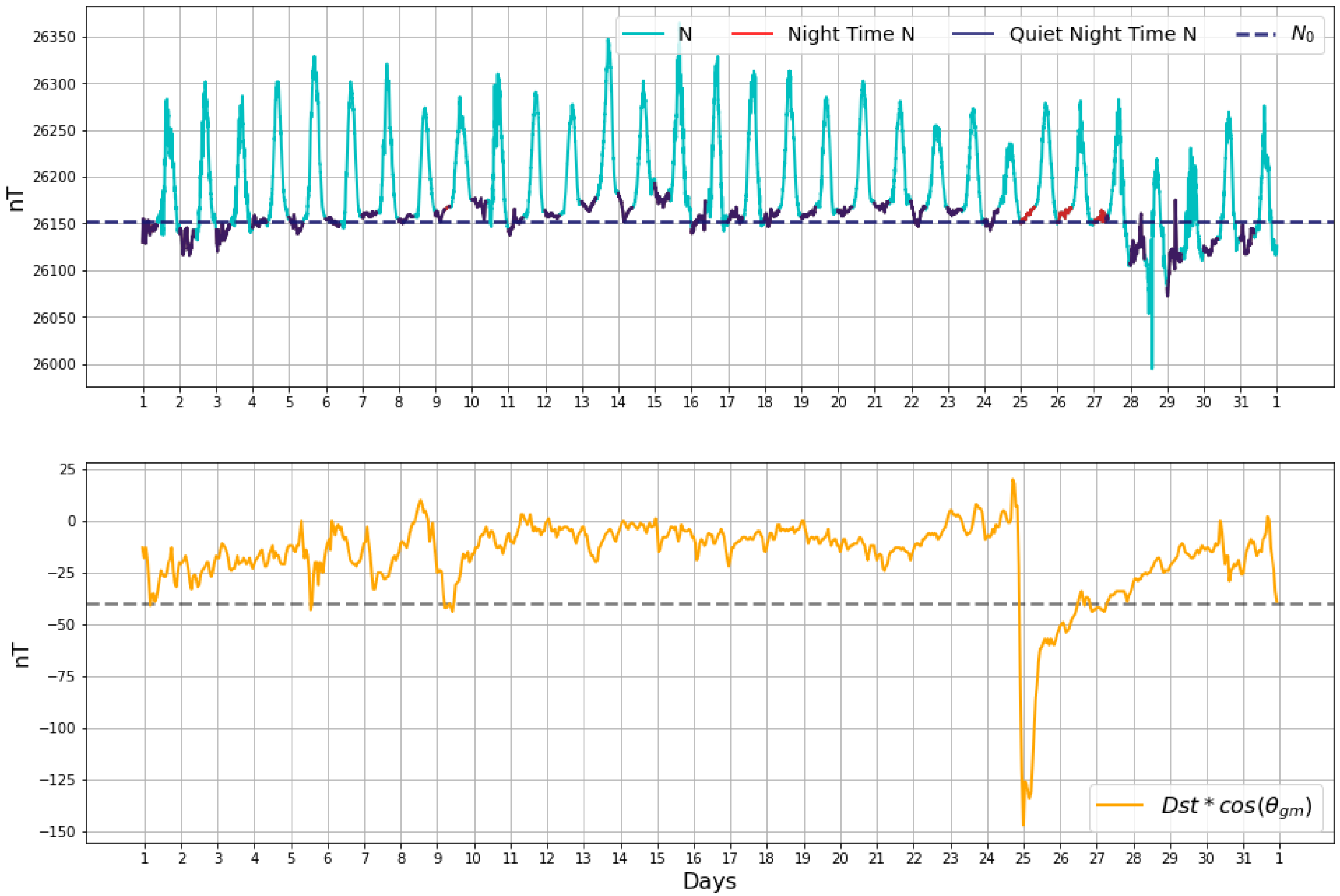

ETH zürich

Geomagnetic Data Calibration Example – Step 2

- Determine the baselines N_0, E_0 and V_0 from the mean of the quiet night time N, E and V data
- We adopt 22 – 4 LT and $|Dst^{*}\cos(\theta_{gm})| < 40$ nT as the night time and geomagnetic activity criterias, respectively

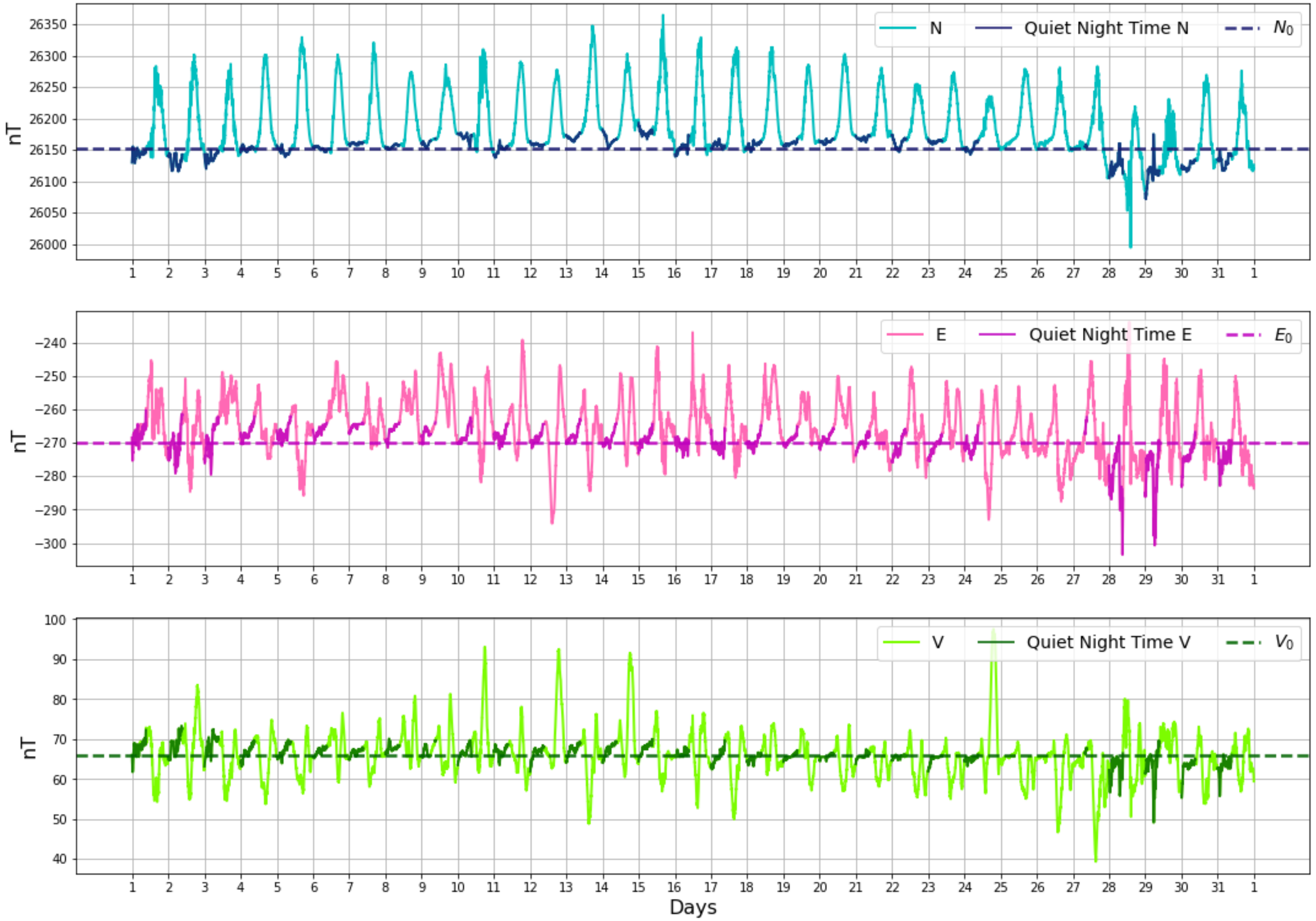

Geomagnetic Data Calibration Example – Step 3

- Calculate time series of N_{var}, E_{var} and V_{var} by subtracting the baselines from the raw time series

$$
\begin{aligned}
\mathrm{N}_{\mathrm{var}}(\mathrm{t}) &= \mathrm{N}(\mathrm{t}) - \mathrm{N}_0 \\
E_{var}(t) &= E(t) - E_0 \\
V_{var}(t) &= V(t) - V_0
\end{aligned}
$$

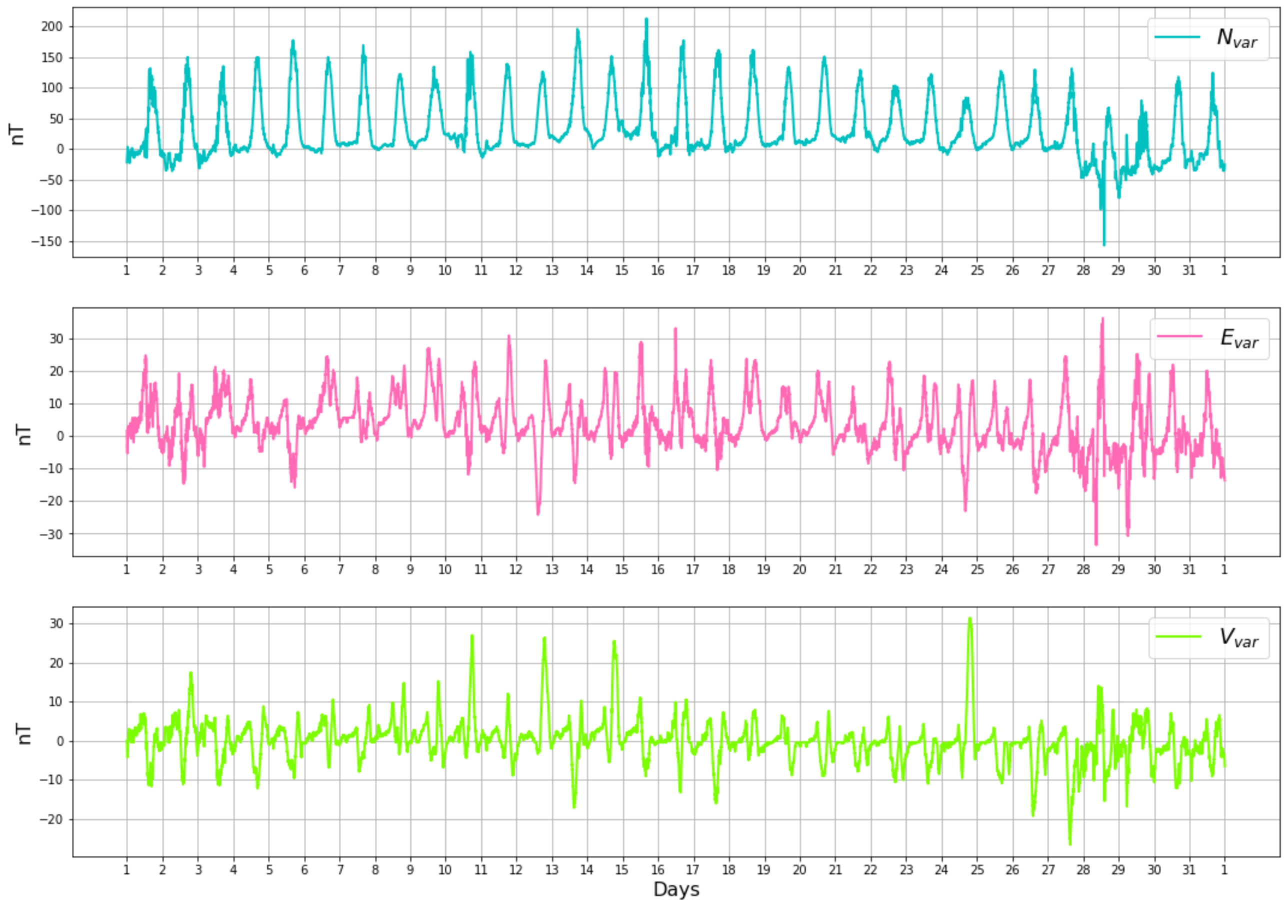

Geomagnetic Data Calibration Example – Step 4

- Calculate new baselines $N_{0,new}$, $E_{0,new}$ and $V_{0,new}$ using from synthetic baselines calculated using CHAOS geomagnetic model and N_{var}, E_{var} and V_{var}

$$N_{0,new}(t) = \sqrt{H_{model}^2 - E_{var}^2} - N_{var}(t)$$

$$D_{0,new}(t) = D_{model} - \tan^{-1}\left(\frac{E_{va*r}(t)}{N_{0,new} + N_{var}(t)}\right)$$

$$V_{0,new}(t) = Z_{model} - V_{var}(t)$$

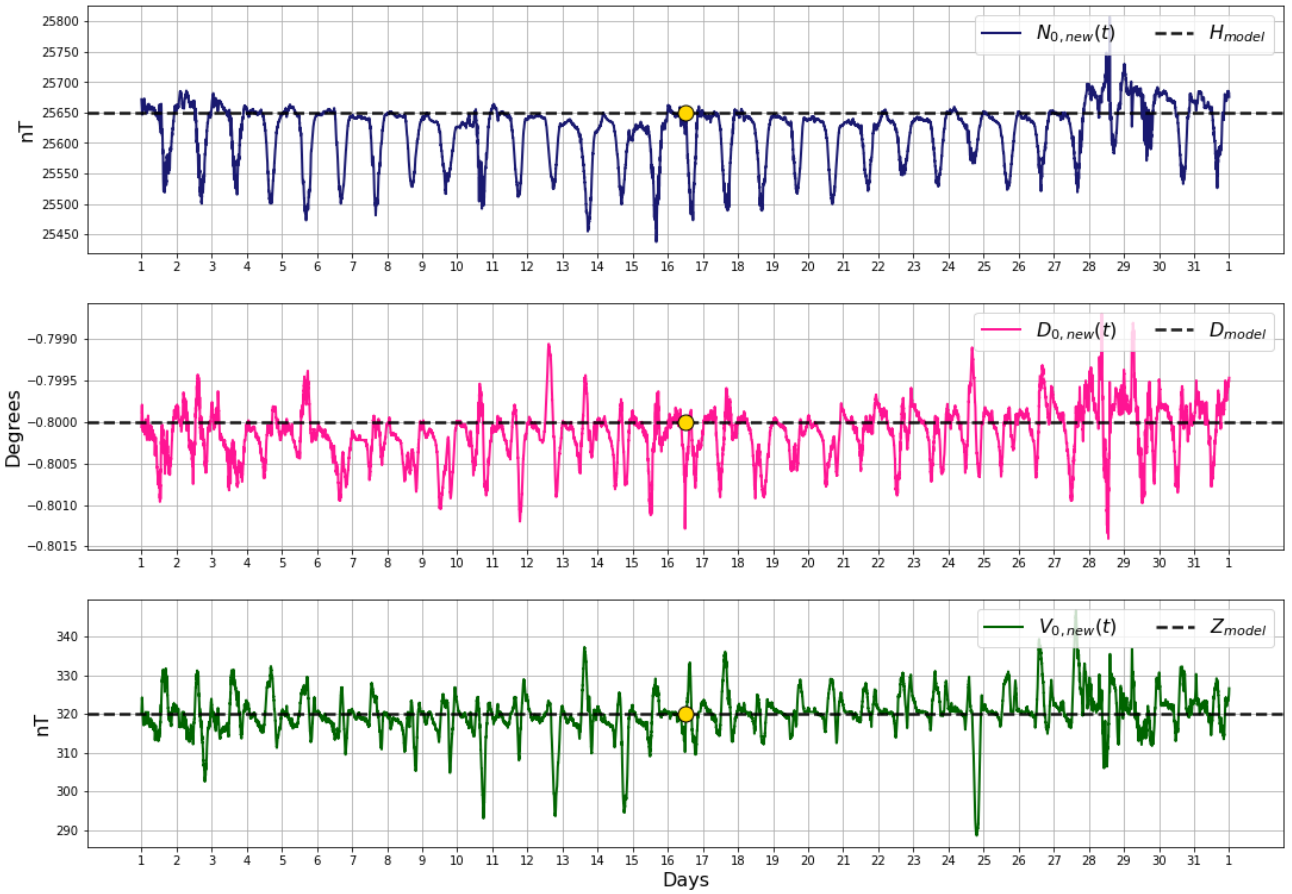

Geomagnetic Data Calibration Example – Step 5

- Calculate calibrated geomagnetic field components H_{cal}, D_{cal}, Z_{cal} from new baselines $N_{0,new}$, $D_{0,new}$ and $V_{0,new}$ and variometer data N_{var}, E_{var}, V_{var}

$$H_{cal}(t) = \sqrt{(N_{0,new} + N_{var}(t))^2 + E_{var}^2(t)}$$

$$D_{cal}(t) = D_{0,new} + \tan^{-1}\left(\frac{E_{var}(t)}{N_{0,new} + N_{var}(t)}\right)$$

$$Z_{cal}(t) = V_{0,new} + V_{var}(t)$$

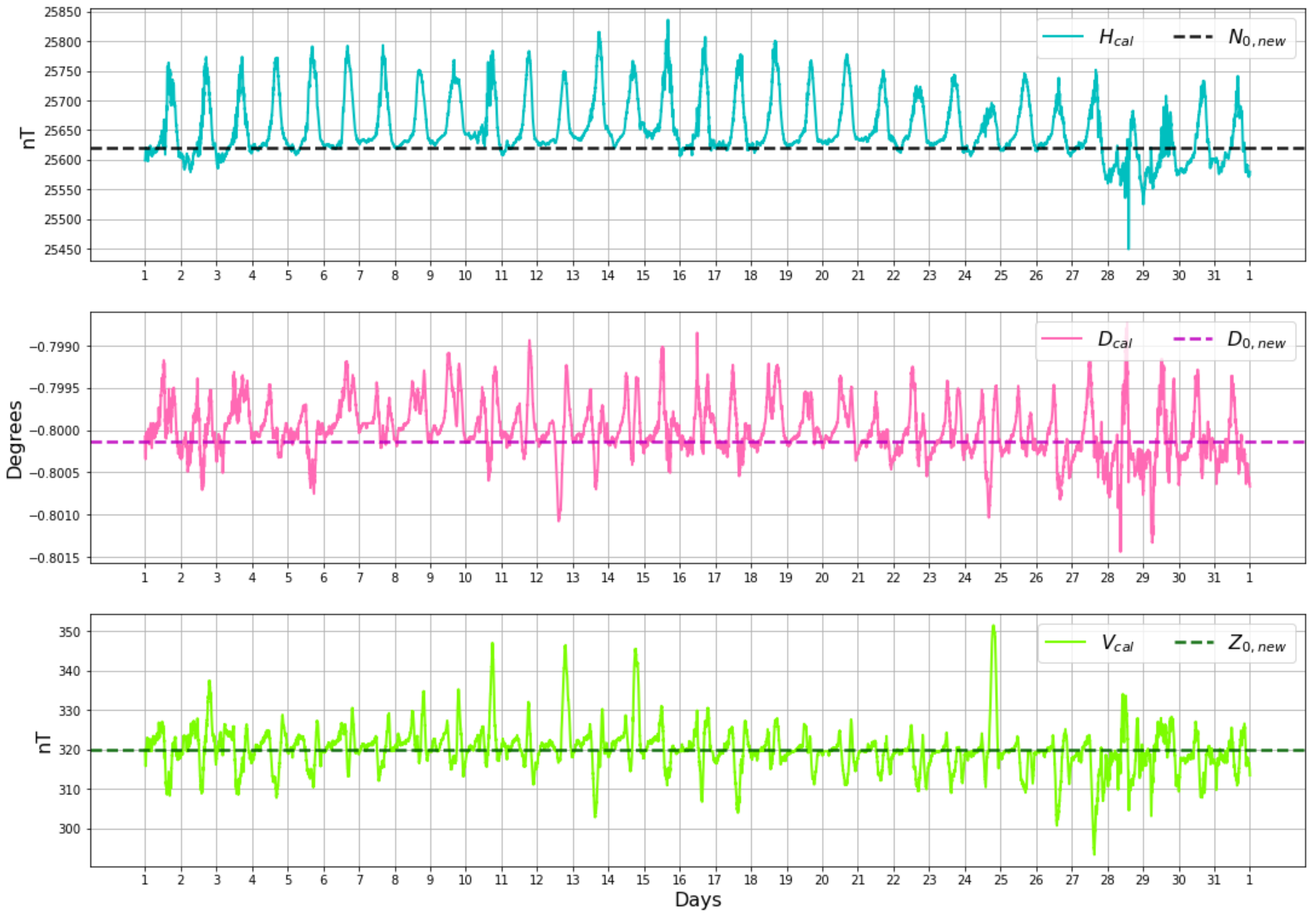

Geomagnetic Data Calibration – Examples

Huancayo (HUA) Magnetic Observatory, year: 2014, lat = -12.05º, lon = -75.33º

Pre-Calibration

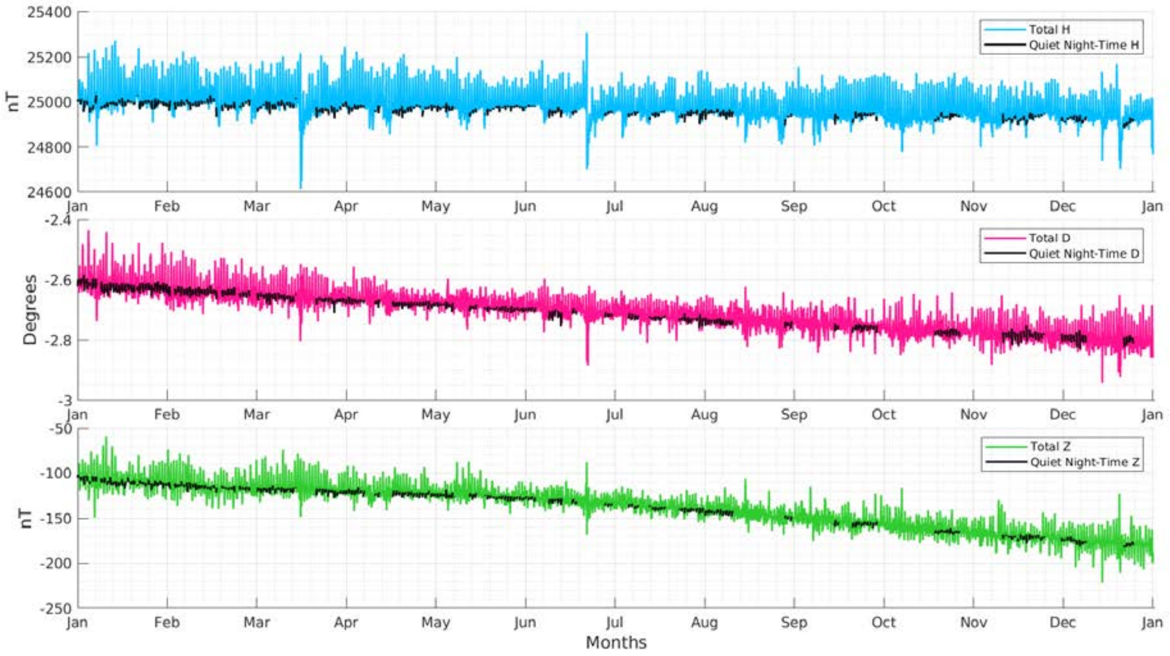

Post-Calibration

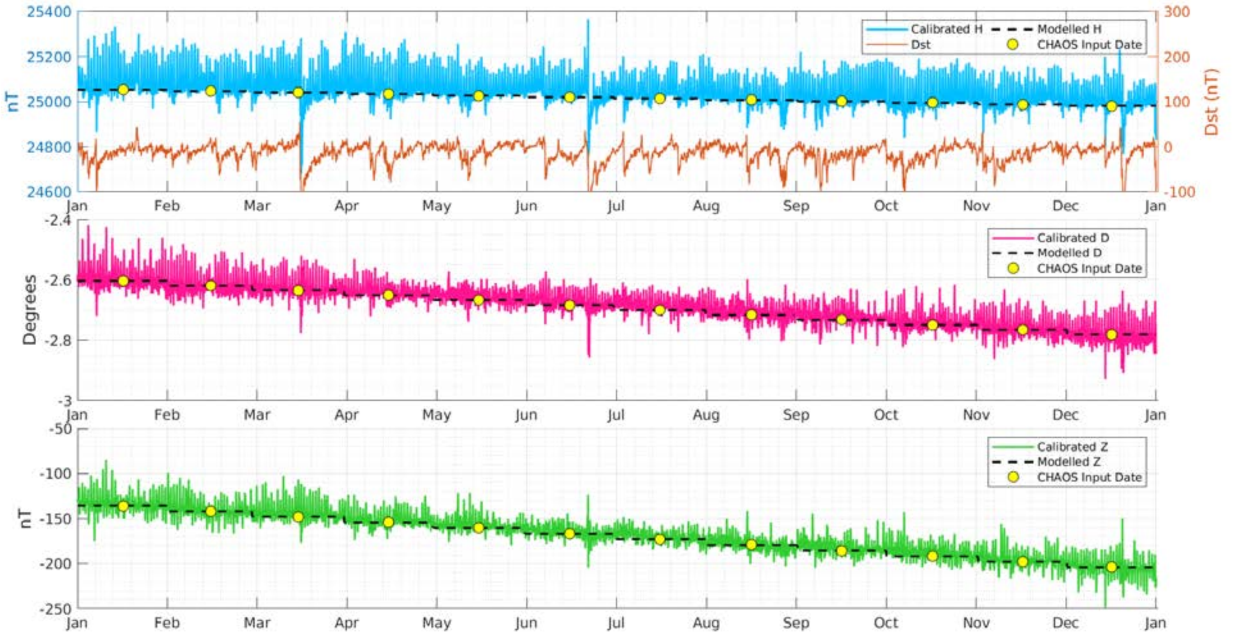

Geomagnetic Data Calibration – Examples

Station: OSNO (Osorno), Year: 2009, lat = -40.34°, lon = -73.09°

Pre-Calibration

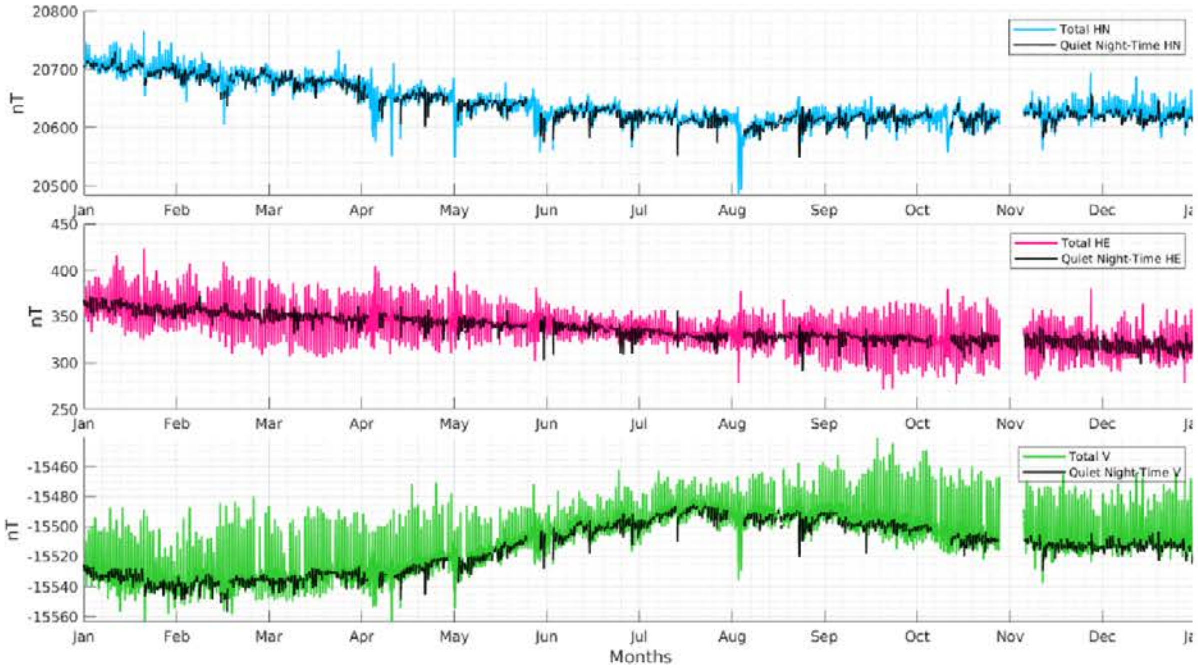

Post-Calibration

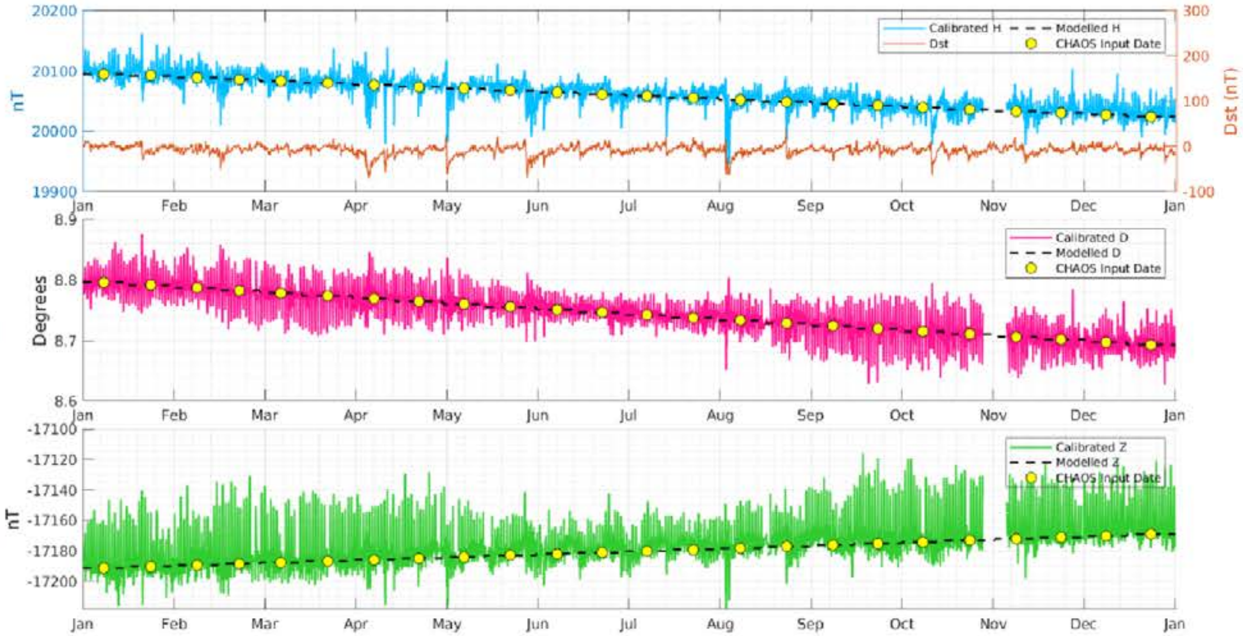

Geomagnetic Data Calibration – Examples

Station: DAW (Dawson City), Year: 2012, lat = 12.41º, lon = 130.92º

Pre-Calibration

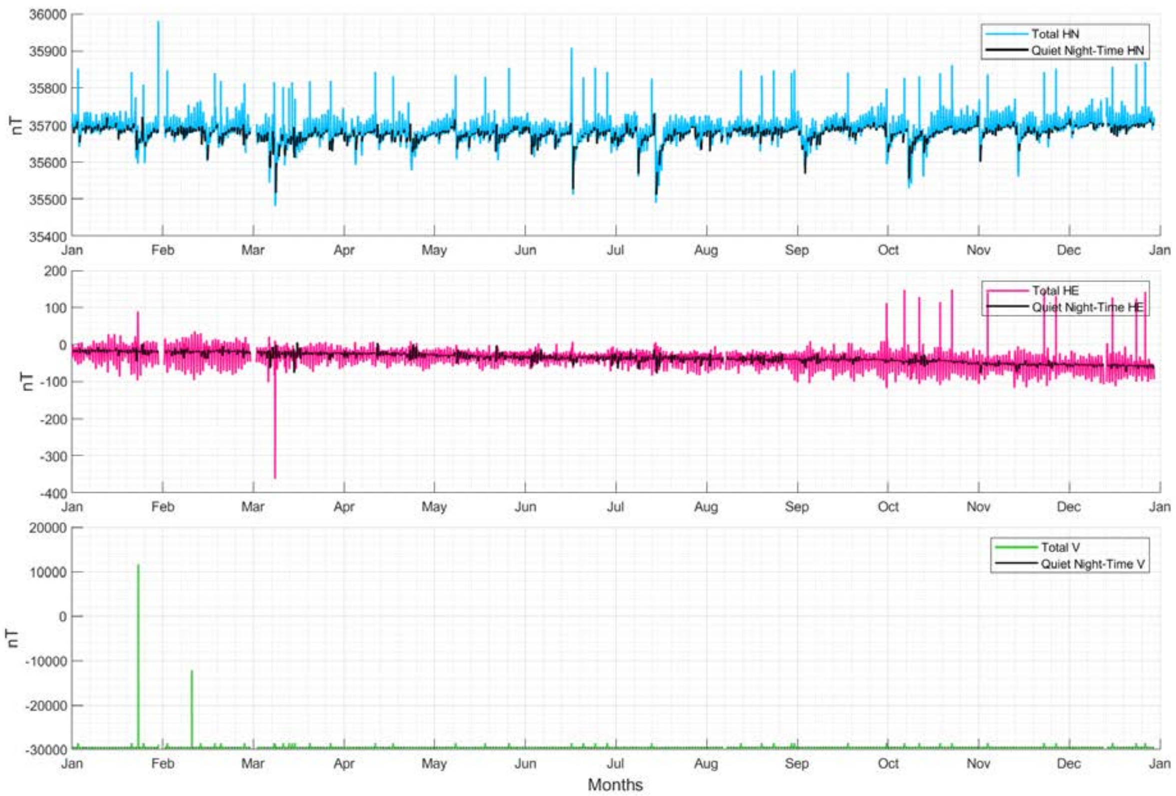

Post-Calibration

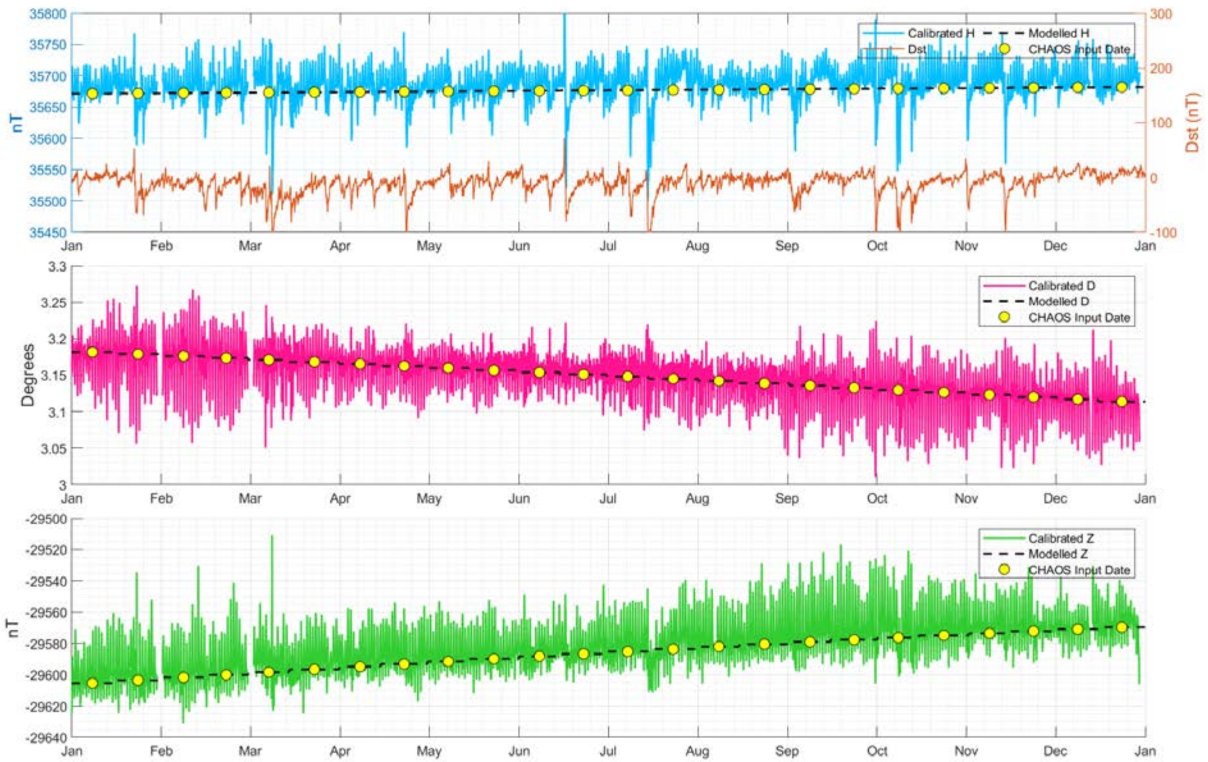

Geomagnetic Data Calibration – Examples

Station: JIC (Jicamarca), Year: 2010, lat = -11.95°, lon = -76.88°

Pre-Calibration

Post-Calibration

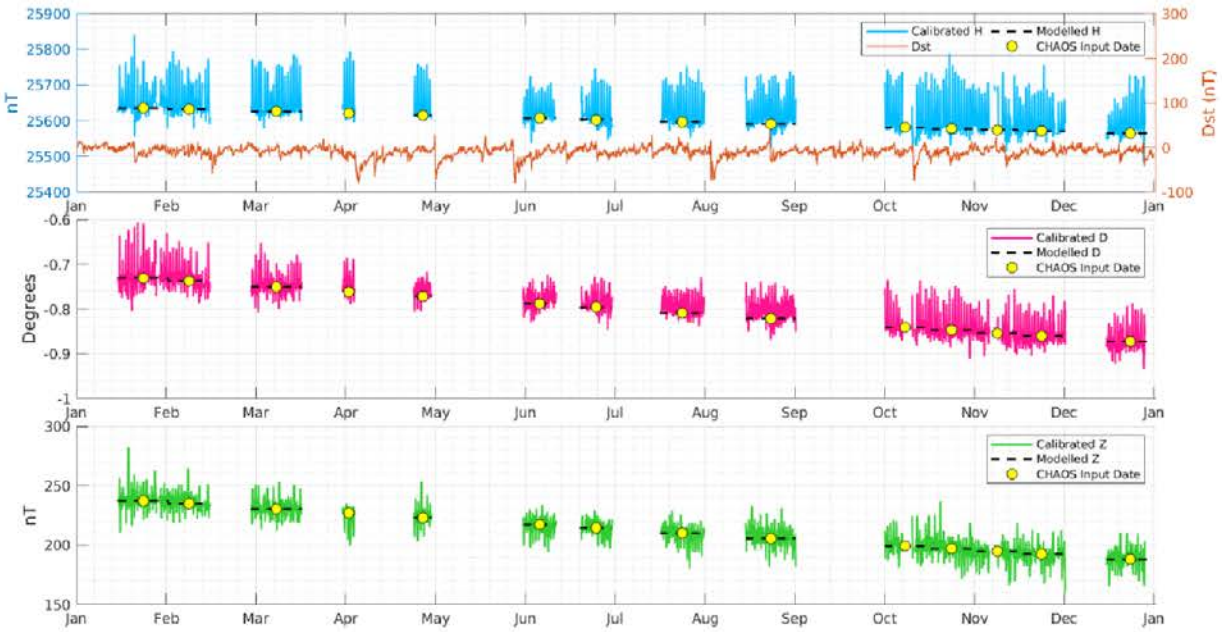

Geomagnetic Data Calibration – Examples

Station: JIC (Jicamarca), Year: 2010, lat = -11.95º, lon = -76.88º

Pre-Calibration

Post-Calibration

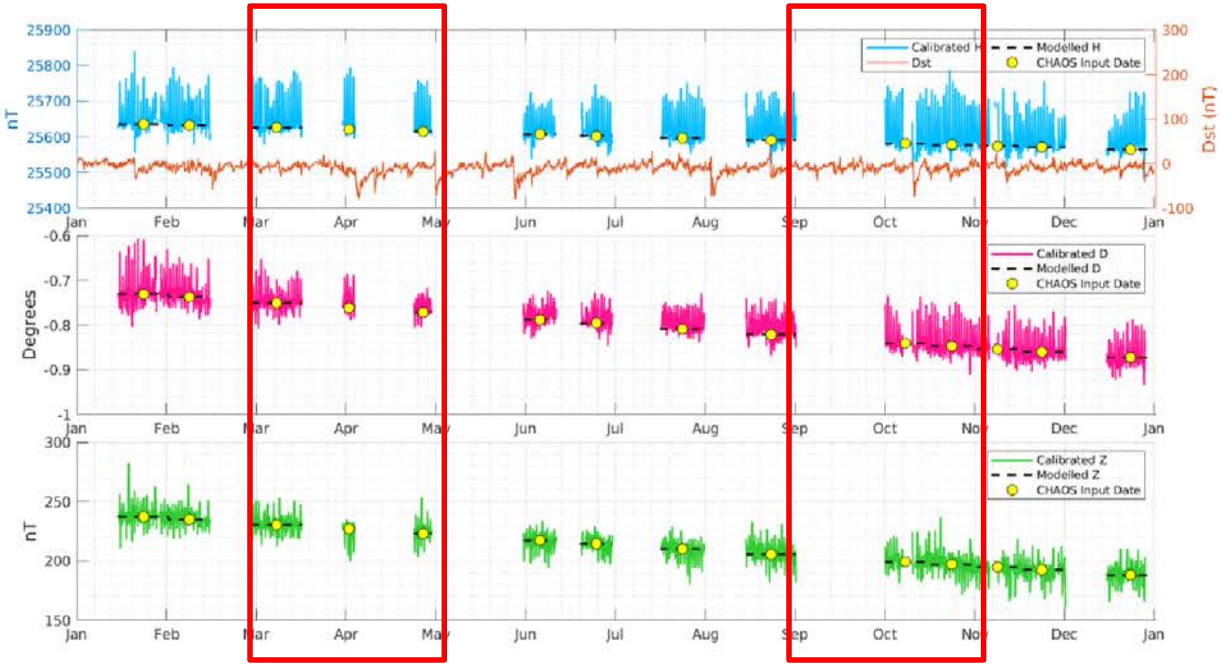

ETH zürich

Calibration of South America Data

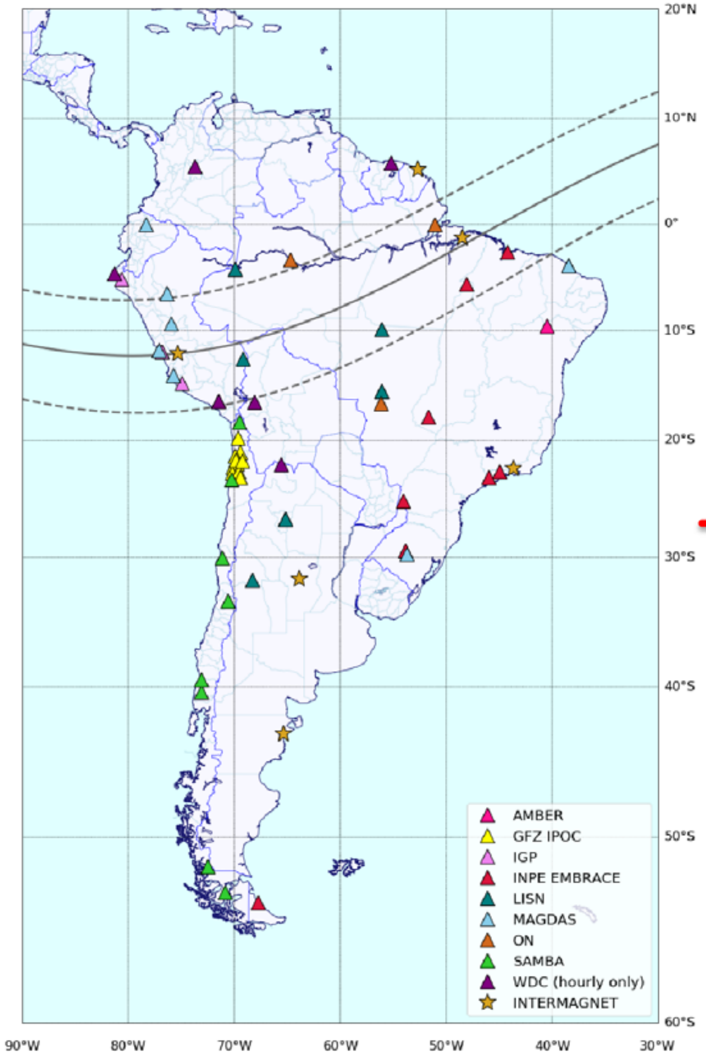

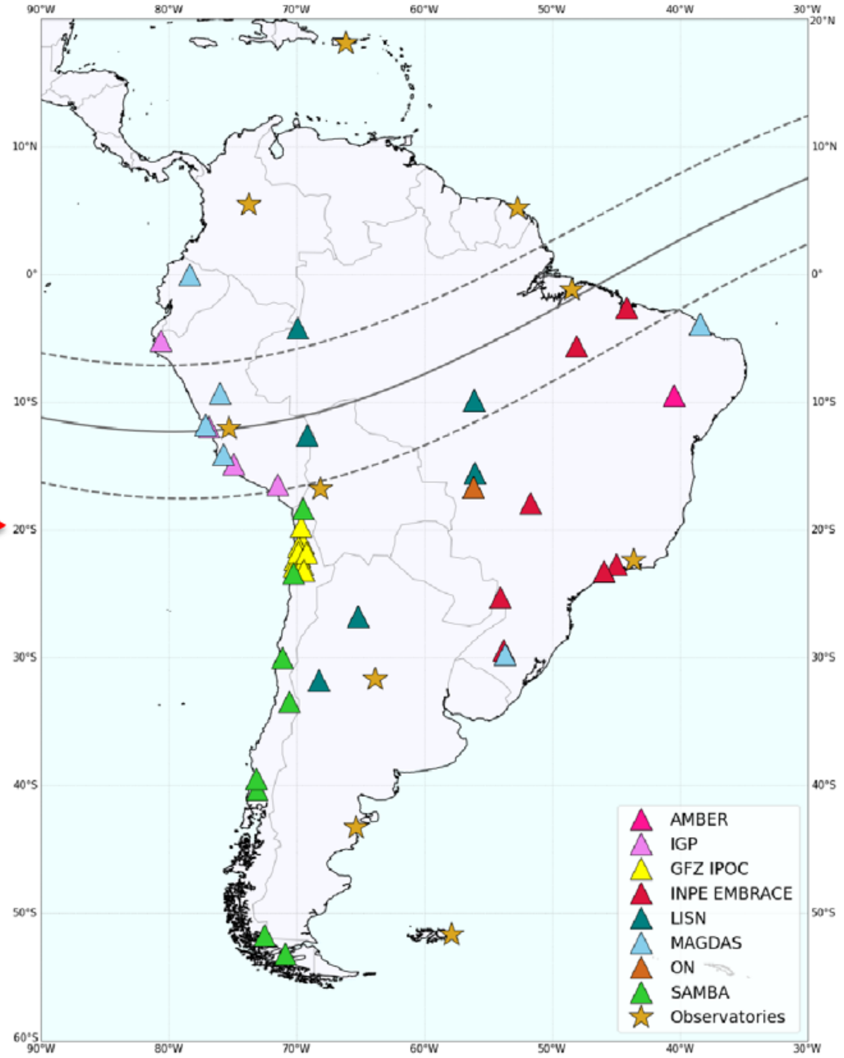

Calibration of South America Data

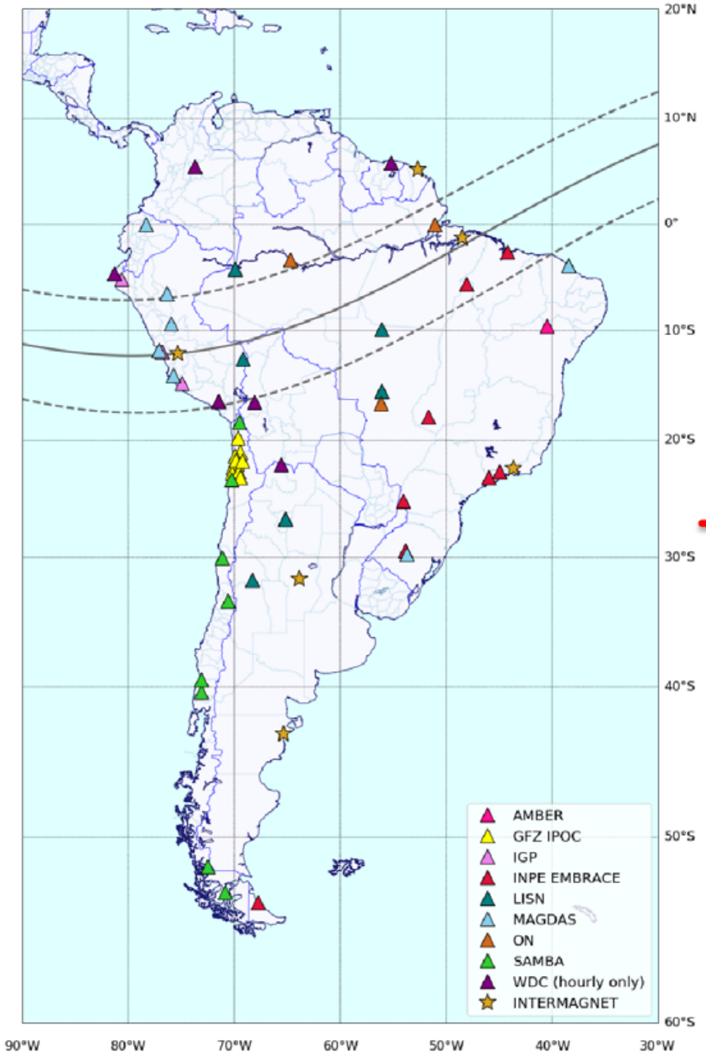

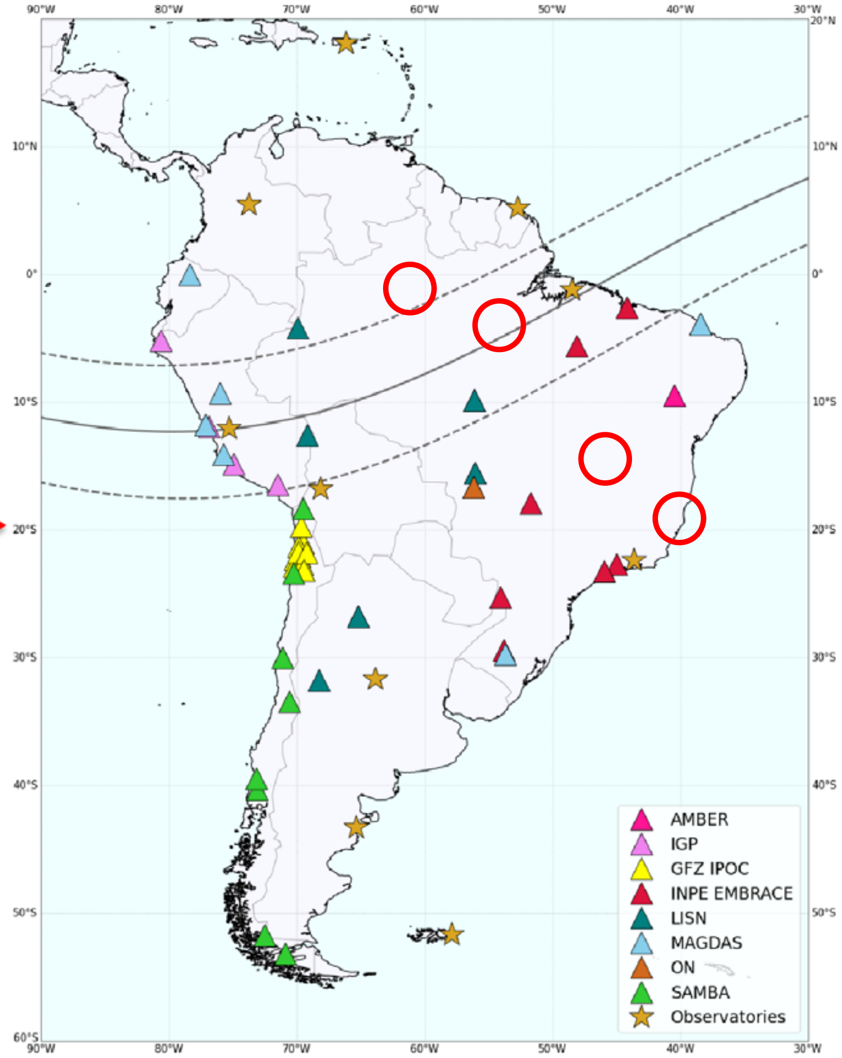

Calibration of Australian Data (Filippo Cicchetti)

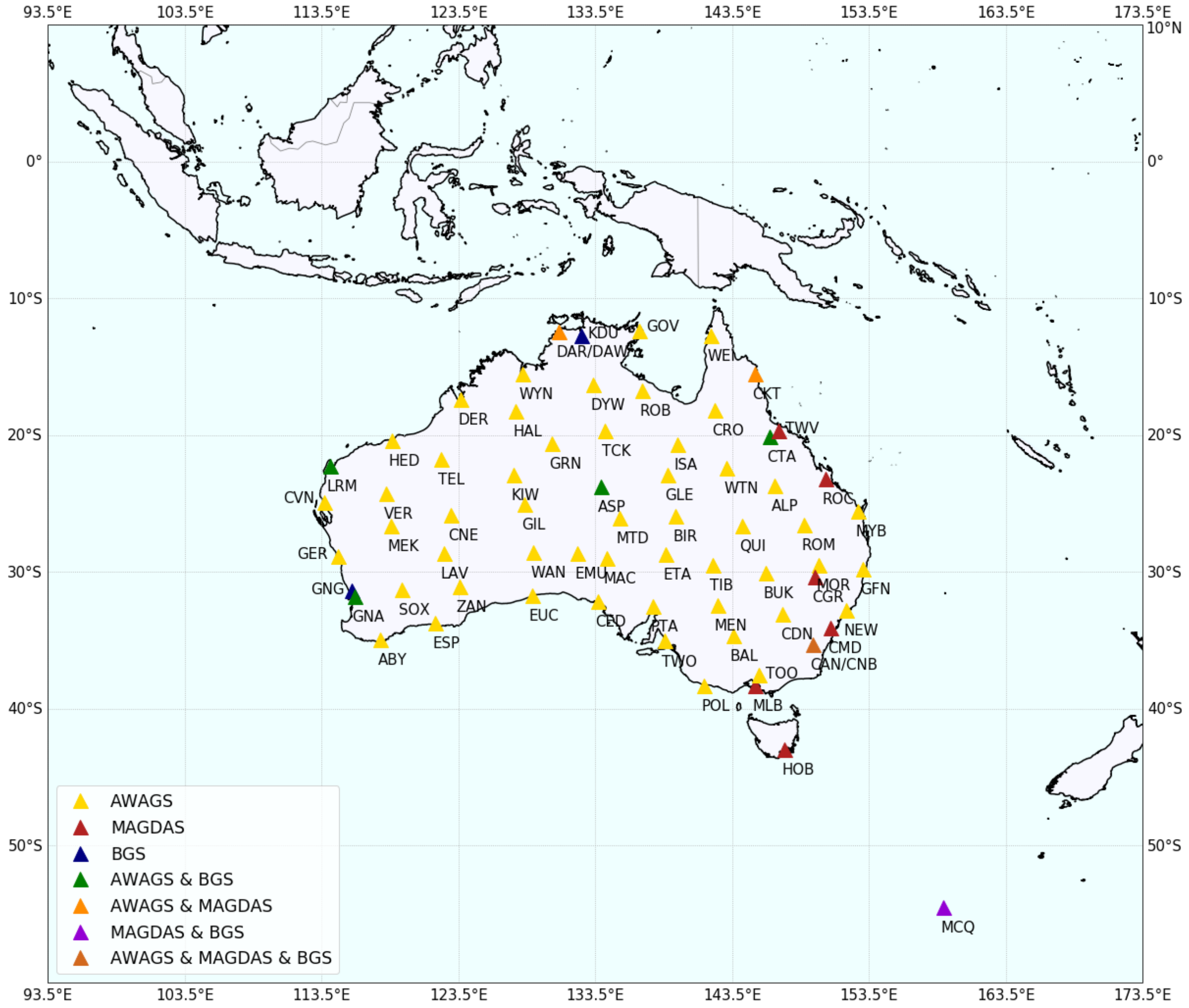

Calibration of Chinese Data (Shan Xu)

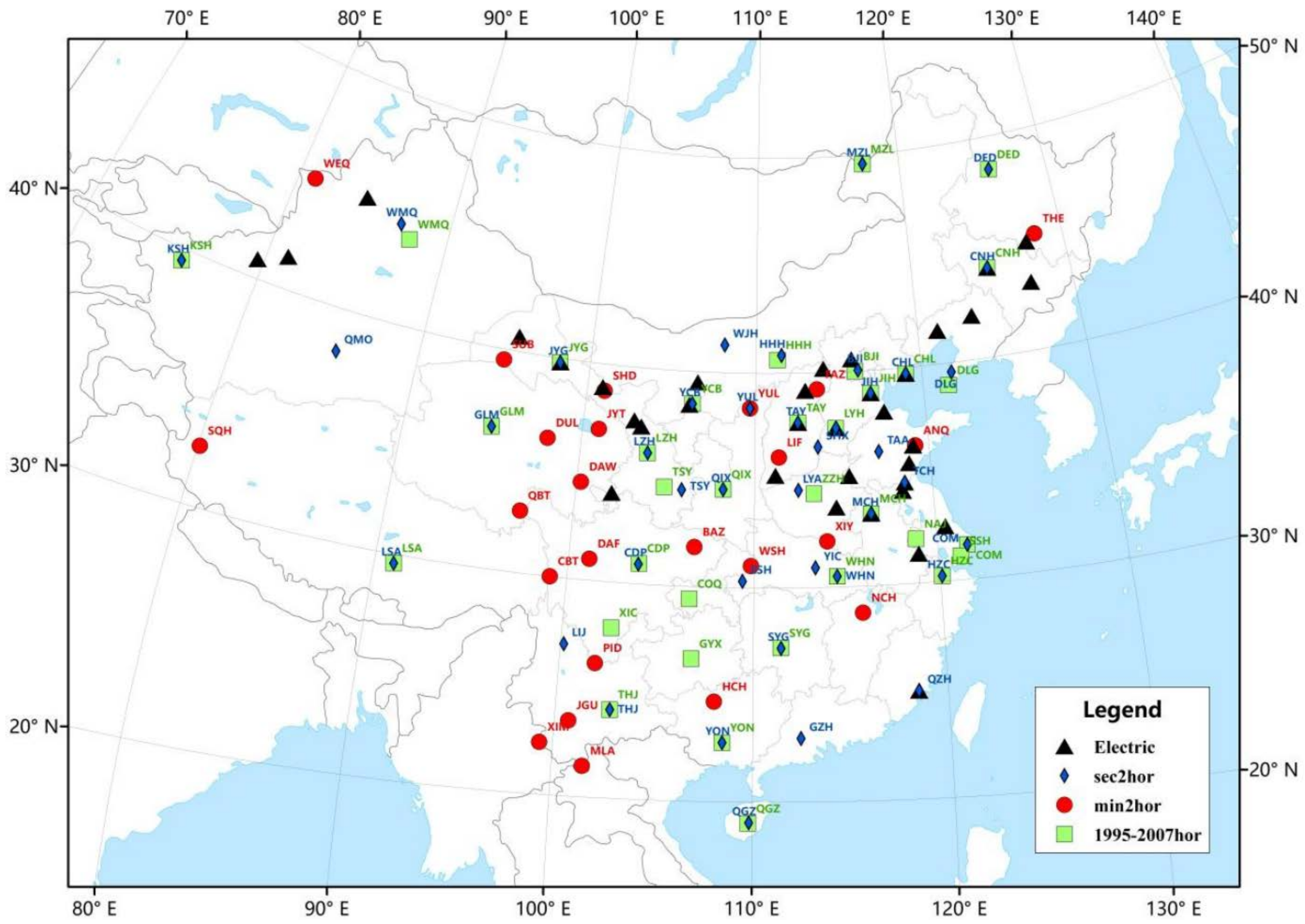

Preliminary Results - Tippers in South America

- Tippers were calculated using a multivariate robust processing code*;

- Large tippers near the coast - Geomagnetic Coast Effect;

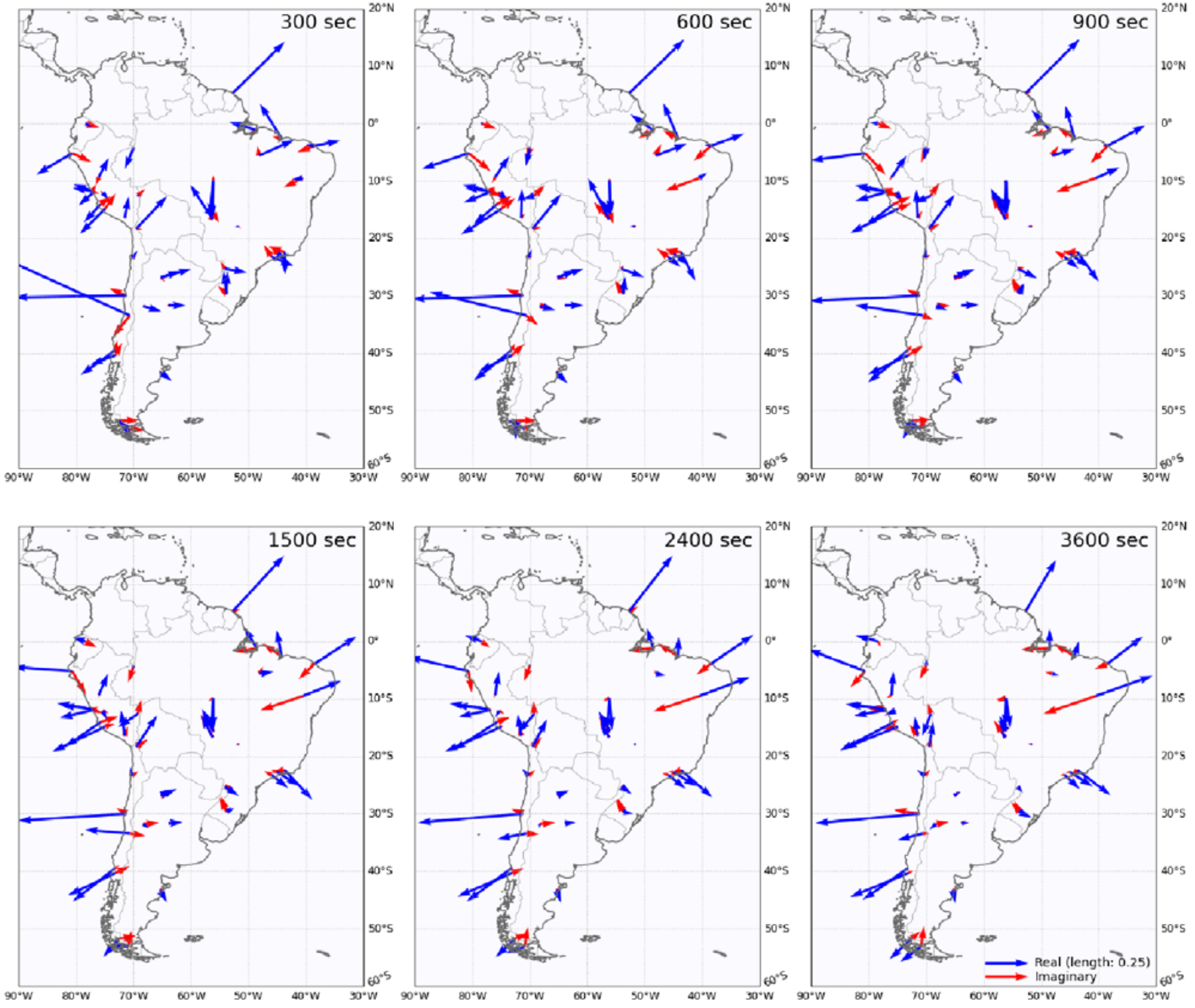

* Püthe et al (2014)

Preliminary Results - Tippers in Australia

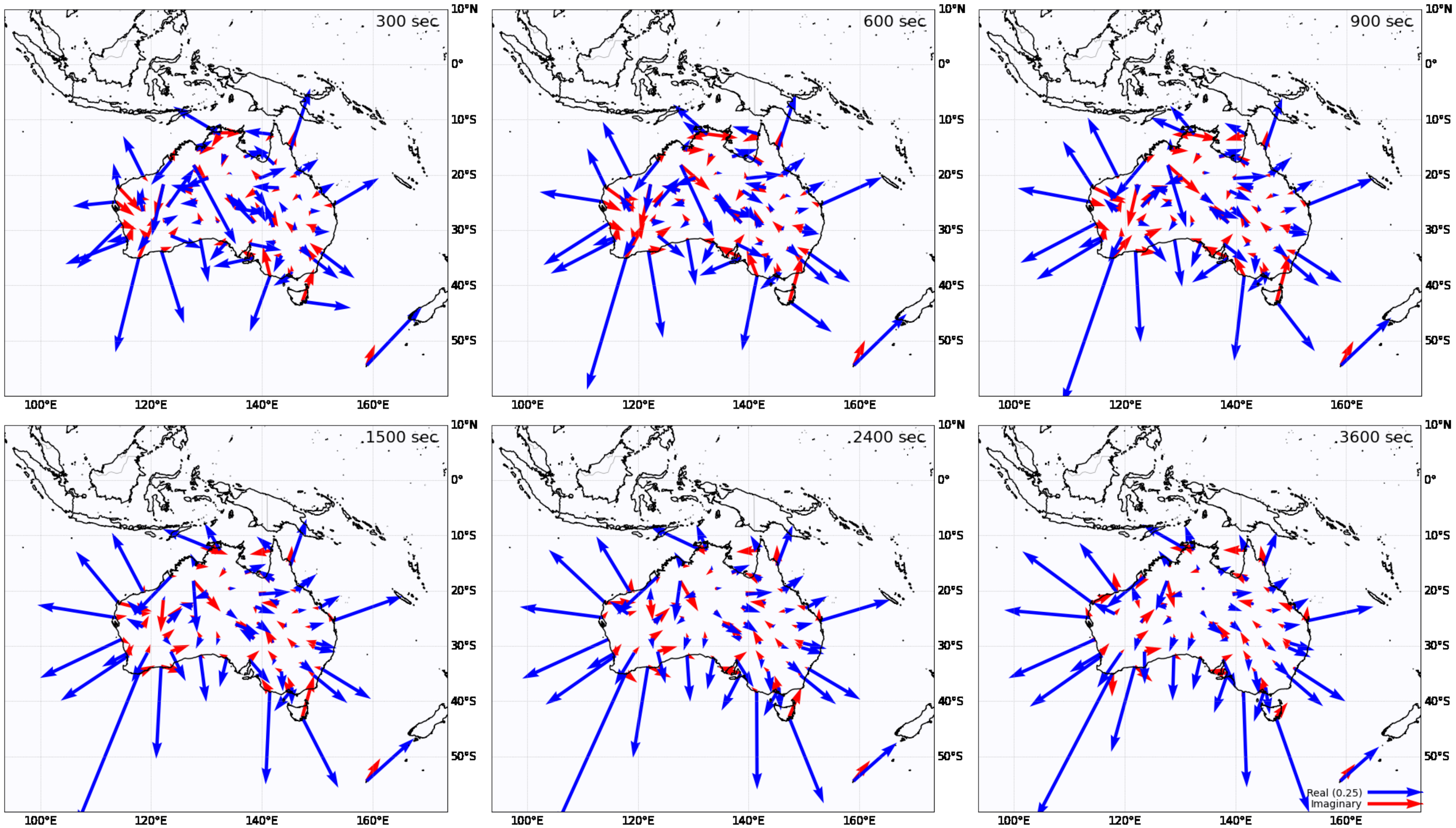

Thanks

ETH zürich

One equation, two unknowns: towards reconstruction of source current and subsurface conductivity structures

Alexander Grayver

Project Meeting
10 Feb 2021

esa eo SWARM DISC STSE Support To Science Element

The various sources of magnetic field

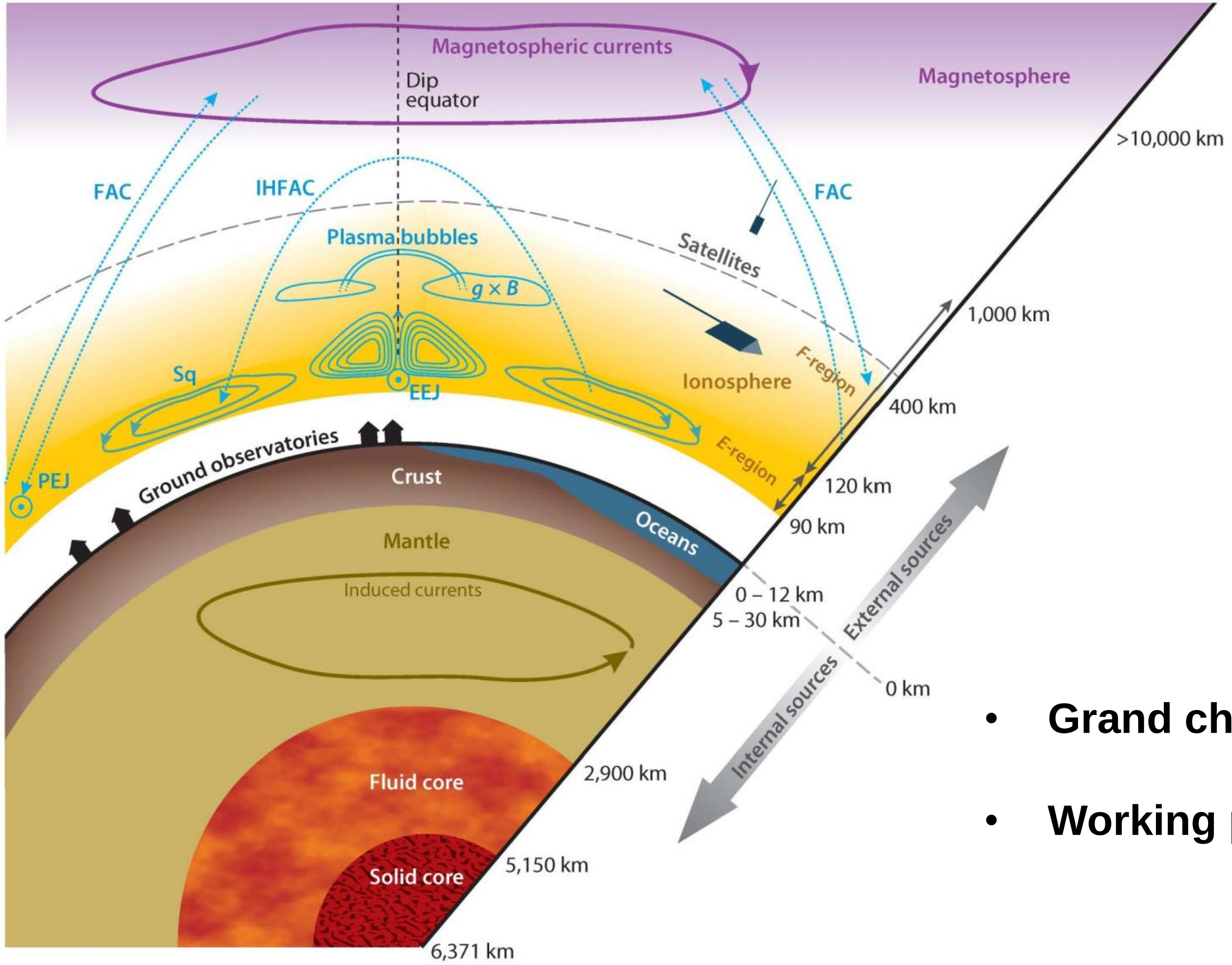

- **Grand challenge**: separate different components
- **Working paradigm**: “one man's noise is another man's signal” *(Edward Ng, NYT, 1990)*

Principle of EM Induction

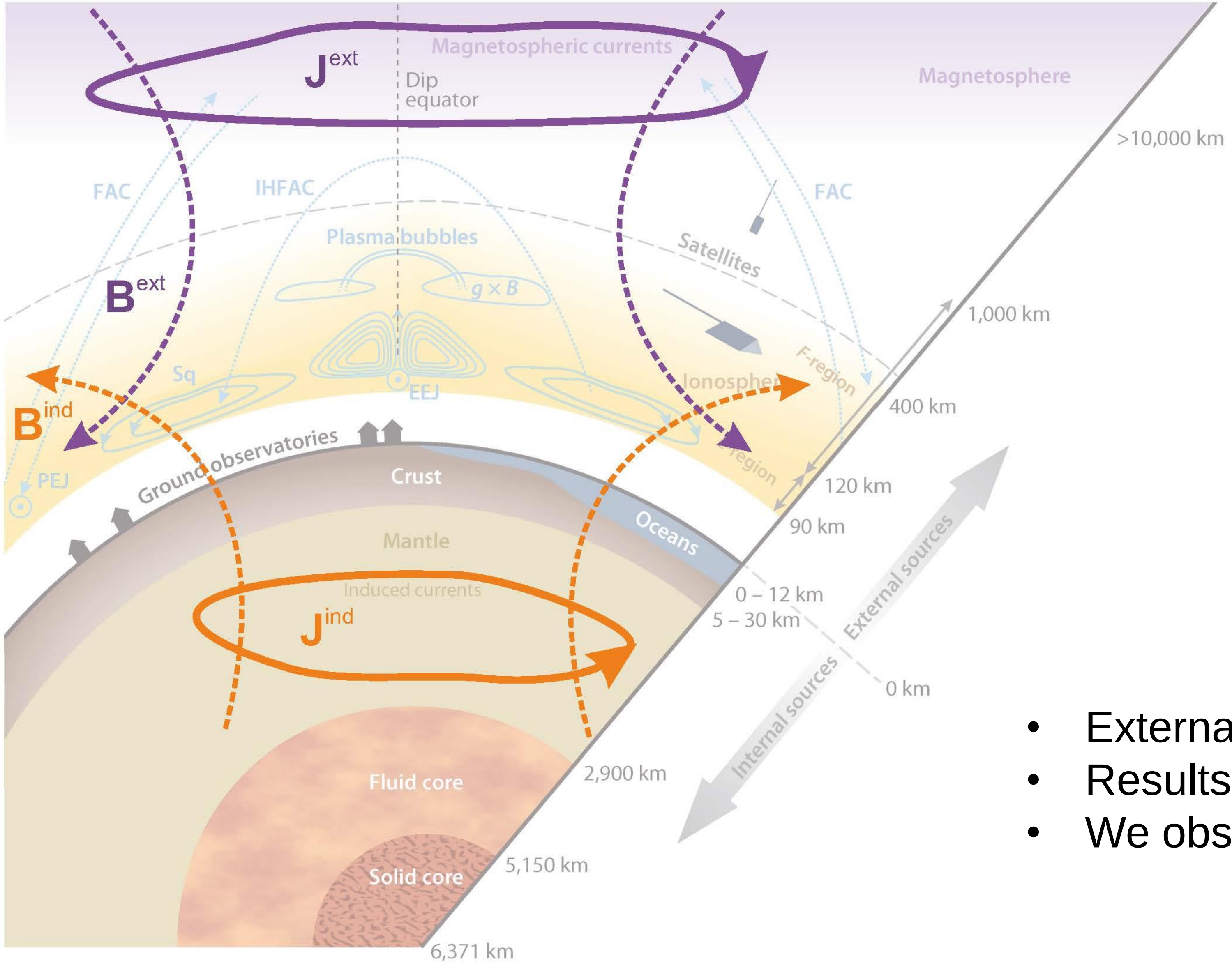

$$\frac{1}{\mu_0}\nabla \times \bar{B} = \sigma \bar{E} + \bar{j}^{ext}$$

$$\nabla \times \bar{E} = -\frac{\partial \bar{B}}{\partial t}$$

- External currents induce secondary currents J^{ind}
- Results in secondary magnetic field B^{ind}
- We observe sum $B^{obs} = B^{ext} + B^{ind}$

Potential method

Assume

$$\vec{B}(\vec{r},t) = -\nabla\left[V^e(\vec{r},t) + V^i(\vec{r},t)\right]$$

then

$$V^e(\vec{r},t) = \mathrm{Re}\left\{a\sum_{n=1}^{N}\sum_{m=-n}^{m}\varepsilon_n^m(t)\left(\frac{r}{a}\right)^n S_n^m(\theta,\phi)\right\}$$

$$V^i(\vec{r},t) = \mathrm{Re}\left\{a\sum_{k=1}^{K}\sum_{l=-k}^{k}\iota_k^l(t)\left(\frac{a}{r}\right)^{k+1} S_k^l(\theta,\phi)\right\},$$

$$S_n^m(\theta,\phi) = P_n^{|m|}(\cos\theta)\exp\left(\mathrm{i}m\phi\right)$$

ALLGEMEINE THEORIE

DES

ERDMAGNETISMUS

VON

CARL FRIEDRICH GAUSS.

Resultate aus den Beobachtungen des magnetischen Vereins im Jahre 1838.
Herausg. v. GAUSS u. WEBER. Leipzig 1839.

Potential method

Assume

$$\vec{B}(\vec{r},t;\sigma) = -\nabla\left[V^e(\vec{r},t) + V^i(\vec{r},t;\sigma)\right]$$

then

$$V^e(\vec{r},t) = \mathrm{Re}\left\{a\sum_{n=1}^{N}\sum_{m=-n}^{n}\varepsilon_n^m(t)\left(\frac{r}{a}\right)^n S_n^m(\theta,\phi)\right\}$$

$$V^i(\vec{r},t;\sigma) = \mathrm{Re}\left\{a\sum_{k=1}^{K}\sum_{l=-k}^{k}\iota_k^l(t;\sigma)\left(\frac{a}{r}\right)^{k+1} S_k^l(\theta,\phi)\right\},$$

$$S_n^m(\theta,\phi) = P_n^{|m|}(\cos\theta)\exp(im\phi)$$

ALLGEMEINE THEORIE

DES

ERDMAGNETISMUS

VON

CARL FRIEDRICH GAUSS.

Resultate aus den Beobachtungen des magnetischen Vereins im Jahre 1838.
Herausg. v. GAUSS u. WEBER. Leipzig 1839.

Potential method and mantle induction

XV. *The Diurnal Variation of Terrestrial Magnetism.*

By Arthur Schuster, *F.R.S., Professor of Physics in Owens College. With an Appendix by* H. Lamb, *F.R.S., Professor of Mathematics in Owens College.*

Received March 20,—Read March 28, 1889.

I. *Introduction.*

In the year 1839 Gauss published his celebrated Memoir on Terrestrial Magnetism, in which the potential on the Earth's surface was calculated to 26 terms of a series of surface harmonics. It was proved in this Memoir that, if the horizontal components of magnetic force were known all over the Earth, the surface potential could be derived without the help of the vertical forces, and it is well known now how these latter can be used to separate the terms of the potential which depend on internal from those which depend on external sources. Nevertheless Gauss made use of the vertical forces in his calculations of the surface potential in order to ensure a greater degree of accuracy. He assumed for this purpose that magnetic matter was distributed through the interior of the Earth, and mentions the fair agreement between calculated and observed facts as a justification of his assumption. In the latter part of the Memoir it was suggested that the same method should be employed in the investigation of the regular and secular variations.

The use of harmonic analysis to separate internal from external causes has never been put to a practical test, but it seems to me to be especially well adapted to enquiries on the causes of the periodic oscillations of the magnetic needle.

untouched. I now publish the results of an investigation which has been carried as far as the observations at my disposal have allowed me to do. My original conclusions have been fully confirmed, and some further information has been obtained which I believe to be of importance. The results of the calculation point not only to an external source, but to an additional internal source, standing in fixed relationship to the external cause. This we might have expected. A varying potential due to external causes must be accompanied by currents induced in the Earth's body, which, in turn, must affect the magnetic needle. The phase of these currents and their magnitude lead us to form definite conclusions on the average conducting power of the Earth, and it will be seen that there is strong evidence that the average conductivity is very small near the surface, but must be greater further down. In this part of the investigation I had much assistance from my colleague, Professor LAMB.

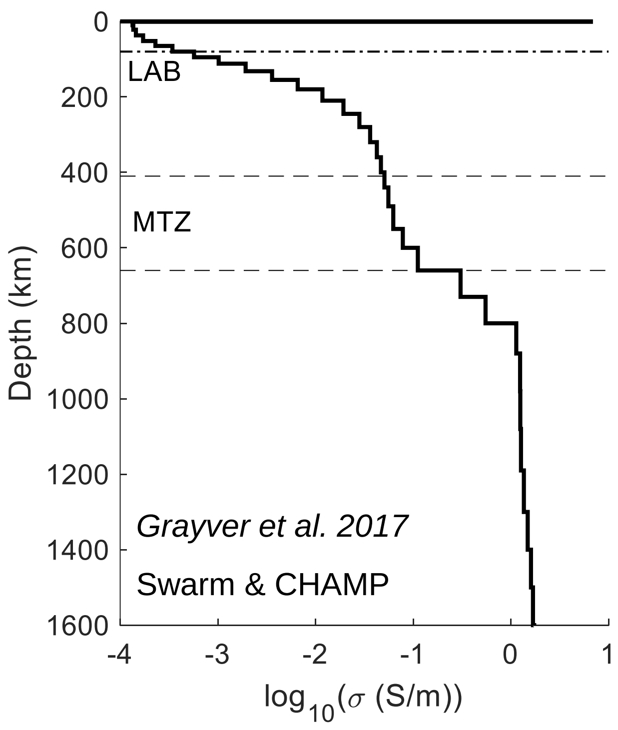

Separate external (inducing) and internal (induced) components of magnetic field

Potential (Gauss) method

- Pros:
  - No prior assumption on subsurface conductivity structure.
  - Mathematical rigor.

- Cons:
  - Potential assumption.
  - Both vertical and (*at least one*) horizontal component are required in practice.
  - Can only separate large-scale signals (*given current observations*).
  - Agnostic to the nature of internal sources.

Alternative method

ETH zürich

Alternative approach

$$\varepsilon_{\mathrm{LS}}(t), \sigma_{\mathrm{LS}} = \min_{\varepsilon,\sigma} \sum_{i=1}^{N_d} \left[B_\theta^{\mathrm{obs}}(\vec{r}_i, t_i) - \sum_{n=1}^{N} \sum_{m=-n}^{n} \int_{-\infty}^{t} B_{n,\theta}^m(\vec{r}_i, t-\tau; \sigma)\varepsilon_n^m(\tau)\mathrm{d}\tau \right]^2 \qquad \varepsilon = \{\varepsilon_n^m \ \forall\ (n,m)\}$$

Grayver et al. 2021, JGR: Space Physics

Alternative approach

$$\varepsilon_{\mathrm{LS}}(t), \sigma_{\mathrm{LS}} = \min_{\varepsilon,\sigma} \sum_{i=1}^{N_d} \left[B_\theta^{\mathrm{obs}}(\vec{r}_i, t_i) - \sum_{n=1}^{N} \sum_{m=-n}^{n} \int_{-\infty}^{t} \overbrace{B_{n,\theta}^{m}(\vec{r}_i, t-\tau; \sigma)}^{\text{“Subsurface” term}} \underbrace{\varepsilon_n^m(\tau)}_{\text{“Source” term}} \mathrm{d}\tau \right]^2 \qquad \varepsilon = \{\varepsilon_n^m \; \forall \, (n,m)\}$$

Grayver et al. 2021, JGR: Space Physics

Alternative approach: reduced version

$$\varepsilon_{\mathrm{LS}}(t) = \min_{\varepsilon} \sum_{i=1}^{N_d} \left[B_\theta^{\mathrm{obs}}(\vec{r}_i, t_i) - \sum_{n=1}^{N} \sum_{m=-n}^{n} \int_{-\infty}^{t} B_{n,\theta}^{m}(\vec{r}_i, t-\tau; \sigma) \underbrace{\varepsilon_n^m(\tau)}_{\text{“Source” term}} \mathrm{d}\tau \right]^2 \qquad \varepsilon = \{\varepsilon_n^m \ \forall \ (n,m)\}$$

Grayver et al. 2021, JGR: Space Physics

Alternative approach

$$\varepsilon^{j}_{\mathrm{LS}}(t) = \min_{\varepsilon} \sum_{i=1}^{N_d} \left[B^{\mathrm{obs}}_{\theta}(\vec{r}_i, t_i) - \sum_{n=1}^{N} \sum_{m=-n}^{n} \int_{-\infty}^{t} B^{m}_{n,\theta}(\vec{r}_i, t-\tau; \sigma)\varepsilon^{m}_{n}(\tau)\mathrm{d}\tau \right]^2 \qquad \varepsilon = \{\varepsilon^m_n \;\forall\; (n,m)\}$$

ε^{1}_{LS} ε^{2}_{LS} ε^{M}_{LS} Time

Time window 1 Time window 2 … Time window *M*

Grayver et al. 2021, JGR: Space Physics

ETH zürich

Separate external (inducing) and internal (induced) components of magnetic field

Potential (Gauss) method

- Pros:
  - No assumption on subsurface conductivity structure.
  - Mathematical rigor

- Cons:
  - Potential assumption.
  - Both vertical and (*at least one*) horizontal component are required in practice.
  - Can only separate large-scale signals (*given current observations*).
  - Agnostic to the nature of internal sources.

Alternative method

- Pros:
  - Works for non-potential fields.
  - Accounts for all scales in the induced field.
  - Isolates fields induced in the mantle.
  - No need to use vertical field.

- Cons:

  Requires a prior subsurface conductivity model

Data (1.12.2013 to 1.12.2019):

- Hourly means from geomagnetic observatories
- Swarm A+B

- Cut-off GM latitude ± 60°
- Only horizontal components are used in model estimation

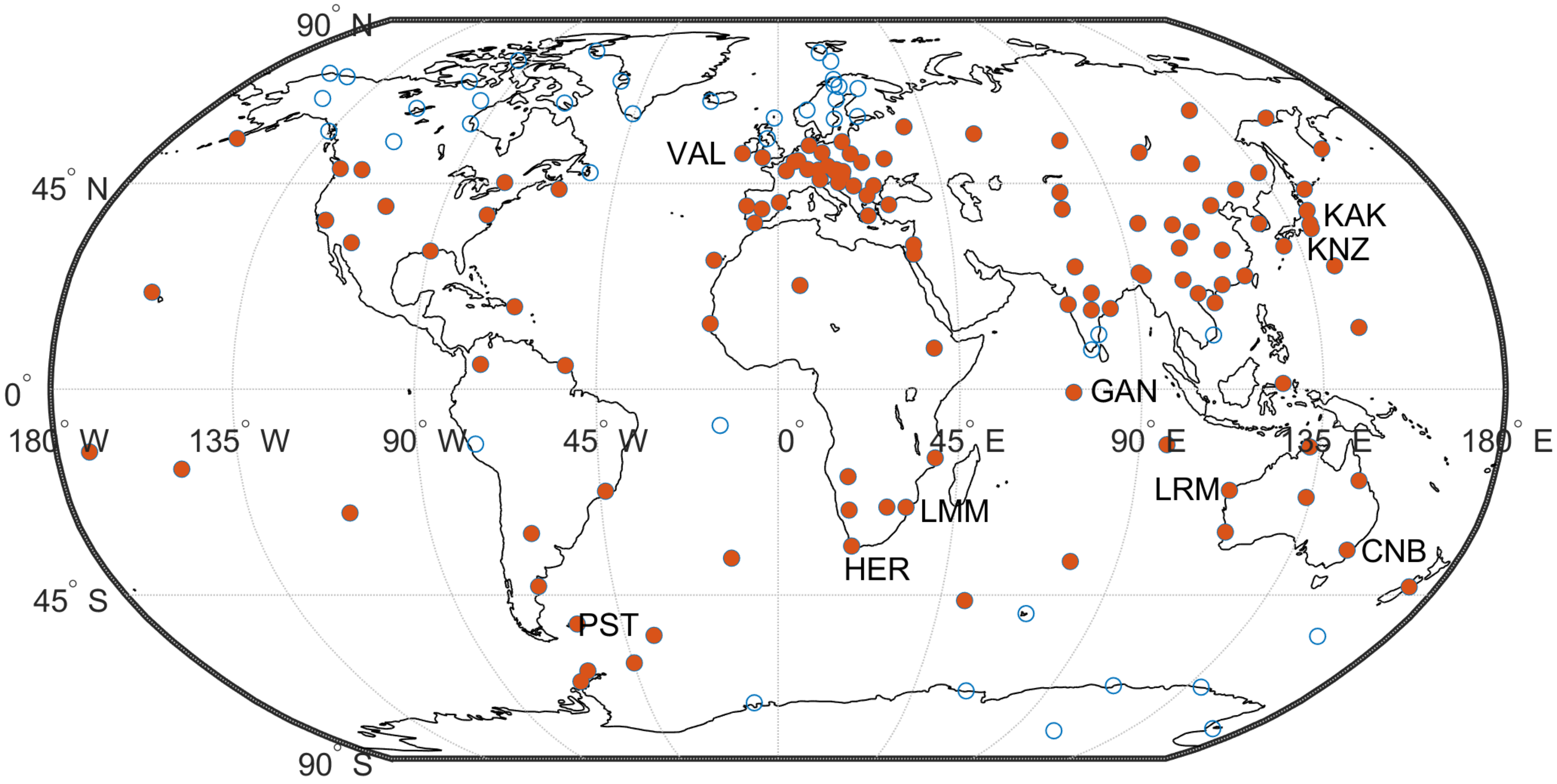

1-D model:

3-D model:

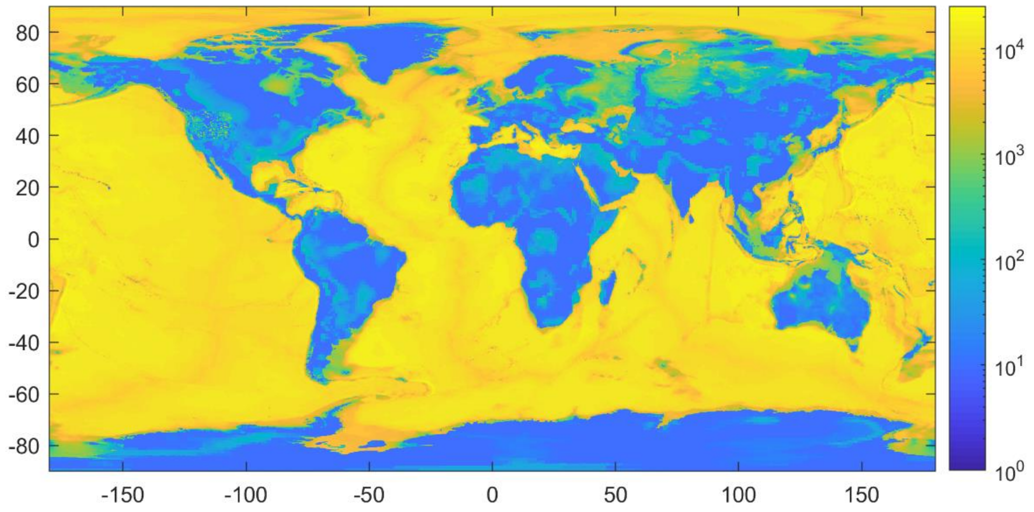

$$S_{\text{const}} = 7000 \text{ Siemens}$$

1-D profile:

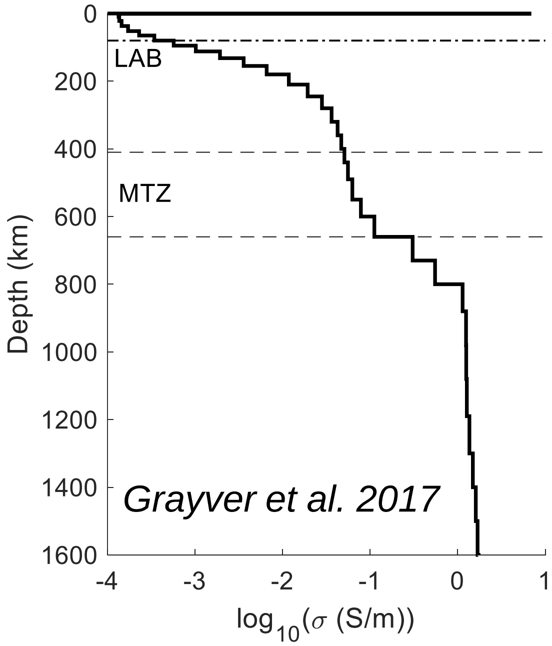

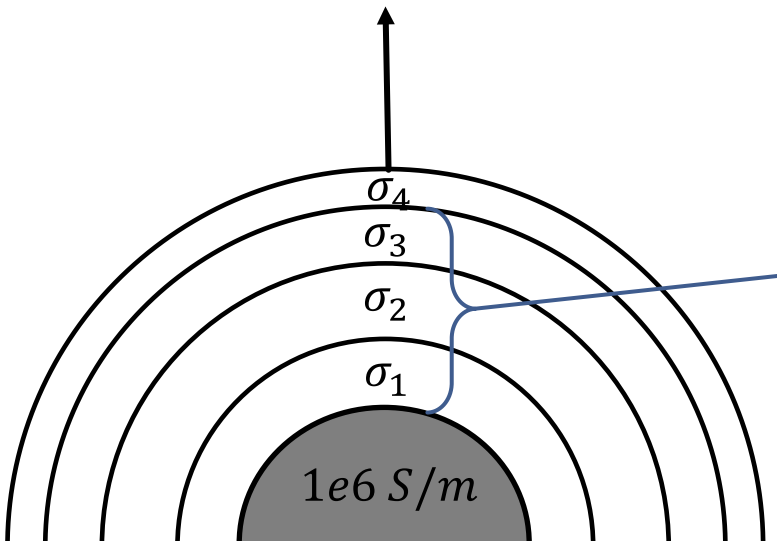

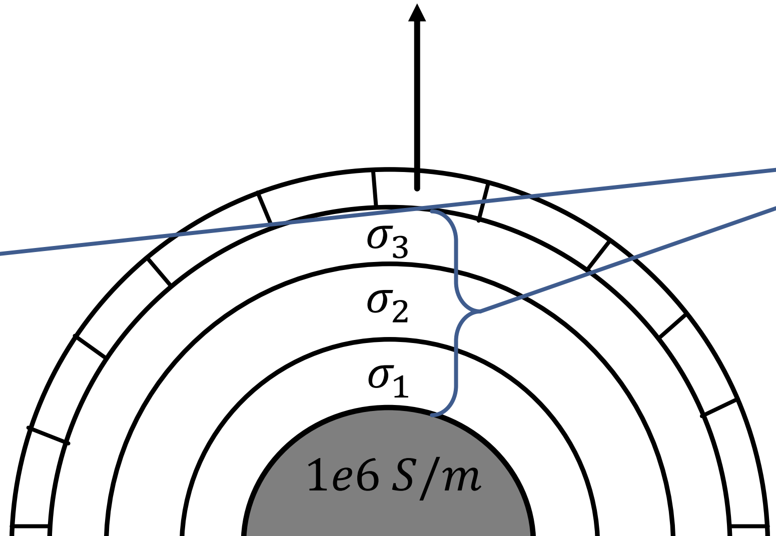

ETH zürich

Coefficient of determination: $$R^2 = 1 - \left[\sum_{i=1}^{N_d} \left(B_i^{\mathrm{obs}} - B_i^{\mathrm{mod}} \right)^2 / \sum_{i=1}^{N_d} \left(B_i^{\mathrm{obs}} - \overline{B}^{\mathrm{obs}} \right)^2 \right]$$

Observatories

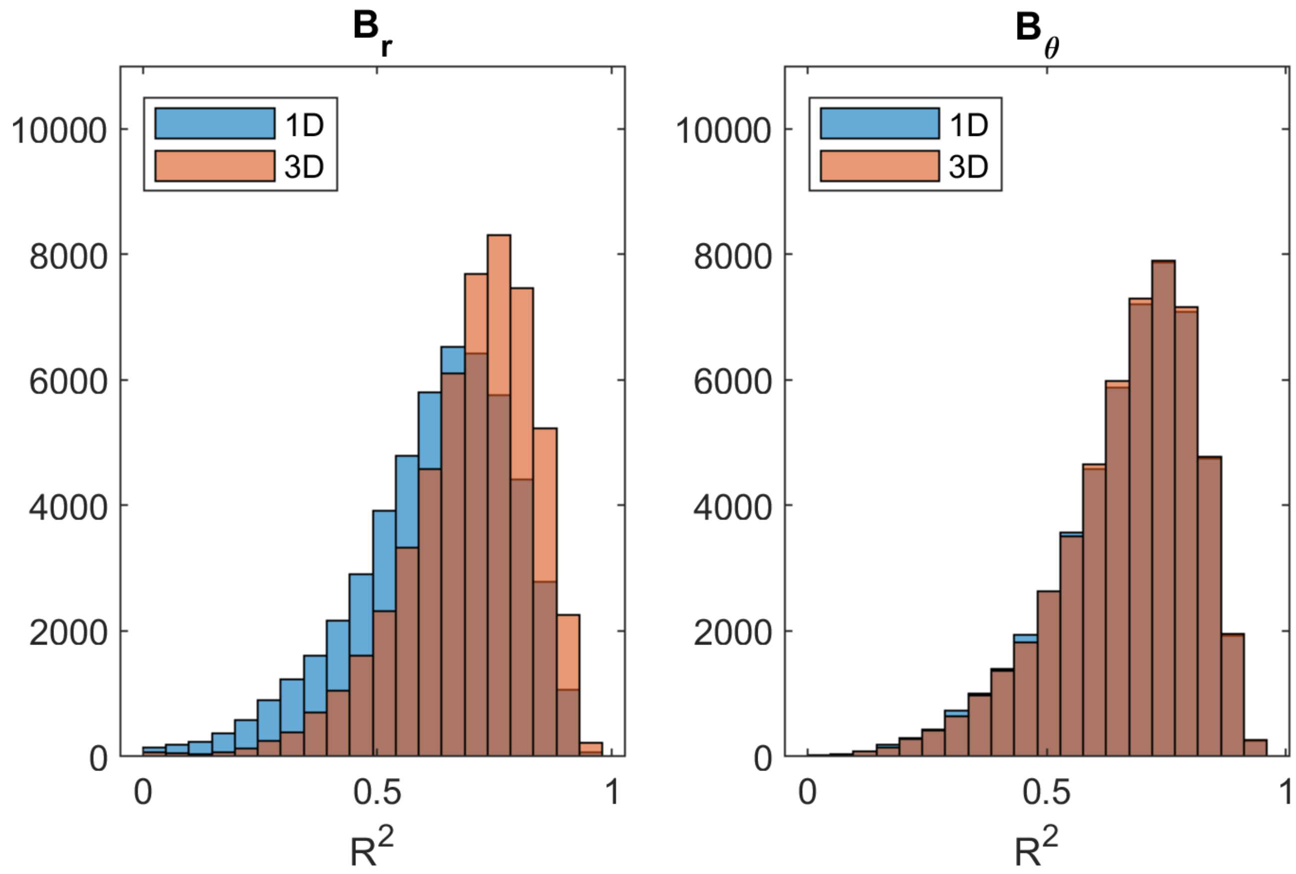

- Radial component is much better fit with a 3-D conductivity model

Coefficient of determination: $$R^2 = 1 - \left[\sum_{i=1}^{N_d} \left(B_i^{\mathrm{obs}} - B_i^{\mathrm{mod}}\right)^2 / \sum_{i=1}^{N_d} \left(B_i^{\mathrm{obs}} - \overline{B}^{\mathrm{obs}}\right)^2 \right]$$

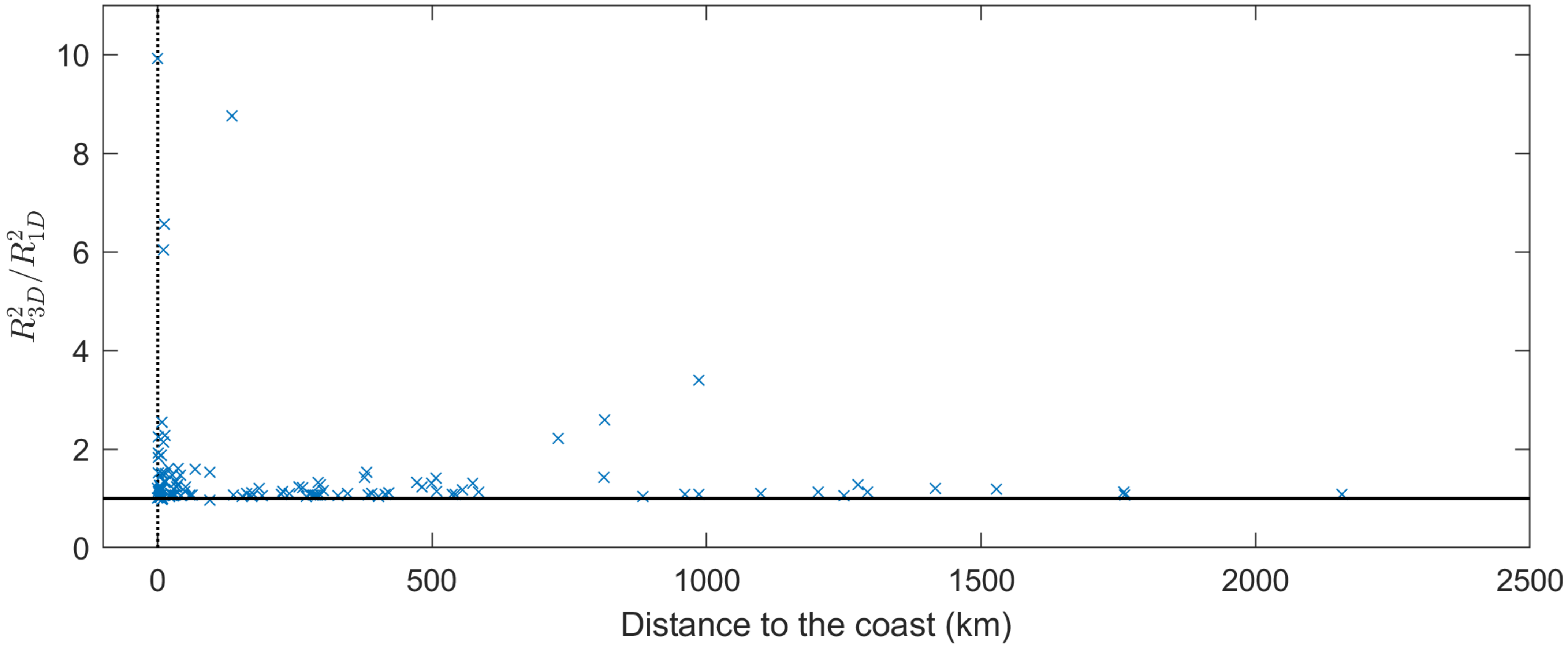

Coefficient of determination: $$R_j^2 = 1 - \frac{\langle \mathbf{b}_j^{\mathrm{obs}} - \mathbf{b}_j^{\mathrm{mod}}, \mathbf{b}_j^{\mathrm{obs}} - \mathbf{b}_j^{\mathrm{mod}} \rangle}{\langle \mathbf{b}_j^{\mathrm{obs}} - \bar{b}_j^{\mathrm{obs}}, \mathbf{b}_j^{\mathrm{obs}} - \bar{b}_j^{\mathrm{obs}} \rangle}$$

Swarm A+B

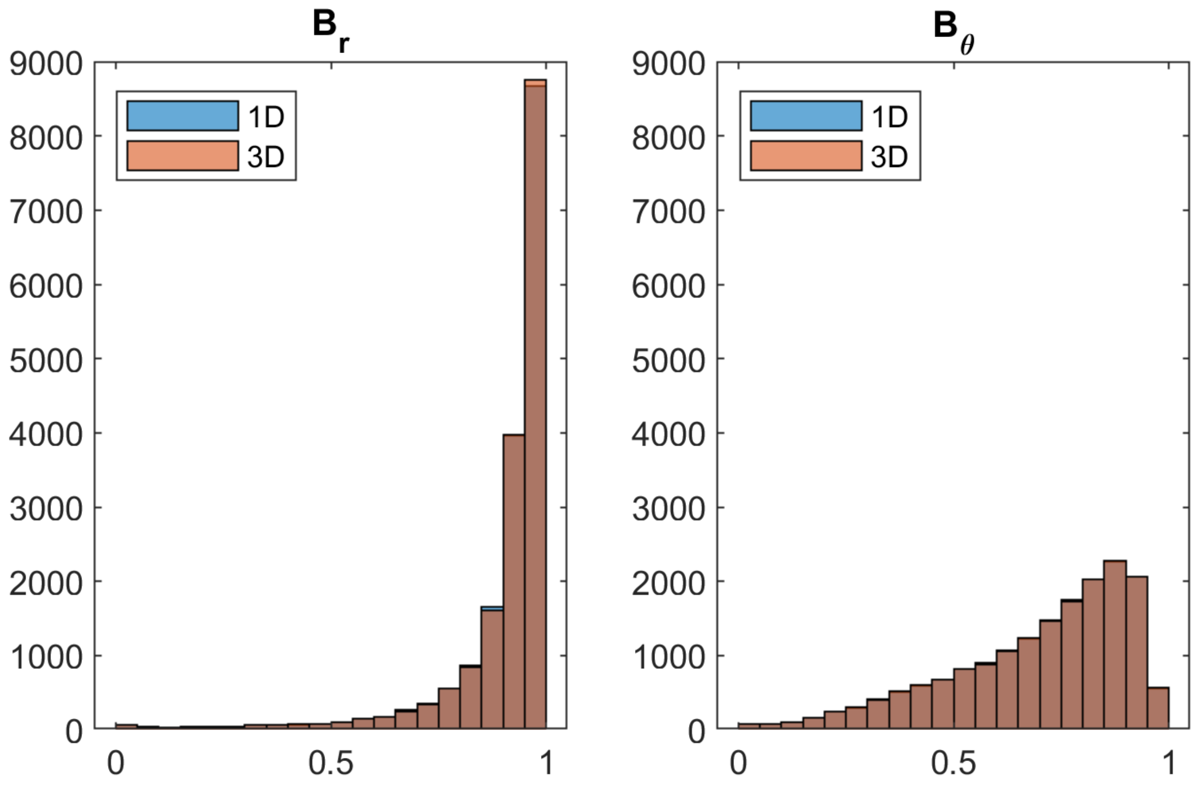

- Nearly no sign of 3-D induction effects at satellite altitude
- Much higher R^2 for radial component than for horizontal

On land

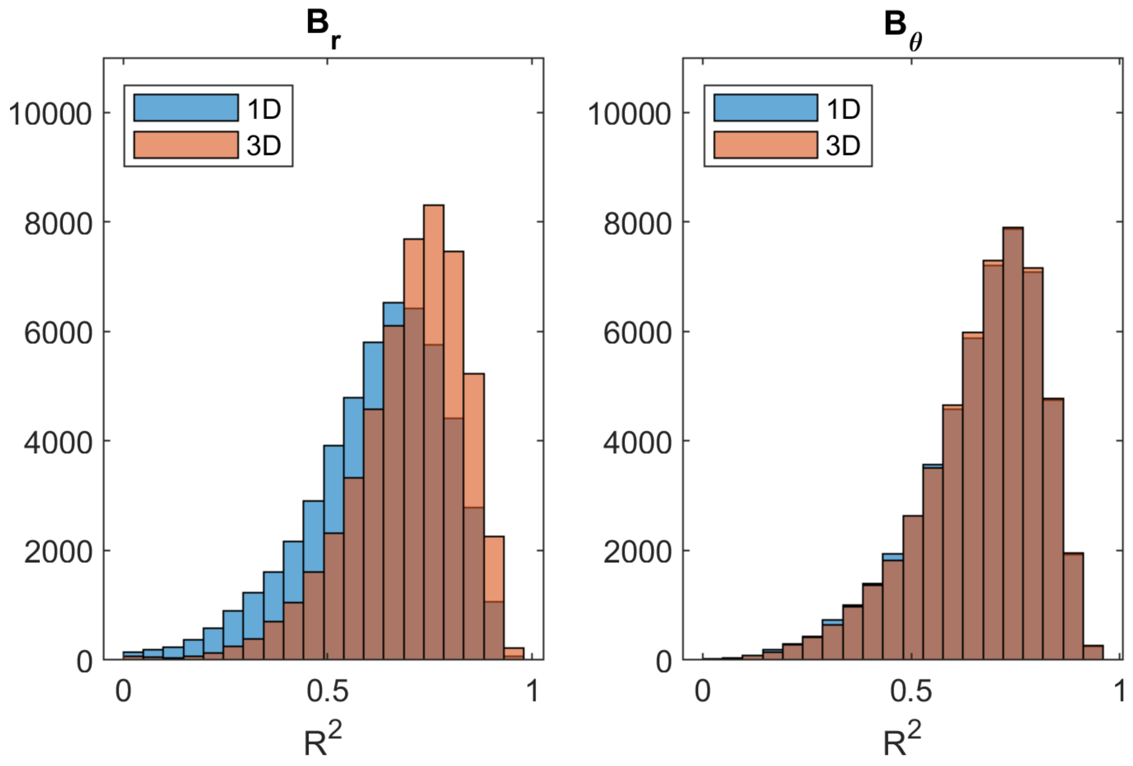

At satellite

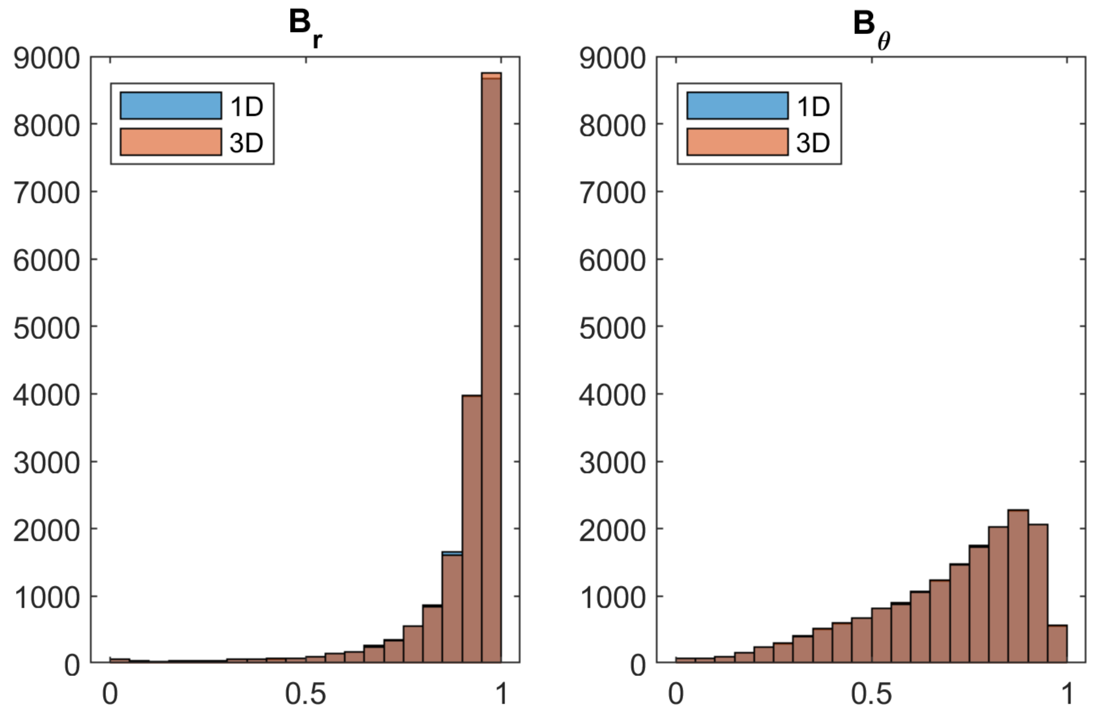

- Nearly no sign of 3-D induction effects at satellite altitude
- Much higher R^2 for radial component than for horizontal

Conclusions and outlook

- Discussed the external/internal magnetic field separation.
- Demonstrated an improved approach to estimate external field
- Enables
  - better characterization of external source structure for mantle induction studies.
  - modelling geomagnetic storms in near real-time.
  - amenable to incorporation in core/crustal field modelling frameworks (CHAOS7)

- Recovery of source and mantle structures demands data redundancy (*seismology enjoys it, but we do not…*)
- Ionospheric contamination of «magnetospheric» coefficients